NAVAL POSTGRADUATE SCHOOL

MONTEREY, CALIFORNIA

THESIS

PERFORMANCE ANALYSIS OF IEEE 802.11G TCM WAVEFORMS TRANSMITTED OVER A CHANNEL WITH PULSE-NOISE INTERFERENCE

by

Athanasios Drivas

June 2007

Thesis Advisor:	Clark Robertson
Thesis Co Advisor:	Tri Ha

Approved for public release; distribution unlimited

THIS PAGE INTENTIONALLY LEFT BLANK

REPORT DOCUMENTATION PAGE			Form Approved OMB No. 0704-0188
Public reporting burden for this collection of information is estimated to average 1 hour per response, including the time for reviewing instruction, searching existing data sources, gathering and maintaining the data needed, and completing and reviewing the collection of information. Send comments regarding this burden estimate or any other aspect of this collection of information, including suggestions for reducing this burden, to Washington headquarters Services, Directorate for Information Operations and Reports, 1215 Jefferson Davis Highway, Suite 1204, Arlington, VA 22202-4302, and to the Office of Management and Budget, Paperwork Reduction Project (0704-0188) Washington DC 20503.			
1. AGENCY USE ONLY *(Leave blank)*	**2. REPORT DATE** June 2007	**3. REPORT TYPE AND DATES COVERED** Master's Thesis	
4. TITLE AND SUBTITLE: Performance Analysis of *IEEE* 802.11*g* TCM Waveforms Transmitted Over a Channel with Pulse-Noise Interference.			**5. FUNDING NUMBERS**
6. AUTHOR Athanasios Drivas			
7. PERFORMING ORGANIZATION NAME(S) AND ADDRESS(ES) Naval Postgraduate School Monterey, CA 93943-5000			**8. PERFORMING ORGANIZATION REPORT NUMBER**
9. SPONSORING /MONITORING AGENCY NAME(S) AND ADDRESS(ES) N/A			**10. SPONSORING/MONITORING AGENCY REPORT NUMBER**
11. SUPPLEMENTARY NOTES The views expressed in this thesis are those of the author and do not reflect the official policy or position of the Department of Defense or the U.S. Government.			
12a. DISTRIBUTION / AVAILABILITY STATEMENT Approved for public release; distribution unlimited			**12b. DISTRIBUTION CODE** A

13. ABSTRACT (maximum 200 words)

Trellis-coded modulation (TCM) is a technique that introduces forward error correction (FEC) coding without increasing the bandwidth of the channel signal. TCM combines binary convolution codes with *M*-ary signal constellation. The application of TCM combines FEC coding and *M*-ary modulation in one operation. The objective of this thesis is to investigate the performance of an orthogonal frequency-division multiplexing (OFDM) based *IEEE* 802.11*g* wireless local area network (WLAN) standard receiver when the waveform is transmitted over an additive white Gaussian noise (AWGN) environment combined with pulse-noise-interference (PNI), for the trellis-coded modulation (TCM) waveform specified by the WLAN standard. In addition to a TCM waveform consisting of a rate r=2/3, 4-state, 8-state and 16-state (K=1, K=2, K=3 and K=4 memory elements) convolution code with 8-phase-shift keying (8-PSK) modulation (analogous to the *IEEE* 802.11*g* TCM mode), improvements to the TCM system will be considered. Specifically, two rate r=1/2 convolution codes independently encoding data on the I and Q channels will be modulated with two 4-pulse amplitude modulation (4-PAM) waveforms. Both K=1 and K=2, K=2 and K=3, and K=2 and K=4 convolution codes (constant number of states and constant constraint length, respectively) will be considered.

14. SUBJECT TERMS *IEEE* 802.11*g* WLAN Standard, Trellis Coded Modulation, Hard decision decoding, Additive White Gaussian Noise, Pulse-noise Interference, 8-PSK, 4-PAM.	**15. NUMBER OF PAGES** 163
	16. PRICE CODE

17. SECURITY CLASSIFICATION OF REPORT	**18. SECURITY CLASSIFICATION OF THIS PAGE**	**19. SECURITY CLASSIFICATION OF ABSTRACT**	**20. LIMITATION OF ABSTRACT**
Unclassified	Unclassified	Unclassified	UL

NSN 7540-01-280-5500 Standard Form 298 (Rev. 2-89)
Prescribed by ANSI Std. 239-18

THIS PAGE INTENTIONALLY LEFT BLANK

Approved for public release; distribution unlimited

PERFORMANCE ANALYSIS OF IEEE 802.11G TCM WAVEFORMS TRANSMITTED OVER A CHANNEL WITH PULSE-NOISE INTERFERENCE

Athanasios Drivas
Lieutenant Junior Grade, Hellenic Navy
Bachelor of Naval Science, Hellenic Naval Academy, 1999

Submitted in partial fulfillment of the
requirements for the degree of

MASTER OF SCIENCE IN ELECTRICAL ENGINEERING

from the

NAVAL POSTGRADUATE SCHOOL
June 2007

Author: Athanasios Drivas

Approved by: Clark Robertson
Thesis Advisor

Tri Ha
Co-advisor

Jeffrey B. Knorr
Chairman, Department of Electrical and Computer Engineering

THIS PAGE INTENTIONALLY LEFT BLANK

ABSTRACT

Trellis-coded modulation (TCM) is a technique that introduces forward error correction (FEC) coding without increasing the bandwidth of the channel signal. TCM combines binary convolution codes with *M*-ary signal constellation. The application of TCM combines FEC coding and *M*-ary modulation in one operation. The objective of this thesis is to investigate the performance of an orthogonal frequency-division multiplexing (OFDM) based *IEEE* 802.11*g* wireless local area network (WLAN) standard receiver when the waveform is transmitted over an additive white Gaussian noise (AWGN) environment combined with pulse-noise-interference (PNI), for the trellis-coded modulation (TCM) waveform specified by the WLAN standard. In addition to a TCM waveform consisting of a rate $r=2/3$, 4-state, 8-state and 16-state ($K=1$, $K=2$, $K=3$ and $K=4$ memory elements) convolution code with 8-phase-shift keying (8-PSK) modulation (analogous to the *IEEE* 802.11*g* TCM mode), improvements to the TCM system will be considered. Specifically, two rate $r=1/2$ convolution codes independently encoding data on the I and Q channels will be modulated with two 4-pulse amplitude modulation (4-PAM) waveforms. Both $K=1$ and $K=2$, $K=2$ and $K=3$, and $K=2$ and $K=4$ convolution codes (constant number of states and constant constraint length, respectively) will be considered.

THIS PAGE INTENTIONALLY LEFT BLANK

TABLE OF CONTENTS

LIST OF FIGURES

THIS PAGE INTENTIONALLY LEFT BLANK

LIST OF TABLES

THIS PAGE INTENTIONALLY LEFT BLANK

ACKNOWLEDGMENTS

I dedicate this work to my beloved parents, Charalampos and Mary Driva, for the educational enlightenment and the generous support they have given me during my educational and military carrier.

I would also like to devote this work to my lovely wife, Dimitra Sotiriou, for her continuous loving support and the happiness that she brings to my life.

Also, I would like to extend my sincere appreciation to Professor Clark Robertson for his constant support, guidance and encouragement in order to complete this work.

Finally, I am grateful to the Hellenic Navy for giving me the opportunity to expand my educational horizons at Naval Postgraduate School.

THIS PAGE INTENTIONALLY LEFT BLANK

EXECUTIVE SUMMARY

Trellis-coded modulation (TCM) is a technique that introduces forward error correction (FEC) coding without increasing the bandwidth of the channel signal. TCM combines binary convolutional codes with *M*-ary modulation in one operation. The waveform is assumed to be transmitted over a channel with both additive white Gaussian noise (AWGN) and pulse-noise interference (PNI). In addition to a TCM waveform consisting of a rate r=2/3 convolutional code with 8-phase-shift keying (8-PSK) modulation (analogous to the *IEEE* 802.11*g* TCM mode) and a TCM system consisting of two rate r=1/2 convolutional codes encoding data that is modulated on the I and Q channels, respectively, with 4-pulse amplitude modulation (4-PAM) is examined. As compared to an r=2/3, 8-PSK TCM system, the decoding complexity of the r=1/2, 4-PAM TCM system is significantly less when the number of encoder memory elements is large. All results obtained in this thesis are the result of modeling the systems such that the resulting models can be analyzed analytically.

Initially, in this thesis the performance of a non-TCM system with rate r=2/3 convolutional coding and 8-PSK modulation in both AWGN and PNI for flat, slowly fading Nakagami channels with the number of encoder memory elements K as a parameter was evaluated. In AWGN, performance of the non-TCM system improves as the number of encoder memory elements K increases. In both AWGN and PNI, as K increases, the performance of the system improves in terms of both E_b/N_o and E_b/N_I . PNI is less effective as the number of memory elements increases. For flat, slowly fading Nakagami channels with AWGN, the effect of the Nakagami fading channel decreases as the fading figure m increases, and the Nakagami fading channel has the least effect when K=8 as compared to K=2. For flat, slowly fading Nakagami channels with both AWGN and PNI, as m increases performance improves. PNI only degrades the performance when m>1, and for $1/2 \le m \le 1$, PNI does not degrade performance but actually improves it. Another interesting point is that for m>2, the effect of the Nakagami fading channel does not significantly change the performance of the system with respect to PNI as m

increases. For K=8, the system performance is significantly better, both in an absolute and a relative sense, compared to K=2.

Next, the performance of the two different TCM waveforms previously mentioned was investigated for the AWGN channel. The performance of the two TCM systems was compared with conventional systems, all designed such that the data rate and signal bandwidth are the same. The two TCM systems were compared in two different ways. First, the two TCM systems were compared for the same number of encoder memory elements devoted to overall encoding. In other words, if the 8-PSK/TCM r=2/3 encoder has K memory elements, then each of the r=1/2 encoders in the 4-PAM/TCM alternative system has K/2 memory elements for a total of K memory elements. Second, the two TCM systems were compared when, if the 8-PSK/TCM r=2/3 encoder has K memory elements, then each of the 4-PAM/TCM r=1/2 encoders has K memory elements for a total of 2K memory elements.

As compared to an r=2/3, 8-PSK TCM system, the decoding complexity of the r=1/2, 4-PAM TCM system is significantly less when the number of encoder memory elements is large; hence, the latter system has an advantage compared to the former system. If we consider both coding gain improvement and decoding complexity, the r=1/2, 4-PAM TCM system is preferred since the coding gain disadvantage, when it exists, is insignificant (a maximum of 0.67 dB) compared to the advantage of decreased decoding complexity. When the two TCM systems are compared for the same total number of encoder memory elements, the r=2/3, 8-PSK TCM system is superior to the r=1/2, 4-PAM TCM system.

In addition to AWGN, the performance of the two TCM systems in PNI was investigated. For both TCM systems, the effect of varying the number of encoder memory elements when PNI is present was examined. It was found that as the number of encoder memory elements increases the negative effect of PNI decreases. When the total number of memory elements in the r=1/2, 4-PAM TCM system is twice that of the r=2/3, 8-PSK TCM system (each r=1/2 encoder has the same number of memory elements as the r=2/3 encoder), the r=1/2, 4-PAM TCM system has better immunity to PNI than the r=2/3, 8-PSK TCM system. When the two TCM systems were compared for the same

total number of encoder memory elements, the r=2/3, 8-PSK TCM system has better immunity to PNI than the r=1/2, 4-PAM TCM system.

The results derived from the comparison of the two TCM schemes having the same bandwidth and data rate imply that the type of comparison used plays a vital role in the selection of which system will be used. We can choose to either sacrifice coding gain in favor of reducing decoding complexity, or we can maximize coding gain at the expense of decoding complexity. In some situations, both reduced decoding complexity and improved coding gain can be obtained simultaneously.

THIS PAGE INTENTIONALLY LEFT BLANK

I. INTRODUCTION

A. BACKGROUND

Over the last few years, the demand of flexible and reliable wireless communications in both the military and commercial field has led to the research and development of wireless local area networks (WLAN). The first wireless protocol which became standard in June 1997 was *IEEE* (Institute of Electrical and Electronics Engineers) standard 802.11, which set the basis for wireless networking development. The 802.11 standard provides three physical layer (PHY) specifications, including 1-2 Mbps frequency-hopping spread spectrum (FHSS) and 1-2 Mbps direct sequence spread spectrum (DSSS) in the 2.4 GHz ISM band, but two more versions of the original standard were introduced [1].

The first variation on 802.11 was the standard specification 802.11*b* which increased data rates beyond 10 Mbps, which was the wired Ethernet limit at the time. 802.11*b* maintained compatibility with the original 802.11 DSSS standard and at the same time incorporated complimentary code keying (CCK) so as to obtain a data rate of 11 Mbps. A scheme with greater range, Packet Binary Convolutional Code (PBCC™), was also provided as an option with data rates of 5.5 and 11 Mbps [1].

The second variation on 802.11 was the standard specification 802.11*a* which was designed to achieve data rates up to 54 Mbps and uses the 5.2 GHz frequency band, so the 802.11*a* standard is not interoperable with either 802.11*b* or the initial 802.11 WLAN protocol.[1] In addition, 802.11*a* uses a multi-carrier modulation technique known as orthogonal frequency-division multiplexing (OFDM), which was chosen because of its ability to mitigate multi-path effects and also achieve high data rates. On the other hand, 802.11*b* specifies a single carrier system [2].

In March 2000, the *IEEE* 802.11 Working Group was formed in order to explore the feasibility of expanding the data rate of the 802.11*b* standard to data rates greater than 20 Mbps. In July 2000, the 802.11 Working Group became Task Group G (TG g), with a mission to define the next standard for higher data rates in the 2.4 GHz band. In November 2000, the 802.11*g* standard was chosen [1].

The 802.11*g* standard exploits existing technologies from the original CCK-OFDM and PBCC-22 proposals. OFDM technology was used in the 802.11*g* standard, and 802.11*g* requires mandatory implementation of 802.11*b* modes but offers optional CCK-OFDM and PBCC-22 modes. The 802.11*g* standard implements the high data rates (54 Mbps) of the 802.11*a* standard in the 2.4 GHz band and, at the same time, provides compatibility with installed 802.11*b* equipment [1].

B. ERROR CORRECTION CODING

In the modern communication world there is an increasing demand for reliable and efficient communications. This demand has been accelerated by the use in our everyday life of wireless local area networks where the transmitted information is severely affected by a noisy transmission environment. There is also increasing demand for high data transmission rates and an acceptable cost of implementing the new designs. One of the most important concerns in designing communications systems is how information bit errors are controlled so that the data can be reliably reproduced. Generally, the communications engineer must address the challenge that the information be reliably transmitted in a noisy environment at the highest feasible rate while keeping implementation costs within acceptable limits [4].

In 1948 Shannon [3] introduced the theory that if the data are properly encoded, then, without sacrificing the rate of data transmission, the errors that are created by a noisy channel can be reduced to any desired level as long as the data rate is less than the channel capacity [4]. Generally, in principle we want to increase the data rate and, at the same time, minimize the required bandwidth and transmitted power. Ideally, the communication system will operate at or near the Shannon limit.

The performance of an error correction coded communication system is measured by the probability of decoder error (bit error probability) and the coding gain of the system relative to an uncoded communication system with the same transmission data rate [4]. The design of a communication system should minimize bit error probability, required signal power, bandwidth, and decoding complexity [4]. There are two major error control strategies: automatic repeat request (ARQ) and forward error correction

(FEC) coding. Many coded systems employ some form of FEC, which is "an application of error-correcting codes that automatically correct errors detected at the receiver"[4].

FEC coding increase the reliability of the system by adding redundant bits to the information data bits in a particular pattern such that the recovery of the information data bits is enhanced. The major disadvantage for a fixed information bit rate is that the implementation of FEC coding results in an increase of the signal bandwidth [5].

In communication applications such as data transmission over telephone networks where there are severe bandwidth limitations, error correction coding is not a viable solution.

Traditionally, with FEC coding, encoding and modulation are treated in separate stages in the transmitter. Trellis-coded modulation (TCM) treats the FEC coding and modulation in an combined manner rather than as separate operations. TCM is a form of coded modulation based on convolution codes and achieves coding gain without an increase in channel signal bandwidth [5].

C. TCM CONCEPT

For many years after the publication of Shannon's paper, research was concentrated on how to design good codes and efficient decoding algorithms, and in the early 1970s it was believed that the achievement of significant coding gains over conventional uncoded modulation could only come with signal bandwidth expansion. Ungerboeck and Csajka in June 1976 [6], introduced for first time the concept of TCM, where coding gains are achieved over conventional uncoded modulation without degrading bandwidth efficiency or reducing the effective information rate.

The basic principles of TCM were published in 1982 [7], and TCM rapidly transitioned from research to practical implementation. From [7] "the essential new concept of TCM that led to the afore-mentioned gains was to use signal-set expansion to provide redundancy for coding and to design coding and signal-mapping functions jointly so as to maximize directly the free distance (minimum Euclidean distance) between

coded signal sequences". The key point of TCM is, instead of using redundant bits, signals that represent symbols, where some of the bits represented by the symbol are redundant and some are not, are transmitted.

D. OBJECTIVE

The objective of this thesis is to examine the performance of TCM waveforms transmitted over a channel with both additive white Gaussian noise (AWGN) and pulse-noise interference (PNI). Specifically, a TCM waveform consisting of a rate r=2/3, 2-state, 4-state, 8-state, and 16-state convolutional code with 8-phase-shift keying (8-PSK) modulation (analogous to the *IEEE* 802.11*g* TCM mode) is examined. In addition, improvements to this TCM system are considered. Specifically, two rate r=1/2 convolutional codes independently encoding data are each modulated with 4-pulse amplitude modulation (4-PAM) waveforms on the I and Q channels to implement an alternative TCM system having the same data rate and channel bandwidth as the original 8-PSK, r=2/3 TCM system.

In this thesis the performance of the TCM systems described is also compared with conventional systems designed such that the data rate and signal bandwidth are the same for all systems. The two TCM systems are compared in two different ways. First, the two TCM systems are compared for the same number of encoder memory elements devoted to overall encoding. In other words, if the 8-PSK/TCM r=2/3 encoder has K memory elements, then each of the r=1/2 encoders in the 4-PAM/TCM alternative system has K/2 memory elements for a total of K memory elements. Second, the two TCM systems are compared, when if the 8-PSK/TCM r=2/3 encoder has K memory elements, then each of the 4-PAM/TCM r=1/2 encoders has K memory elements for a total of 2K memory elements.

All results obtained in this thesis are the result of modeling the systems such that the resulting models can be analyzed analytically. With the exemption of QPSK TCM, the effects of PNI on TCM systems has not been previously analyzed.

E. OUTLINE

The chapter outline of this thesis is organized into the introduction and five additional chapters. In Chapter II, the basic theory of TCM is reviewed, including mapping by set partitioning, minimum Euclidean distance, the Generic Ungerboeck encoder, and the bit error probability of TCM. In Chapter III, the performance of a conventional rate r=2/3 convolutional encoded system with 8-PSK modulation transmitted over a flat, slowly fading Nakagami channel in both AWGN and PNI is analyzed. Chapter IV is an examination of the performance of TCM signals transmitted over channels with both AWGN and PNI. Finally, in Chapter V the conclusions based on the results obtained from the analysis in the previous chapters are presented.

THIS PAGE INTENTIONALLY LEFT BLANK

II. TCM MAIN ELEMENTS

A. TCM CONTRIBUTION

As discussed in Chapter I, TCM is a combined coding and modulation technique which gives positive coding gain without increasing the signal bandwidth. After the publication of the basic principles of TCM in 1982 [7], the International Telegraph and Telephone Consultative Committee (CCITT) adopted a TCM scheme with a 4 dB coding gain for use in high-speed voice band modems in 1984. This was a significant advance considering that the practical limit for data modems for uncoded transmission over voice band channels was 9.6 kbit/s at the time. Since then, data modems which employ TCM techniques have achieved reliable data transmission rates over voice band channels of 14.4 kbit/s and higher. Trellis coded modulation is a method that combines an ordinary $r=m/(m+1)$ convolutional encoder with M-ary modulation while maintaining a constant symbol transmission rate and channel bandwidth. The potential to transmit signals over bandwidth-constrained channels with increased data rates, coding gain, and no bandwidth expansion makes TCM suitable for satellite, mobile, and networking applications.

B. TCM THEORY

In TCM, the transmitted symbols are modulated with schemes that can be described by an M-ary constellation such as M-ary phase-shift-keying (MPSK) or M-ary quadrature amplitude modulation (MQAM).

TCM introduces redundant bits through signal set expansion rather than additional transmitted symbols, and one performance comparison that is made is with uncoded systems that have the same spectral efficiency. With TCM the spectral efficiency is defined as the number of information bits per transmitted symbol, and any comparison with uncoded systems is made with those which have the same average energy per transmitted symbol and the same spectral efficiency.

In an environment with power limitations, the communication system must achieve the desired performance with the smallest possible power. Error-correction

coding, which adds extra bits to the information bit stream, increases the power efficiency as well as the required bandwidth. In an environment with bandwidth limitations, a high-order modulation scheme such as *M*PSK increases the spectral efficiency but increases power requirements. TCM combines the operations of modulation and coding in one step and introduces error correction coding without increasing bandwidth.

The concept of TCM is introduced with an example. From [11] we have the example of a digital communication system which transmits two information bits every T seconds.

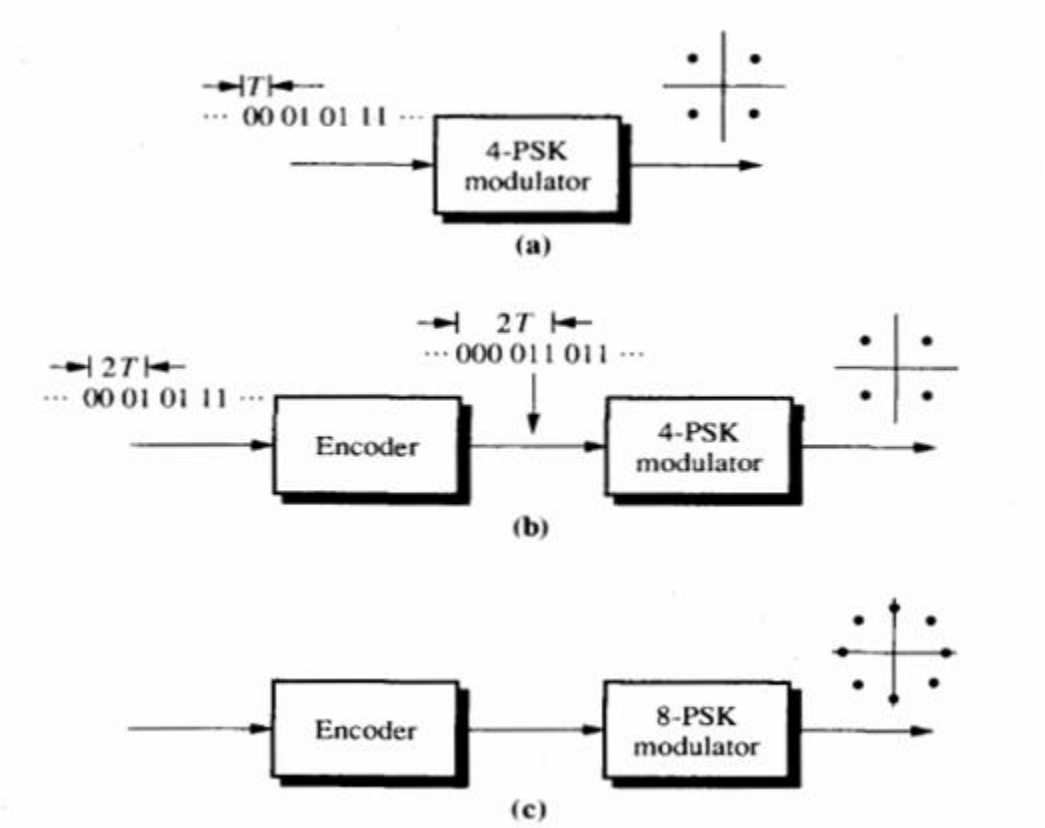

Figure 1. Three digital communication schemes transmitting two information bits every T seconds: (a) uncoded transmission with QPSK (b) QPSK with a rate r=2/3 convolutional encoder and bandwidth expansion (c) 8-PSK with a rate r=2/3 convolutional encoder and no bandwidth expansion. (From: [4]).

The first choice, shown in Figure 1a, uses quadriphase-shift keying (QPSK) modulation with no coding. In this case, every symbol represents two information bits. The second choice, shown in Figure 1b, uses QPSK modulation combined with a rate r=2/3 convolutional encoder. In this situation every signal carries 4⁄3 information bits and in order to match the information rate of the uncoded system each channel symbol must have a duration of 2T/3 seconds. This implies a bandwidth expansion 3/2, or 50% relative to the uncoded system. The third choice, shown in Figure 1c, uses 8-PSK modulation with a r=2/3 convolutional encoder. In this situation two information bits are represented by every symbol, and there is no bandwidth expansion since the channel symbol rate is unchanged. In the preceding example, since 8-PSK is used, there is one extra bit for every two information bits for error correction coding, but the redundant bits are not obtained by transmitting extra bits as with traditional FEC but instead by expanding the size of the signal constellation relative to the uncoded system.

With TCM, if we use convolutional codes that maximize the minimum free Hamming distance between codewords and the code and the signal mapping are designed independently, then we may not achieve a positive coding gain. On the other hand, if we jointly design the code and the signal mapping and maximize the minimum Euclidean distance between signal sequences, we can achieve positive coding gain without increasing the average energy of the signal set or expanding the bandwidth [4].

C. TCM SIGNAL SET EXPANSION

In order to design a TCM system three basic steps must be followed. The first step is the appropriate selection of the signal constellation that meets the spectral efficiency specifications. Second is the selection of the code. The last step is to label the signal set in order to maximize the minimum squared-Euclidean distance d_{free}^2 of the overall TCM system. The technique used to assign these labels is called *mapping by set partitioning* [4].

Referring to the example of Figure 1, we recall that with QPSK two information bits are transmitted per unit time T. If we want to apply error correction coding without increasing the signal bandwidth for the same information bit rate, we use 8-PSK

modulation where each transmitted symbol represents three bits. In Figure 2 we show the partitioning of the 8-PSK constellation where the minimum squared-Euclidean distance, the distance between the signal points within the same subset, is maximized at each stage of the partition tree. The original constellation was partitioned initially in two sets, each containing four symbols, and at the second partition stage there are four sets, each containing two symbols. As we follow the paths of the tree structure, the minimum squared-Euclidean distance between the signal points within the same subset is maximized.

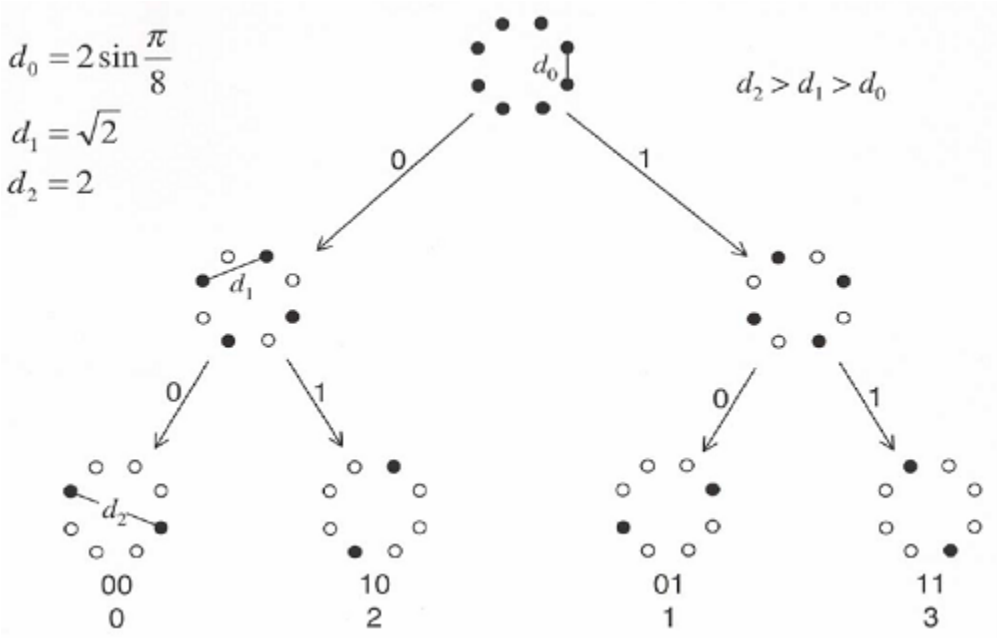

Figure 2. Partitioning of 8-PSK constellation. (From: [5]).

Similarly, if we start with either 8-PSK or 8-QAM, then three information bits are transmitted per unit time T. If we want to apply error correction coding without increasing the signal bandwidth for the same information bit rate, we use either 16-PSK or 16-QAM modulation where each transmitted symbol now represents four bits. In Figure 3 we show the partitioning of a 16-QAM constellation that maximizes the Euclidean distance between signal points within the same subset at each stage of the partition tree. The original constellation was initially partitioned into four sets, each containing four symbols. In the second partition stage there are eight sets, each containing two symbols. Finally, in the last partition stage there are sixteen sets, each

containing one symbol. As with the previous example with 8-PSK, the minimum squared-Euclidean distance between the signal points within the same subset is maximized.

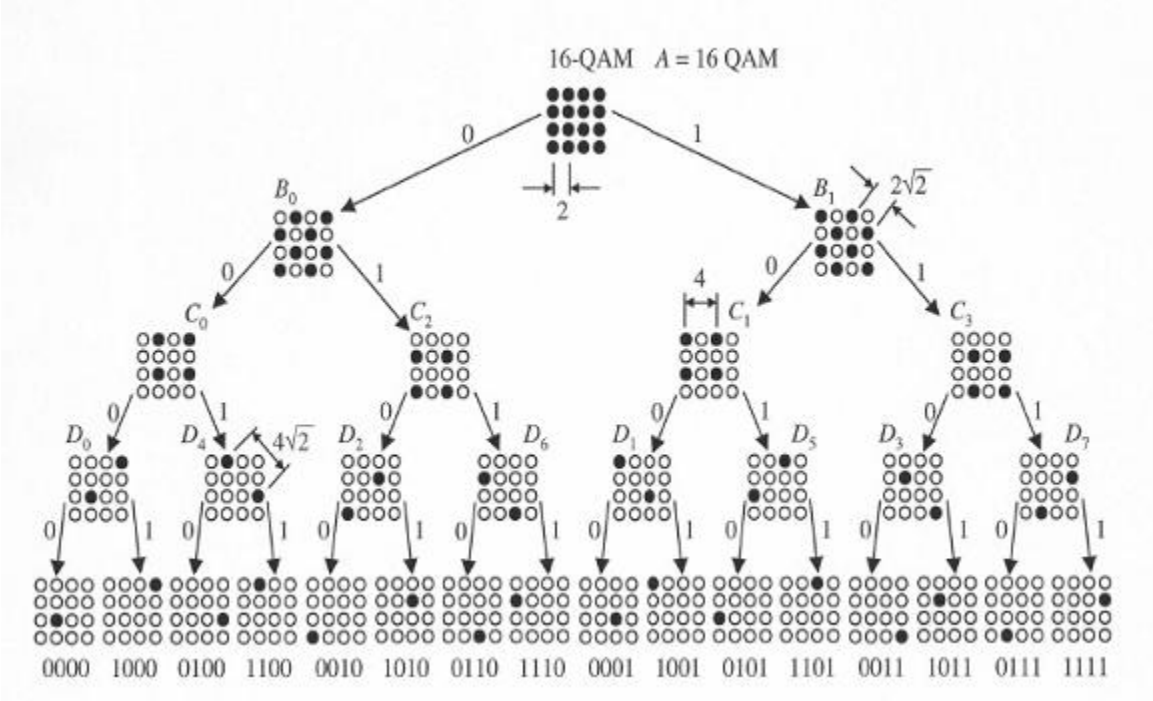

Figure 3. Partitioning of 16-QAM constellation. (From: [5]).

D. TCM ENCODER

For TCM with 8-PSK there are two options. The first option is to apply one of the two information bits to a r=1/2 convolutional encoder where the output of the encoder selects one of four signal subsets. The information bit not applied to the encoder selects the signal within the selected subset. Figure 4 is an example of this type of TCM system. The output of the r=1/2 encoder can be described by a trellis diagram similar to that for conventional encoders. In this case, where there is one uncoded bit, each branch is associated with two possible combinations of three bits. This is referred to as a parallel branch transition.

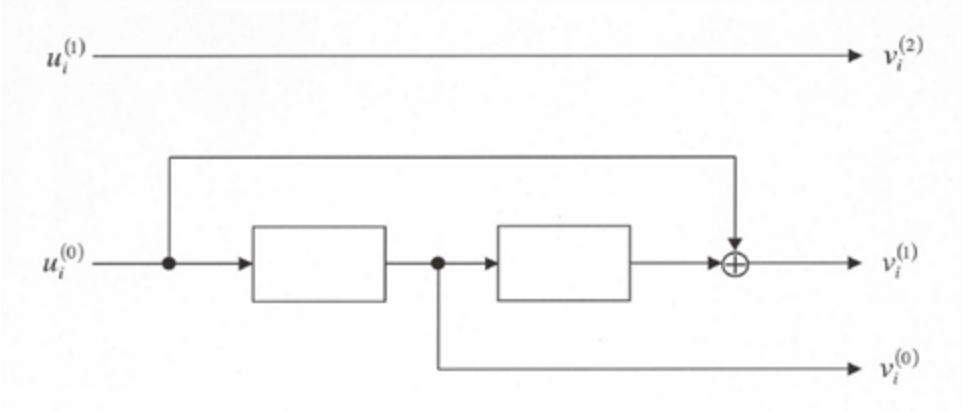

Figure 4. TCM encoder with a single parallel transition/branch for 8-ary signaling. (From: [5]).

Another option is to apply two information bits to a r=2/3 convolutional encoder where the output of the encoder selects one of the eight signal subsets from the third partition level of the 8-PSK constellation, where each set contains one symbol. In this case the parallel transitions are eliminated. Figure 5 is an example of a TCM system with a r=2/3 encoder and no parallel transitions.

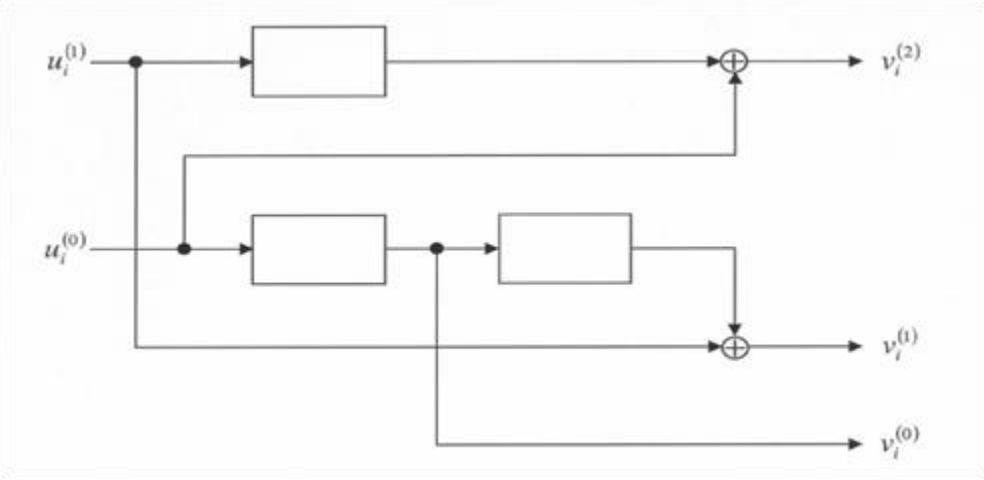

Figure 5. TCM encoder with no parallel transition/branch for 8-ary signaling. (From: [5]).

Figure 6 is the trellis diagram of the TCM encoder shown in Figure 4. Each branch has a single parallel transition.

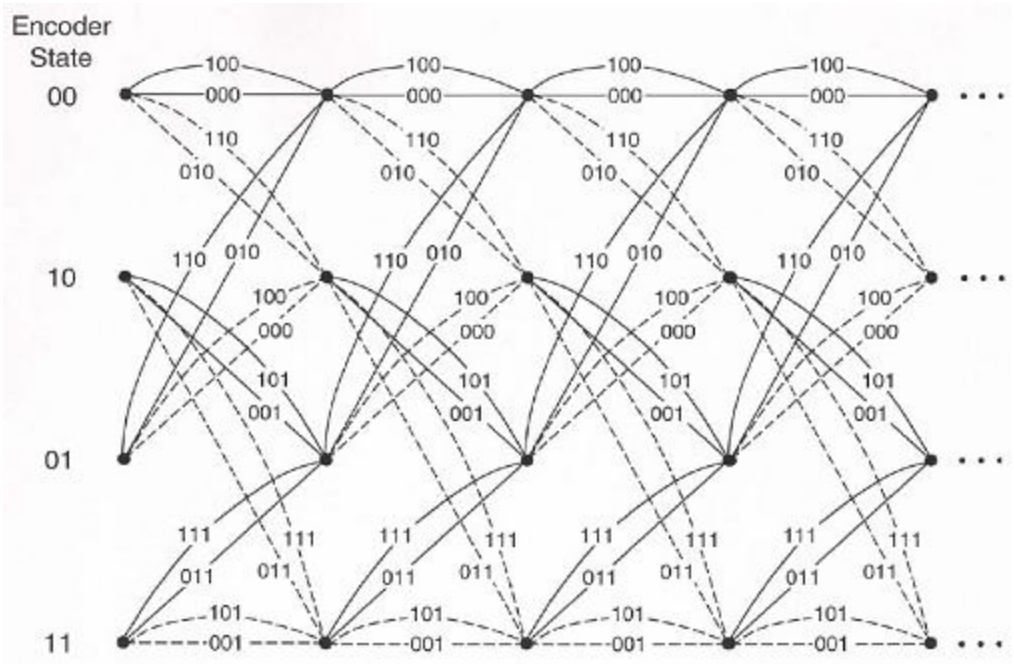

Figure 6. Trellis diagram for TCM encoder with a single parallel transition/branch for 8-ary signaling. (From: [5]).

The preceding can be generalized to m information bits per unit time and 2^{m+1}–ary signaling. In this case the natural uncoded modulation techniques are either 2^m-QAM or 2^m-PSK. For TCM, either 2^{m+1}-QAM or 2^{m+1}-PSK is used, and the constellation is partitioned as before.

In general, there are m different TCM implementations. If we apply one of the m information bits to a convolutional encoder with code rate r=1/2, then the output of the encoder selects a symbol subset from the second partition level where each symbol subset contains 2^{m-1} symbols. The $(m-1)$ remaining uncoded bits select one of the 2^{m-1} symbols signal from the selected subset. In this case each branch of TCM trellis has $2^{m-1}-1$ parallel transitions. If we apply two information bits to a r=2/3 convolutional encoder, the output of the encoder selects a symbol subset from the third partition level where each symbol subset contains 2^{m-2} symbols. The $(m-2)$ remaining uncoded bits select one of the 2^{m-2} symbols signal from the selected subset. In this case each branch of TCM trellis has $2^{m-2}-1$ parallel transitions. If we continue the above process until all m information

bits are applied to an $r=m/(m+1)$ convolutional encoder, then the output of the encoder selects a symbol subset from the $(m+1)$ partition level where each symbol subset contains only one symbol. In this case there are no parallel transitions, which results in no error floor due to parallel transitions, but as m increases and the code rate increases, so does decoder complexity. Figure 7 shows a generic Ungerboeck TCM encoder.

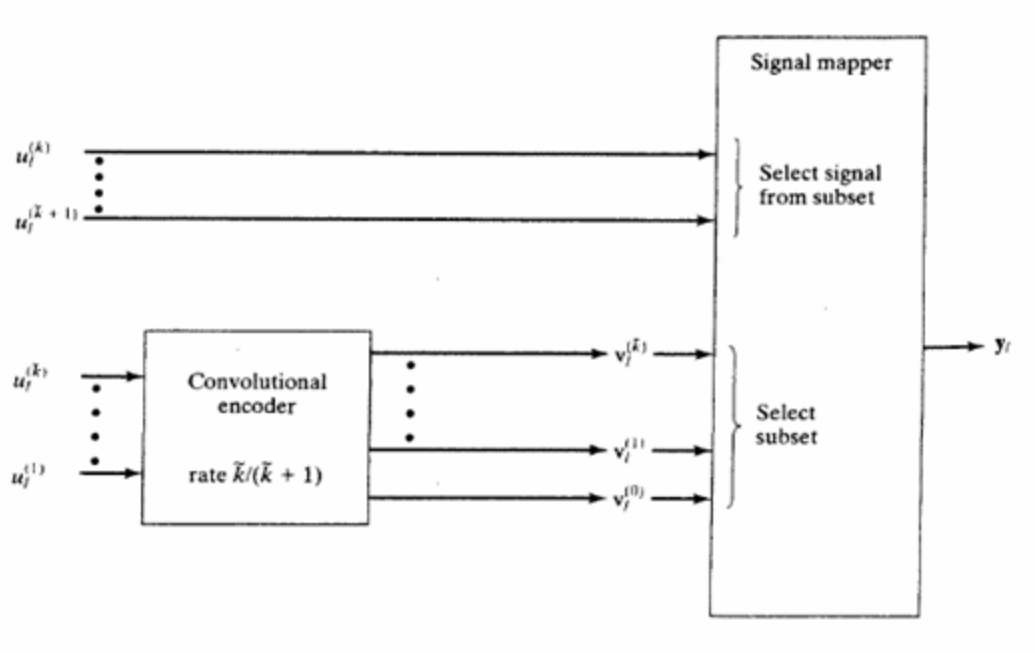

Figure 7. Set partitioning TCM encoder diagram. (From: [4]).

E. PERFORMANCE OF TCM SYSTEMS

A probability bit error analysis of TCM systems is much more complicated than for conventional convolutionally encoded systems because the TCM system is nonlinear, which means that probability bit error depends on the particular code sequence which is transmitted.

The first step in analyzing the performance of a TCM system is to obtain the average input-output weight enumerating function (AIOWEF) $T_{ave}(X,Y)$. In order to obtain the AIOWEF, the error trellis of the convolutional code is required [12].

The error trellis of the convolutional code is an alternative graphical representation of the code that is equivalent to the state diagram of the specific code. A well known algorithm for decoding is the Viterbi algorithm (VA), which is a maximum-likelihood decoding algorithm and relatively simple to implement. From [13] the "Viterbi algorithm decodes the convolutional code by selecting the most likely path through the trellis which represents the received code sequence and is associated with a given received information sequence".

As stated in [12], the error vector of code sequence v and code sequence v´ is defined as $e(v,v') = v \oplus v'$ where v is the code sequence and v´ is the estimate of the code sequence. Without loss of generality v´=0 (the all zero path) can be chosen since the convolutional code is linear. Now e=v, and the conventional trellis is identical to the error trellis with the only difference being one of interpretation. In the conventional trellis each branch is labeled with the encoder output which corresponds to that specific transition, whereas in the error trellis each branch is labeled with the error vector which corresponds to that specific transition [12].

From the theory of convolutional codes[12] we recall that each branch in the signal flow graph is labeled with a branch gain X^d, where d is the encoder output weight for the specific branch, Y^j, where j is the information weight of that branch, and Z, which represents the length of the branch. The transmittance of the branch is the product of $X^d Y^j Z$.

For TCM we use the error trellis of the convolutional code and obtain the signal flow graph by labeling each branch of the error trellis with $\Delta^2{}_e(X)Y^j$.

The term $\Delta^2{}_e(X)$ is the average Euclidean weight enumerator (AEWE), which represents the average of the squared Euclidean distance enumerating function for all pairs of signal points in the constellation having the same error vector. The AEWE is defined [4] by:

$$\Delta_e^2(X) = \frac{1}{M}\sum_{v} X^{\Delta_v^2(e)} \qquad (2.1)$$

where $\Delta_v^2(e)$ is the squared-Euclidean distance between **v** and some arbitrary reference **v´** and there are *M* sequences **v** which have the same error vector relative to some arbitrary reference **v´**. As a result, the (AEWE) depends both on the mapping and the signal constellation [12].

In order to illustrate the derivation of the AIOWEF, we present an example from [12] that uses 4-PAM modulation in conjunction with a *r*=1/2, K=2 convolutional encoder.

Figure 8 shows the 4-PAM constellation with Gray mapping. In Gray mapping adjacent symbols differ in only one bit position.

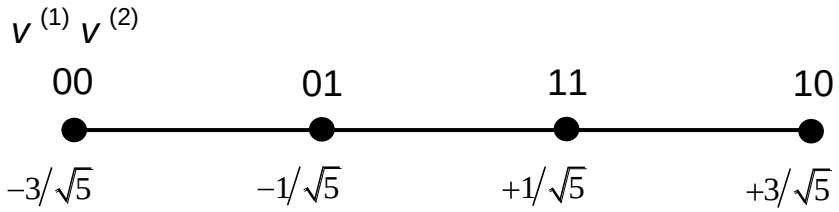

Figure 8. 4-PAM constellation plot. (From: [12]).

For Gray mapped 4-PAM [12], ***e*(00,01)=*e*(11,10)=01** and

$$\Delta_{01}^2(\mathrm{X}) = \frac{1}{2}\mathrm{X}^{4/5} + \frac{1}{2}\mathrm{X}^{4/5} = \mathrm{X}^{0.8}$$

In the same way ***e*(00,11)=*e*(01,10)=11**, and

$$\Delta_{11}^2(\mathrm{X}) = \frac{1}{2}\mathrm{X}^{16/5} + \frac{1}{2}\mathrm{X}^{16/5} = \mathrm{X}^{3.2}$$

Similarly, ***e*(00,10)=*e*(01,11)=10**, and

$$\Delta_{10}^2(\mathrm{X}) = \frac{1}{2}\mathrm{X}^{36/5} + \frac{1}{2}\mathrm{X}^{4/5} = \frac{1}{2}\mathrm{X}^{7.2} + \frac{1}{2}\mathrm{X}^{0.8}$$

Finally, ***e*(00,00)=*e*(11,11)= *e*(01,01)=*e*(10,10)=00** ,and

$$\Delta_{00}^2(\mathrm{X}) = \frac{1}{4}\mathrm{X}^{0} + \frac{1}{4}\mathrm{X}^{0} + \frac{1}{4}\mathrm{X}^{0} + \frac{1}{4}\mathrm{X}^{0} = \mathrm{X}^{0} = 1$$

Table 1 lists the Hamming distance and squared-Euclidean distances. It is clear that the Hamming distance and the squared-Euclidean distance are not linearly related for all **v** relative to some arbitrary reference **v´**.

Table 1. Hamming distance and squared-Euclidean distance for 4-PAM with Gray mapping. (From: [12]).

$w(00)=0$	$\Delta_{00}^2(\mathrm{X})=\mathrm{X}^0$
$w(01)=1$	$\Delta_{01}^2(\mathrm{X})=\mathrm{X}^{0.8}$
$w(10)=1$	$\Delta_{10}^2(\mathrm{X})=\frac{1}{2}\mathrm{X}^{7.2}+\frac{1}{2}\mathrm{X}^{0.8}$
$w(11)=2$	$\Delta_{11}^2(\mathrm{X})=\mathrm{X}^{3.2}$

Figure 9 shows r=1/2, K=2 convolutional encoder and Figure 10 shows the associated error trellis. The signal flow graph for Gray mapped 4-PAM/TCM is obtained from the error trellis and Table 1 and is shown in Figure 11.

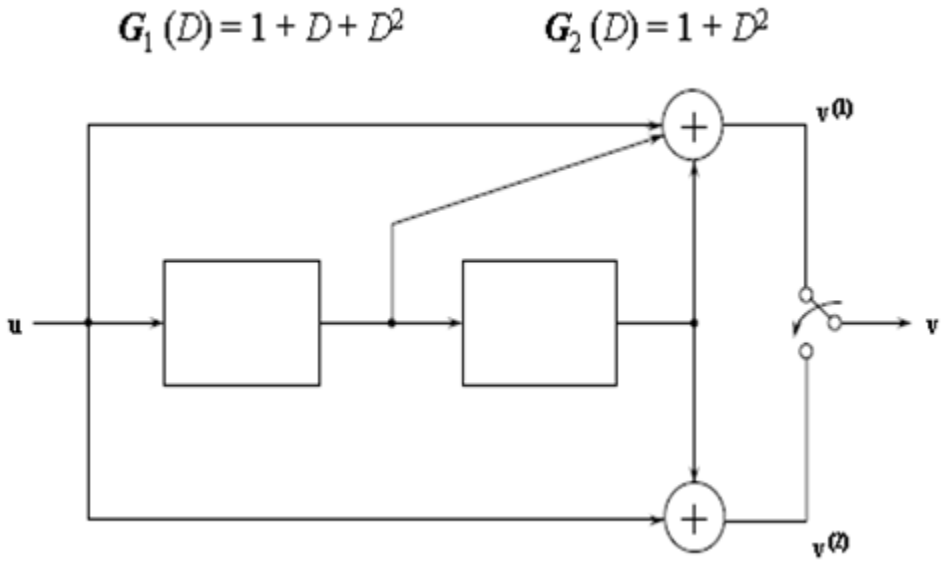

Figure 9. Code rate r=1/2,K=2 convolutional encoder. (From: [5]).

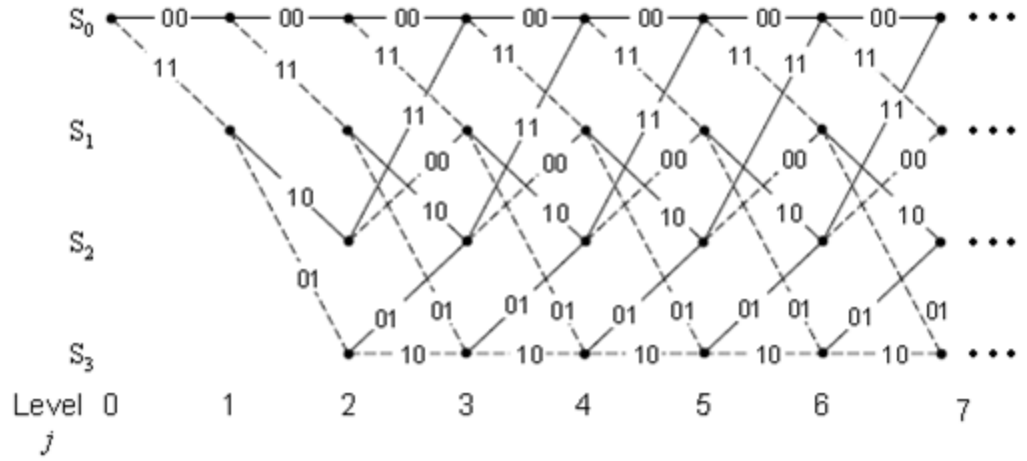

Figure 10. Error trellis for r=1/2,K=2 convolutional encoder. (From: [5]).

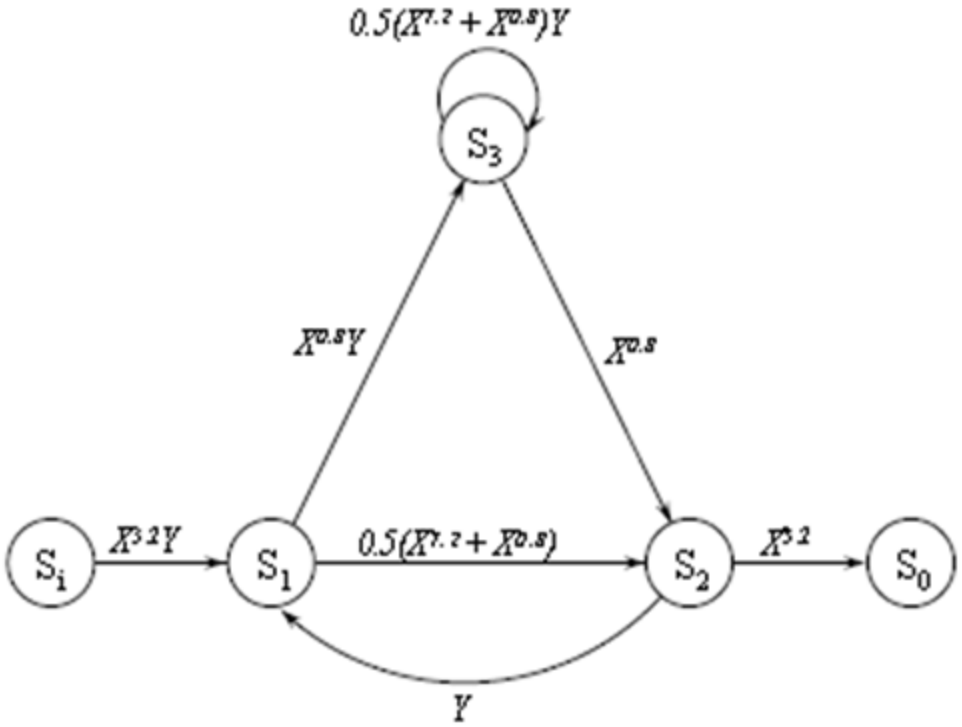

Figure 11. Signal flow graph for r=1/2, K=2 convolutional encoder with Gray mapped 4-PAM/TCM. (From: [5]).

Using the transfer function method, we calculate the AIOWEF as [12]

$$T_{ave}(X,Y) = \frac{X^{7.2}Y\left[\frac{1}{2}+\frac{3}{4}X^{0.8}Y+\frac{1}{2}X^{6.4}-\frac{1}{2}X^{7.2}Y-\frac{1}{4}X^{13.6}Y\right]}{1-X^{0.8}Y+\frac{3}{4}X^{1.6}Y^2-X^{7.2}Y+\frac{1}{2}X^{8.0}Y^2+\frac{1}{4}X^{14.4}Y^2} \tag{2.2}$$

From the geometric series expansion

$$\frac{1}{1-x} = 1+x+x^2+x^3+x^4+..... \tag{2.3}$$

the AIOWEF in equation (2.2) is given by

$$\begin{aligned} T_{ave}(X,Y) = {} & \frac{(X^{7.2}+X^{13.6})Y}{2}+\left(\frac{5X^{8.0}}{4}+\frac{X^{14.4}}{2}-\frac{X^{15.8}}{4}+\frac{X^{20.8}}{2}\right)Y^2 \\ & +\left(\frac{13X^{8.8}}{8}+\frac{15X^{15.2}}{8}-\frac{X^{16.6}}{4}+\frac{5X^{21.6}}{8}-\frac{X^{23.0}}{4}+\frac{3X^{28.0}}{8}\right)Y^3 \\ & +\left(\frac{33X^{9.6}}{16}+...\right)Y^4+... \end{aligned} \tag{2.4}$$

By inspection of the AIOWEF, we see that for an arbitrary sequence there are an average of 1/2 paths with a squared-Euclidean distance of 7.2 associated with one information bit error. There are an average of 5/4 code paths with a squared-Euclidean distance of eight associated with two information bit errors, and so on for higher powers of *X*.

F. PROBABILITY OF SEQUENCE AND BIT ERROR FOR TCM SYSTEMS

For TCM systems, an upper bound on the probability of sequence error is given by [5]

$$P_E \le P_E(parallel)+Q\left(\sqrt{\frac{E_{sc}d^2_{free_{nonparallel}}}{2N_0}}\right)\exp\left(\frac{E_{sc}d^2_{free_{nonparallel}}}{4N_0}\right)\times T(X)\Big|_{X=\exp\left(\frac{-E_{sc}}{4N_0}\right)} \tag{2.5}$$

which can be approximated by [5]

$$P_E \approx P_E(parallel) + A_{dfree_{nonparallel}} Q\left(\sqrt{\frac{E_{sc} d^2_{free_{nonparallel}}}{2N_0}}\right) \tag{2.6}$$

where $E_{sc} = r(m+1)E_b$, $P_E(parallel)$ is the probability of choosing an incorrect parallel path, the average output weight enumerating function (AOWEF) $T(X)$ does not account for parallel paths, $A_{dfree_{nonparallel}}$ is the average number of code sequences that have a Euclidean-distance $d_{free_{nonparallel}}$ from the correct sequence, and $d^2_{free_{nonparallel}}$ is the minimum squared-Euclidean distance between all pairs of nonparallel sequences [5].

The upper bound on the probability of bit error is given by [5]

$$P_b \le P_b(parallel) + \frac{1}{m} Q\left(\sqrt{\frac{E_{sc} d^2_{free_{nonparallel}}}{2N_0}}\right) \exp\left(\frac{E_{sc} d^2_{free_{nonparallel}}}{4N_0}\right) \times \left.\frac{\partial T(X,Y)}{\partial Y}\right|_{X=\exp\left(\frac{-E_{sc}}{4N_0}\right), Y=1} \tag{2.7}$$

which can be approximated by [5]

$$P_b \approx P_b(parallel) + \frac{B_{dfree_{nonparallel}}}{m} Q\left(\sqrt{\frac{E_{sc} d^2_{free_{nonparallel}}}{2N_0}}\right) \tag{2.8}$$

where $P_b(parallel)$ is the probability of bit error when we choose an incorrect parallel path, the AIOWEF $T(X,Y)$ does not account for parallel paths, $B_{dfree_{nonparallel}}$ is the total number of information bit errors of all error paths that have a distance $d_{free_{nonparallel}}$ from the correct path [5].

From the above it is clear that in order to obtain the probability of sequence error we must obtain the AOWEF $T_{ave}(X) = T_{ave}(X, Y=1)$. In order to obtain the probability of bit error, we require $\partial T_{ave}(X,Y)/\partial Y$.

Parallel paths are not preferable because, regardless the complexity of the convolutional encoder, they provide an error floor beyond which performance cannot be improved. In this thesis, we consider only TCM with no parallel transitions, obtained by applying the generic Ungerboeck encoder where all *m* information bits are applied to a

$r=m/(m+1)$ convolutional encoder. Since there are no parallel transitions, computation of the probabilities of bit and sequence error is easier. For TCM systems with no parallel transitions, the probability of bit error is upper bounded by [5]

$$P_b < \frac{1}{m}\sum_{i=1}^{\infty} B_{d_i} Q\left(\sqrt{\frac{E_{sc} d_i^2}{2N_0}}\right) \tag{2.9}$$

or

$$P_b < \frac{1}{m} Q\left(\sqrt{\frac{E_{sc} d_{free}^2}{2N_0}}\right) \exp\left(\frac{E_{sc} d_{free}^2}{4N_0}\right) \times \left.\frac{\partial T_{ave}(X,Y)}{\partial Y}\right|_{X=\exp\left(\frac{-E_{sc}}{4N_0}\right), Y=1} \tag{2.10}$$

where B_{d_i} is the total number of information bit errors on all paths that have a Euclidean distance d_i from the correct path and $d_1^2 = d_{free}^2$. When $E_b/N_o >> 1$, we need only the first term in the infinite series in order to approximate the probability of bit error [5]:

$$P_b \approx \frac{B_{d_{free}}}{m} Q\left(\sqrt{\frac{E_{sc} d_{free}^2}{2N_0}}\right) \tag{2.11}$$

In order to calculate the B_{d_i} from the AIOWEF, we compute

$$\left.\frac{\partial T_{ave}(X,Y)}{\partial Y}\right|_{Y=1} = \sum_{i=1}^{\infty} B_{d_i} X^{d_i^2} \tag{2.12}$$

From the AIOWEF, given in (2.4), we derive

$$\begin{aligned}\left.\frac{\partial T_{ave}(X,Y)}{\partial Y}\right|_{Y=1} = {} & \frac{(X^{7.2} + X^{13.6})}{2} + \left(\frac{5X^{8.0}}{2} + X^{14.4} - \frac{X^{15.8}}{2} + X^{20.8}\right) \\ & + \left(\frac{39X^{8.8}}{8} + \frac{45X^{15.2}}{8} - \frac{3X^{16.6}}{4} + \frac{15X^{21.6}}{8} - \frac{3X^{23.0}}{4} + \frac{9X^{28.0}}{8}\right) \\ & + \frac{33X^{9.6}}{4} + \ldots\end{aligned} \tag{2.13}$$

If we rearrange the terms of equation (2.13), we get

$$\left.\frac{\partial T_{ave}(X,Y)}{\partial Y}\right|_{Y=1} = \frac{X^{7.2}}{2} + \frac{5X^{8.0}}{2} + \frac{39X^{8.8}}{8} + \frac{33X^{9.6}}{4} + \ldots \quad (2.14)$$

Comparing equations (2.14) and (2.12), we obtain the $B_{d_i}s$ which are substituted into equation (2.9) to obtain

$$P_b < 0.5Q\left(\sqrt{\frac{3.6E_b}{N_0}}\right) + 2.5Q\left(\sqrt{\frac{4E_b}{N_0}}\right) + 4.875Q\left(\sqrt{\frac{4.4E_b}{N_0}}\right) + 8.25Q\left(\sqrt{\frac{4.8E_b}{N_0}}\right) + \ldots \quad (2.15)$$

since m=1 and $E_{sc} = r(m+1)E_b = E_b$.

In this chapter we reviewed basic elements of TCM theory and derived the bounds on the probability of sequence and bit error. In Chapter III we evaluate the performance of a non-TCM system with r=2/3 convolution coding and 8-PSK modulation in both AWGN and PNI for slowly fading Nakagami channels with K=2, 4, 6, and 8.

III. PERFORMANCE ANALYSIS OF A NON-TCM SYSTEM WITH *r*=2/3 CONVOLUTION CODING AND 8-PSK MODULATION IN AWGN AND PNI FOR FLAT, SLOWLY FADING NAKAGAMI CHANNELS

In this chapter we examine the performance of a conventional rate r=2/3 convolutionally encoded system with 8-PSK modulation in AWGN and PNI for a flat, slowly fading Nakagami channel.

We first examine the effect of AWGN, noise which is present for all communications systems even when there are no other types of noise present. Second, we examine the performance of the communication system for both PNI and AWGN. Next, we introduce a more realistic scenario by analyzing the performance of the system for a multi-path environment which is modeled as a flat, slowly fading Nakagami channel. Finally, we examine the effect of the flat, slowly fading Nakagami channel when both PNI and AWGN are present.

A. PERFORMANCE BOUND FOR HARD DECISION VITERBI DECODING OF CONVOLUTIONAL CODES

As was discussed in Chapter II, the free distance is defined as the minimum Hamming distance between two code sequences. The Viterbi algorithm chooses a path through the code trellis (yields a code sequence) that differs from the received code sequence in the fewest possible places, and by this method the Viterbi algorithm decodes the encoded bits [12].

The best metric to use with the Viterbi algorithm when hard decision decoding (HDD) is used is the minimum Hamming distance between the received sequence and the survivor sequences at each level [12].

In forward error correction (FEC), when the Viterbi algorithm is used for decoding, a commonly used upper bound on the probability bit error is [9]

$$P_b < \frac{1}{k} \sum_{d=d_{free}}^{\infty} B_d P_d \tag{3.1}$$

where k is the number of the information bits per trellis branch, d is the output weight of a specific path, P_d is the probability that the decoder selects a code sequence that is a Hamming distance d from the correct code sequence, and B_d represents the total information weight of all code sequences of weight d and represents the sum of all possible bit errors that can occur when the all-zero code sequence is transmitted. Finally, d_{free} is the minimum Hamming distance between all pairs of non-zero paths.

Table 2 lists the best rate r=2/3, punctured convolutional code information weight structure B_d .

Table 2. Best (maximum free distance) rate r=2/3 punctured convolutional code information weight structure. (From: [12]).

K	d_{free}	B_{free}	B_{free+1}	B_{free+2}	B_{free+3}	B_{free+4}
2	3	1	10	54	226	853
3	4	8	34	180	738	2989
4	5	25	112	357	1858	8406
5	6	75	0	1571	0	31474
6	6	1	81	402	1487	6793
7	8	395	0	6695	0	235288
8	8	97	0	2863	0	56633

1. Probability Bit Error with Hard Decision Decoding in AWGN

A good approximation for the channel probability bit error in the case of 8-PSK modulation in AWGN is [13]

$$p \approx \frac{2}{3} Q\left[\sqrt{6r\frac{E_b}{N_o}}\sin\left(\frac{\pi}{M}\right)\right] \tag{3.2}$$

where r=2/3 and $M=8$.

The probability P_d for hard decision decoding is [12]

$$P_d = \sum_{i=\frac{d+1}{2}}^{d} \binom{d}{i} p^i (1-p)^{d-i} \qquad \text{for } d \text{ odd}$$
$$P_d = \frac{1}{2}\binom{d}{d/2} p^{d/2}(1-p)^{d/2} + \sum_{i=\frac{d+1}{2}}^{d} \binom{d}{i} p^i (1-p)^{d-i} \qquad \text{for } d \text{ even} \tag{3.3}$$

If we substitute equation (3.2) into equation (3.3) and equation (3.3) into equation (3.1) then, with the help of Table 2, we get the overall probability of bit error for HDD in AWGN. In Figure 12 the performance of 8-PSK and r=2/3 convolutionally encoded bits is shown for different numbers of memory elements.

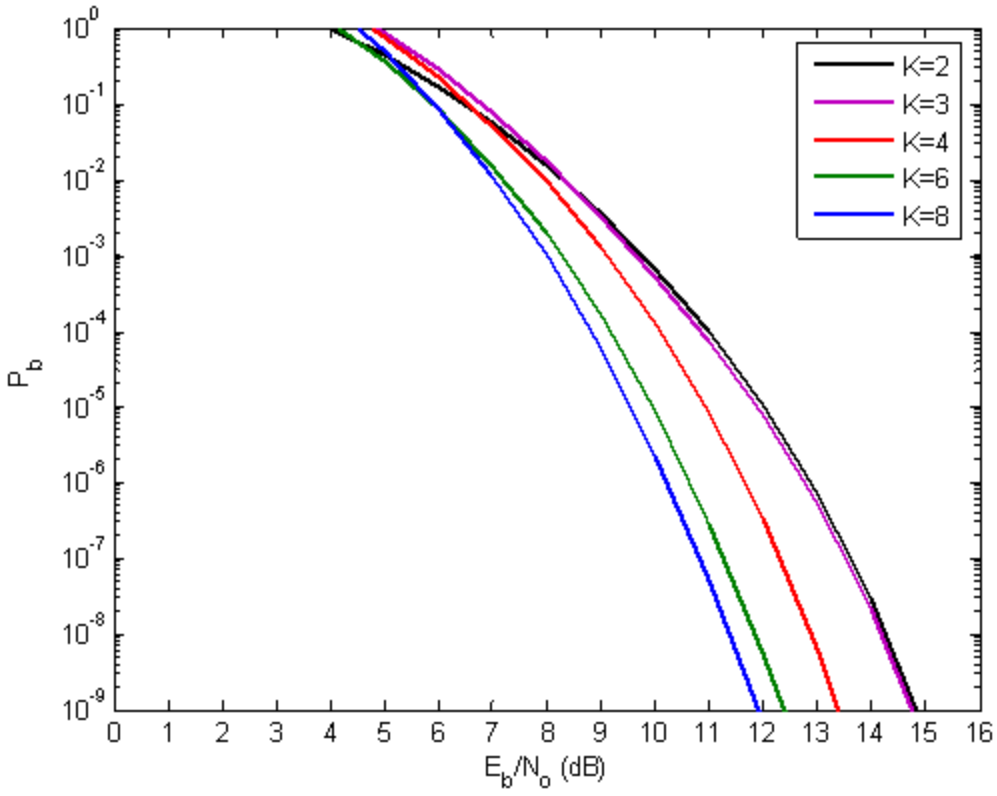

Figure 12. Performance of 8-PSK and r=2/3 convolutionally encoded bits with HDD for different numbers of memory elements in AWGN.

It is obvious that performance improves as the number of encoder memory elements increase. In order to achieve $P_b=10^{-9}$, E_b/N_o=14.85 dB is required for K=2 and E_b/N_o=11.89 dB for K=8. The relative E_b/N_o difference that results from increasing K from two to eight is 2.96 dB. The required probability of bit error P_b for most practical applications is $P_b=10^{-5}$. From Figure 12, in order to achieve $P_b=10^{-5}$, E_b/N_o=9.52 dB is required for K=8 and E_b/N_o=12.01 dB for K=2. The relative E_b/N_o difference that results from increasing K from two to eight is 2.49 dB. In both cases the encoder with K=8 always requires less E_b/N_o compared to encoders with fewer memory elements. It is interesting to note that performance is almost identical for K=2 and K=3.

2. Probability Bit Error with Hard Decision Decoding in AWGN and PNI

We now examine the performance of the receiver in the presence of PNI and AWGN.

With PNI, we assume that the communication system is attacked by a noise-like signal that is turned on and off periodically. If ρ represents the fraction of time that the PNI is turned on, then $(1-\rho)$ represents the fraction of time that the PNI is turned off where $0<\rho\le 1$. In order to derive the channel probability of bit error p, we assume that the PNI does not turn on or off during a bit interval and that the interference's overall average noise power remains constant. In this kind of noisy environment, received symbols are affected by two different levels of noise power since some of the symbols may be affected by AWGN and the rest by both AWGN and PNI. If the power spectral density (PSD) of AWGN is N_o and the PSD of barrage noise interference is N_I, then N_I/ρ is the PSD of the PNI. The total noise power at the output of the receiver for a channel with both AWGN and PNI is

$$\sigma_k^2=\begin{cases}\sigma_o^2 & \text{with AWGN}\\ \sigma_o^2+\sigma_I^2 & \text{with PNI and AWGN}\end{cases} \tag{3.4}$$

where $\sigma_o^2=N_o/T_s$ is the AWGN noise power, $\sigma_I^2=N_I/\rho T_s$ is the PNI noise power, and T_s is the symbol duration.

The channel probability of bit error for both AWGN and PNI is given by

$$p = \Pr(PNI \text{ on})\mathrm{P_b}(PNI \text{ on}) + \Pr(PNI \text{ off})\mathrm{P_b}(PNI \text{ off}) \tag{3.5}$$

where $\rho = \Pr(PNI \text{ on})$ and $(1-\rho) = \Pr(PNI \text{ off})$. From equation (3.2), we get

$$P_b(PNI \text{ off}) = \frac{2}{3} Q\left[\sqrt{6r\frac{E_b}{N_o}}\sin\left(\frac{\pi}{M}\right)\right] \tag{3.6}$$

and

$$P_b(PNI \text{ on}) = \frac{2}{3} Q\left[\sqrt{6r\frac{E_b}{N_o + \frac{N_I}{\rho}}}\sin\left(\frac{\pi}{M}\right)\right] \tag{3.7}$$

Substituting equations (3.6) and (3.7) into equation (3.5), we get the channel probability of bit error for 8-PSK modulation and HDD with both AWGN and PNI as

$$p = \frac{2}{3}\left[\rho Q\left[\sqrt{6r\frac{E_b}{N_o + \frac{N_I}{\rho}}}\sin\left(\frac{\pi}{M}\right)\right] + (1-\rho)Q\left[\sqrt{6r\frac{E_b}{N_o}}\sin\left(\frac{\pi}{M}\right)\right]\right] \tag{3.8}$$

Again the bound on P_b for HDD is given by equation (3.1) after equation (3.8) is substituted into equation (3.3). Results shown in Figure 13 represent the performance of the 8-PSK system with K=2, r=2/3 convolutional encoding for different values of ρ in both AWGN and PNI. All plots are obtained for E_b/N_o=14.27 dB, which results in $P_b=10^{-8}$ when $E_b/N_I >> 1$.

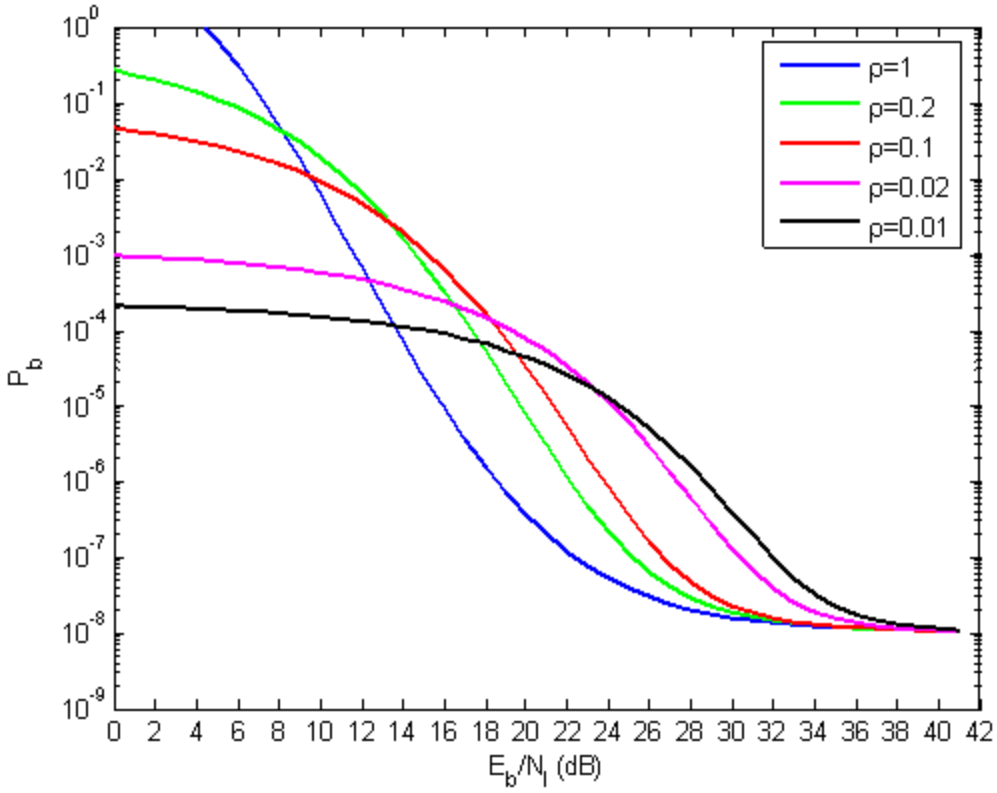

Figure 13. Performance of 8-PSK and K=2, r=2/3 convolutionally encoded bits with HDD for different ρ in both AWGN and PNI.

From Figure 13 we see that PNI can degrade the performance of the system relative to barrage-noise interference (BNI) except when $E_b/N_I >> 1$, when the P_b converges to 10^{-8} since the PNI approaches AWGN.

For $P_b=10^{-5}$, we require E_b/N_I=15.89 dB for BNI, while E_b/N_I=24.51 dB is required for PNI with ρ=0.01. The relative degradation in E_b/N_I between BNI and PNI for the worst case ρ is 8.62 dB for K=2 and E_b/N_o=14.27 dB.

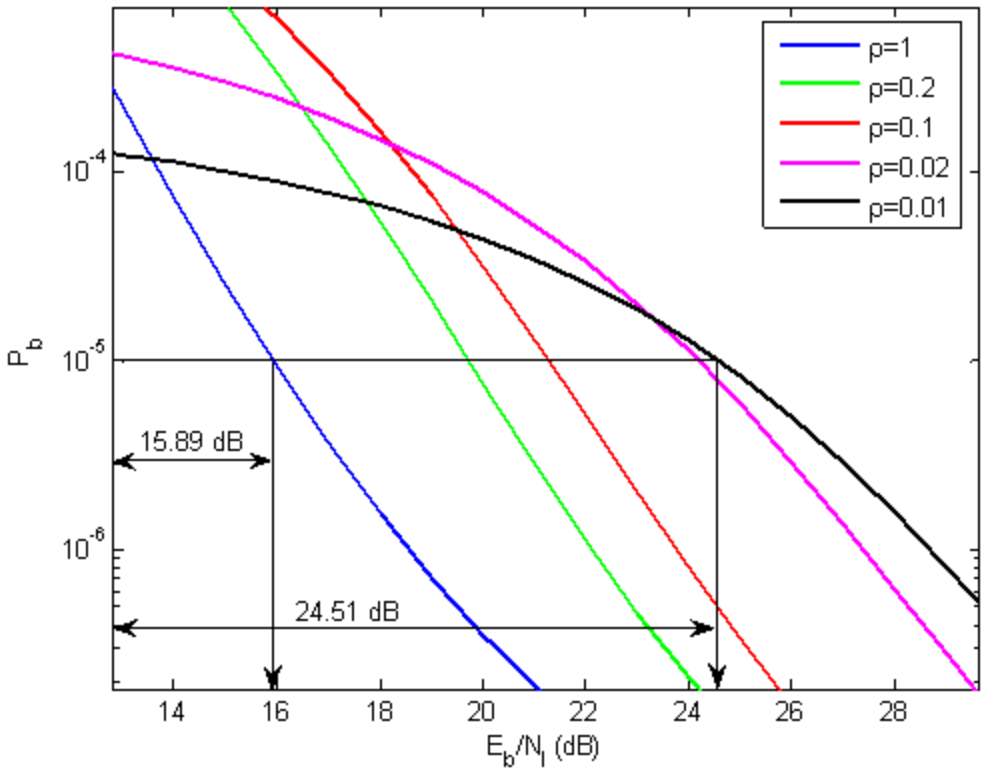

Figure 14. Magnified performance of 8-PSK and K=2, r=2/3 convolutionally encoded bits with HDD for different ρ in both AWGN and PNI.

Figure 14 is a magnified version of Figure 13, where it is obvious that the overall performance is strongly affected by PNI.

The results shown in Figure 15 are for K=4, and all plots are obtained for E_b/N_o=12.89 dB, which results in $P_b=10^{-8}$ when $E_b/N_I>>1$.

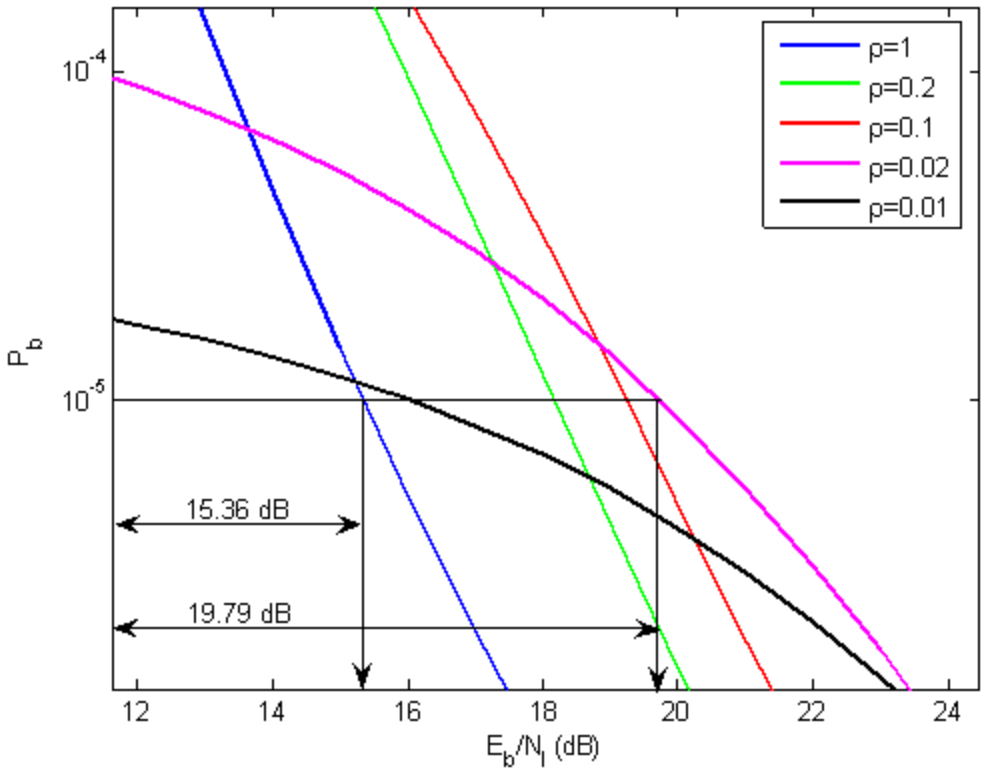

Figure 15. Magnified performance of 8-PSK and K=4, r=2/3 convolutionally encoded bits with HDD for different ρ in both AWGN and PNI.

From Figure 15 we again see that PNI has a significant effect on performance.

For $P_b=10^{-5}$, we require E_b/N_I=15.36 dB for BNI, while E_b/N_I=19.79 dB is required for PNI with ρ=0.02. The relative degradation in E_b/N_I between BNI and PNI for the worst case ρ is 4.43 dB for K=4 and E_b/N_o=12.89 dB.

If we compare the relative E_b/N_I degradation for memory elements K=2 (8.62 dB) and K=4 (4.43 dB), we derive that PNI is less effective as the number of memory elements in the encoder increases.

The results shown in Figure 16 are for K=6, and all plots are obtained for E_b/N_o=11.84 dB, which results in $P_b=10^{-8}$ when $E_b/N_I>>1$.

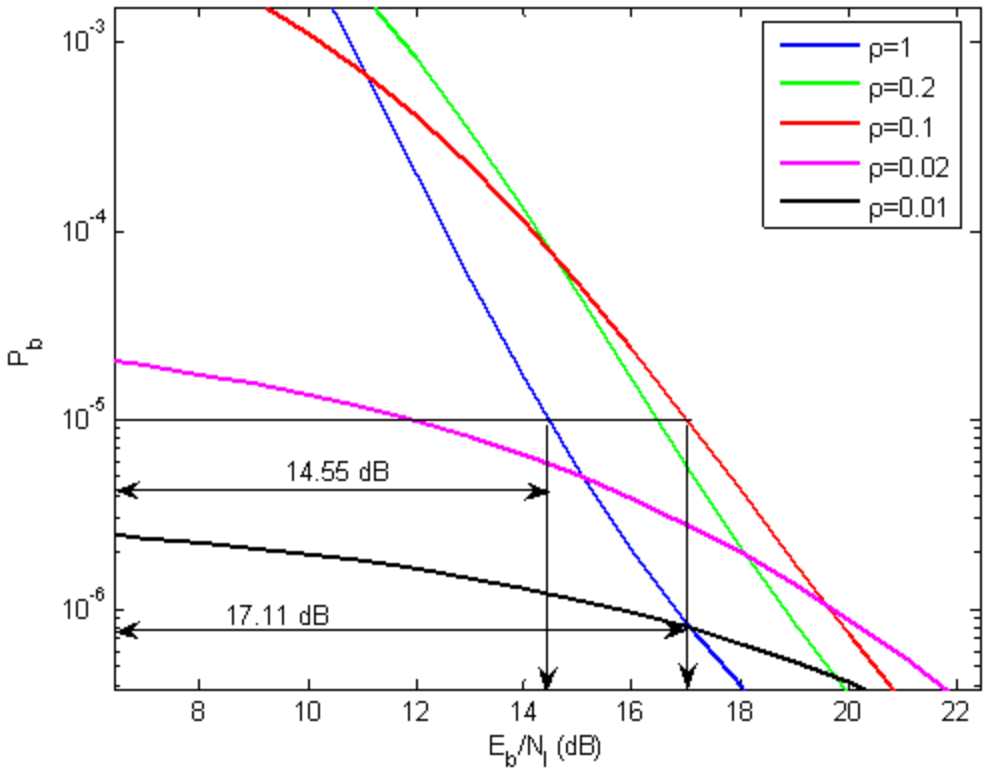

Figure 16. Magnified performance of 8-PSK and K=6, r=2/3 convolutionally encoded bits with HDD for different ρ in both AWGN and PNI.

From Figure 16 we see that PNI has a smaller effect on the performance of the system than for smaller K. For $P_b=10^{-5}$, we require E_b/N_I=14.55 dB for BNI, while E_b/N_I=17.11 dB is required for PNI with ρ=0.1. The relative degradation in E_b/N_I between BNI, and PNI for the worst case ρ is 2.55 dB for K=6 and E_b/N_o=11.84 dB.

The results shown in Figure 17 are for K=8, and all plots are obtained for E_b/N_o=11.35 dB, which results in $P_b=10^{-8}$ when $E_b/N_I>>1$.

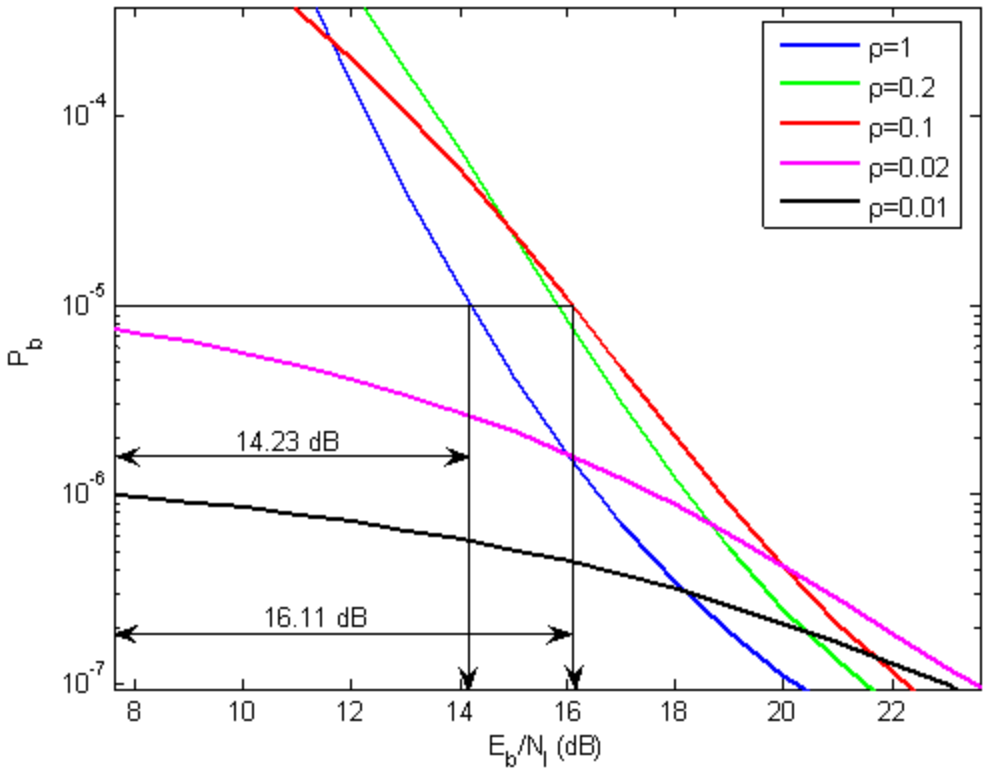

Figure 17. Magnified performance of 8-PSK and K=8, r=2/3 convolutionally encoded bits with HDD for different ρ in both AWGN and PNI.

From Figure 17 we see that PNI has even less effect on performance as compared to smaller K. For $P_b=10^{-5}$, we require E_b/N_I=14.23 dB for the case of BNI, while E_b/N_I=16.11 dB is required for PNI with ρ=0.1. The relative degradation in E_b/N_I between BNI, and PNI for the worst case ρ is 1.87 dB for K=8 and E_b/N_o=11.35 dB.

It is obvious that PNI has less of an effect because we are applying an encoder with K=8, which is the largest number of memory elements compared to previous cases.

Table 3. Performance of 8-PSK with r=2/3 convolution encoding and HDD for both AWGN and PNI.

K	Required E_b/N_o for $P_b=10^{-5}$	Relative E_b/N_I degradation for $P_b=10^{-5}$	Absolute E_b/N_I for $P_b=10^{-5}$ for worst case ρ
2	12 dB	8.62 dB	24.51 dB
4	10.91 dB	4.43 dB	19.79 dB
6	9.94 dB	2.55 dB	17.11 dB
8	9.52 dB	1.87 dB	16.11 dB

Table 3 summarizes the preceding results. From Table 3, we see that as the number of memory elements of the r=2/3 convolution encoder increases, the performance of the system improves (from 12 dB to 9.52 dB) in terms of E_b/N_o and in terms of the relative E_b/N_I degradation (from 8.62 dB to 1.87 dB). Clearly, the PNI is less effective as the number of memory elements increases. The improvement is 6.75 dB. Finally, we see that the absolute E_b/N_I decreases (from 24.51 dB to 16.11 dB) when the number of memory elements is increased, almost an 8.4 dB improvement.

3. Probability Bit Error with Hard Decision Decoding for Flat, Slowly Fading Nakagami Channels and AWGN

In the modern wireless communication world there is a need to reliably transmit high data rates in order to support multimedia applications over wireless communication links. The main characteristic of wireless propagation is that usually there is no line-of-sight (LOS) path for the signal. Most of the time the mobile antennas are surrounded by much higher surrounding structures that restrict wireless propagation and result in signal fading.

In the multipath fading environment, several models have been developed in order to describe the phenomenon. The most characteristic models are the Rayleigh fading model, which applies to non-LOS applications, and the Ricean model, which applies

when there is a LOS propagation path. A channel model that is more flexible is the Nakagami model. The Rayleigh model is a special case of Nakagami model.

For the Nakagami channel model, the amplitude of the received signal a_c is modeled as a Nakagami-*m* random variable. The probability density function (PDF) for the Nakagami-*m* random variable is [9]

$$f_{A_c}(a_c) = \frac{2}{\Gamma(m)}\left(\frac{m}{\Omega}\right)^m a_c^{2m-1} e^{\frac{-ma_c^2}{\Omega}} \tag{3.9}$$

where the Gamma function $\Gamma(m)$ is defined as

$$\Gamma(m) = \int_0^\infty t^{m-1} e^{-t}\, dt \text{ for } m \geq 0 \tag{3.10}$$

Ω is defined as

$$\Omega = E\left[A_c^2\right] \tag{3.11}$$

and A_c is the expected value of the Nakagami-*m* random variable a_c. The parameter *m* is the *fading figure* and is defined as the ratio of moments

$$m = \frac{\Omega^2}{E\left[\ A_c^2 - \Omega^2\ \right]} \text{ for } m \geq \frac{1}{2} \tag{3.12}$$

The fading figure *m* determines if the channel conditions are less or more severe than the Rayleigh model since, for *m*=1, the Nakagami PDF is a Rayleigh PDF. For small *m* $(1/2 \leq m \leq 1)$, fading is very severe, while, for larger values of *m* $(m > 1)$, the fading conditions are less severe. For the special case where $m \to \infty$, there is no fading. The Nakagami-*m* fading model is the best model for the multipath propagation channel which generally occur in mobile wireless communications since the Rayleigh model cannot account for shadowing, a large scale effect for mobile communications.

The average energy per bit-to-AWGN PSD ratio is given by

$$\gamma_b = \frac{E_b}{N_o} = \frac{a_c^2 T_b}{N_o} \tag{3.13}$$

where T_b is the bit duration.

From equation (3.13), we see that γ_b is a random variable since it is a function of a_c^2. Changing variables, we get

$$f_{\Gamma_b}(\gamma_b) = \frac{1}{\Gamma(m)}\left(\frac{m}{\bar{\gamma}_b}\right)^m \gamma_b^{m-1} e^{\frac{-m\gamma_b}{\bar{\gamma}_b}} \tag{3.14}$$

From equation (3.3), we get the conditional probability

$$p(\gamma_b) \approx \frac{2}{3} Q\left[\sqrt{6r\gamma_b \sin^2\left(\frac{\pi}{M}\right)}\right] \tag{3.15}$$

From [17], the overall unconditional probability of channel bit error is

$$p = \int_0^\infty \frac{2}{3} Q\left[\sqrt{6r\gamma_b \sin^2\left(\frac{\pi}{M}\right)}\right] f_{\Gamma_b}(\gamma_b) d\gamma_b \tag{3.16}$$

Substituting equation (3.14) into equation (3.16), we get [17]

$$p = \frac{1}{3} \frac{\Gamma\left(m+\frac{1}{2}\right)\left(\frac{2\sin^2\left(\frac{\pi}{M}\right)\bar{\gamma}_b}{m}\right)^{1/2}}{\sqrt{\pi}\Gamma(m+1)\left(1+\frac{2\sin^2\left(\frac{\pi}{M}\right)\bar{\gamma}_b}{m}\right)^{1/2}} \times_2 F_1\left(1, m+\frac{1}{2}; m+1; \frac{1}{1+\frac{2\sin^2\left(\frac{\pi}{M}\right)\bar{\gamma}_b}{m}}\right) \tag{3.17}$$

where Gauss' hypergeometric function is defined as

$${}_2F_1\left(1, b+\frac{1}{2}; b+1; z\right) = \sum_0^\infty \frac{\left(b+\frac{1}{2}\right)_k z^k}{b+1_{\,k}} \tag{3.18}$$

If we substitute equation (3.17) into equation (3.3), then the overall probability of bit error with HDD for a flat, slowly fading Nakagami channel with AWGN is obtained from equation (3.1).

The results shown in Figure 18 are for different numbers of memory elements and a flat, slowly fading Nakagami channel with *m*=1/2.

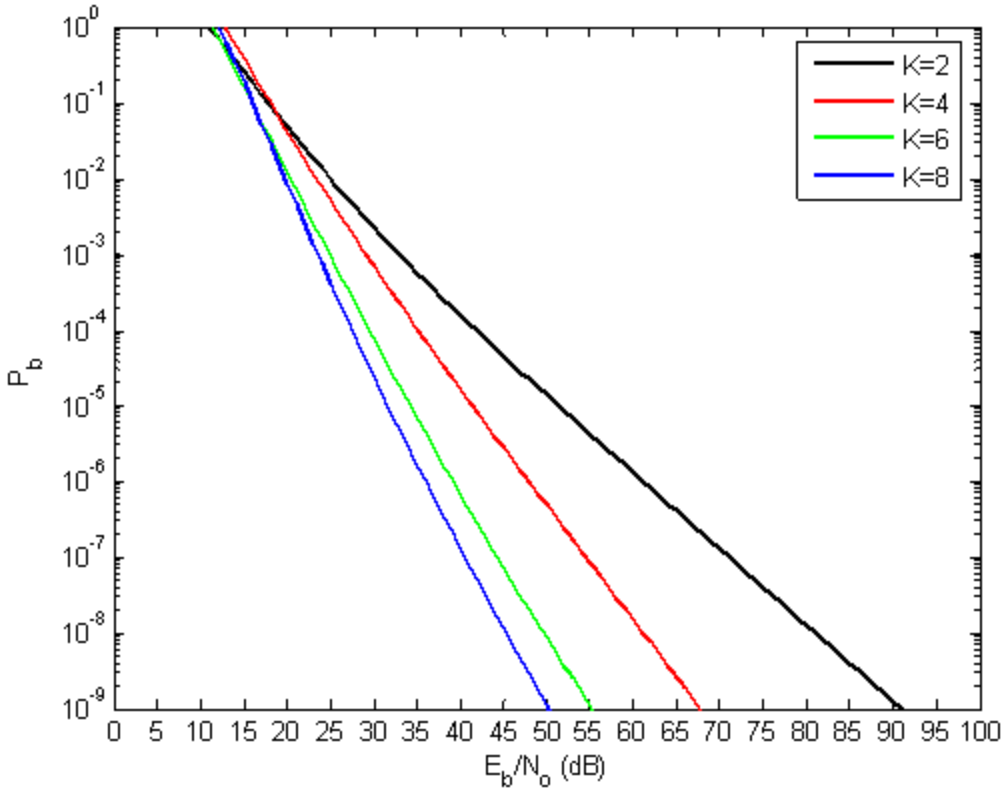

Figure 18. Performance of 8-PSK and r=2/3 convolutionally encoded bits with HDD for different numbers of memory elements and a flat, slowly fading Nakagami channel with m=1/2 in AWGN.

From Figure 18 we see that the effect of Nakagami fading is reduced as the number of memory elements increases. From Figure 19, in order to achieve $P_b=10^{-5}$ when m=1/2, E_b/N_o=31.63 dB is required for K=8 and E_b/N_o=51.47 dB for K=2. The relative E_b/N_o difference that results from increasing K from two to eight is 19.8 dB for m=1/2, which is the worst type of fading. For m=1/2 and K=2, E_b/N_o=51.47 dB is required.

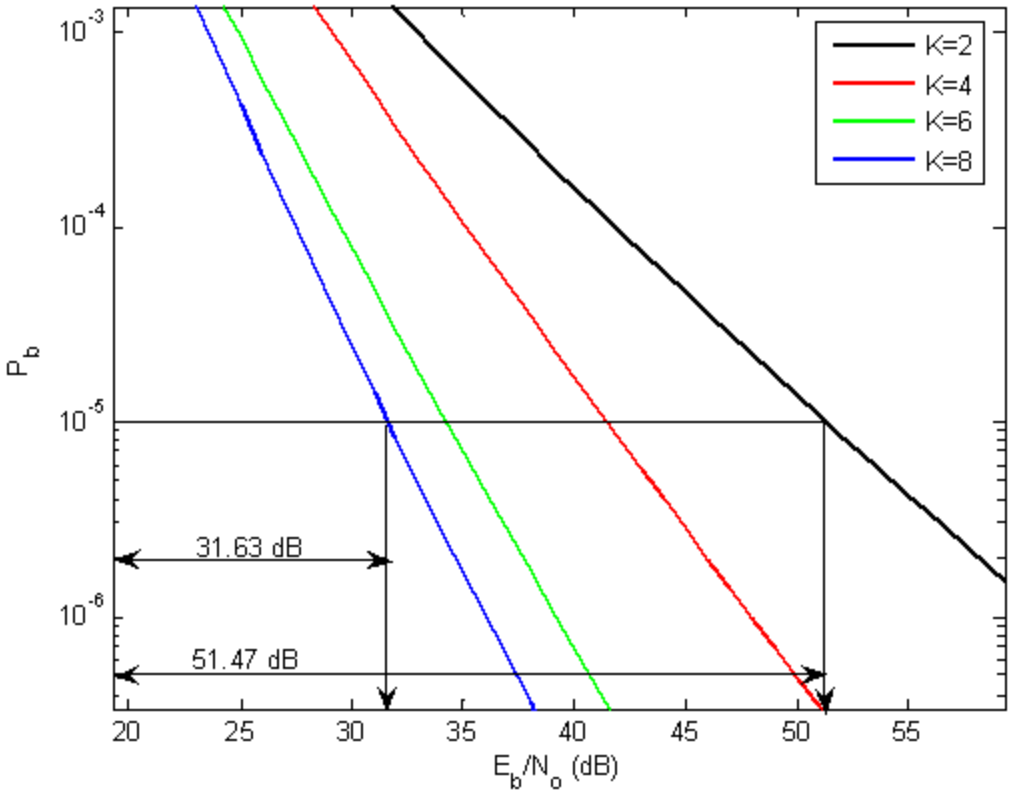

Figure 19. Magnified performance of 8-PSK and r=2/3 convolutionally encoded bits with HDD for different numbers of memory elements and a flat, slowly fading Nakagami channel with m=1/2 in AWGN.

Figure 19 is a magnified version of Figure 18, where it is clear that performance is strongly affected by Nakagami fading channels when K is small and m=1/2.

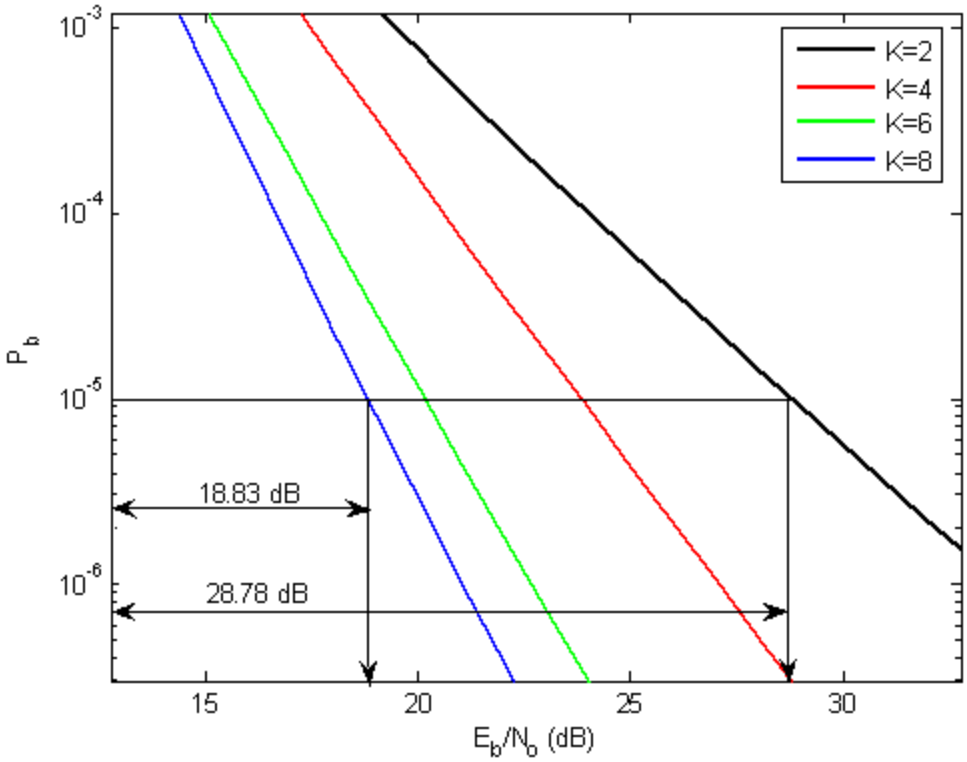

Figure 20. Magnified performance of 8-PSK and r=2/3 convolutionally encoded bits with HDD for different numbers of memory elements and a flat, slowly fading Nakagami channel with m=1 in AWGN.

Results shown in Figure 20 are for m=1. From Figure 20 we see that again the effect of Nakagami fading is reduced as the number of memory elements increases. From Figure 20, in order to achieve $P_b=10^{-5}$ when m=1, E_b/N_o=18.83 dB is required for K=8 and E_b/N_o=28.78 dB for K=2. The relative E_b/N_o difference that results from increasing K from two to eight is 9.95 dB for a fading Nakagami figure m=1. If we compare the coding gain for m=1 (9.95 dB) with that for m=1/2 (19.8 dB), we see that the increase in m results in improved performance. Another point is the reduction of the E_b/N_o required, where for K=2 and m=1 we have E_b/N_o=28.78 dB as compared to E_b/N_o=51.47 dB for K=2 and m=1/2.

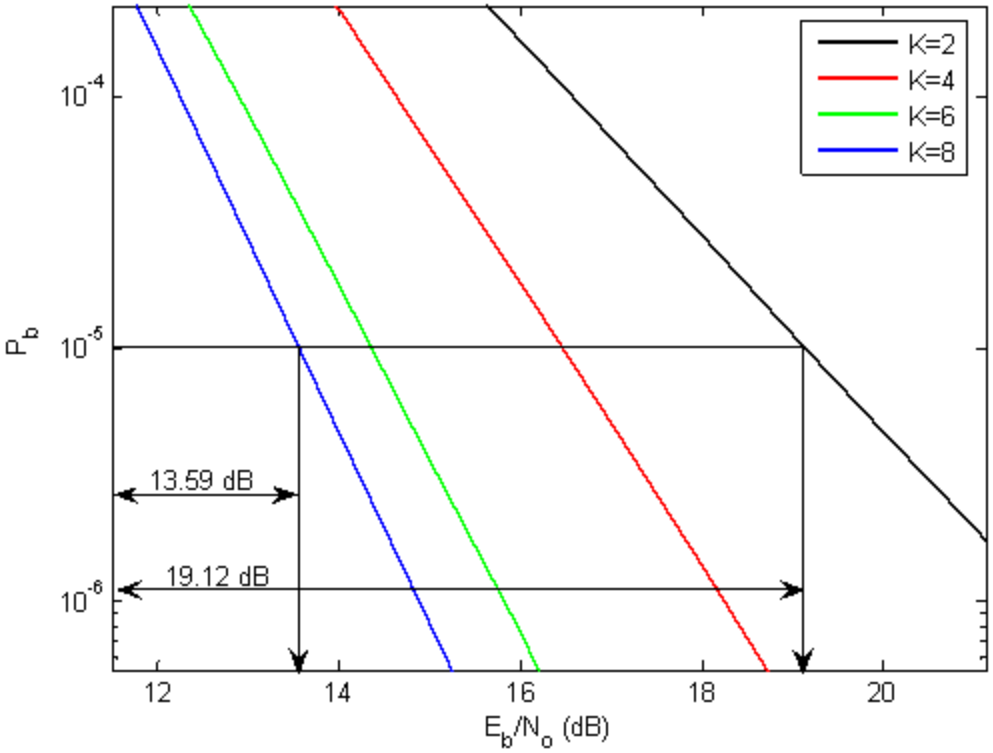

Figure 21. Magnified performance of 8-PSK and r=2/3 convolutionally encoded bits with HDD for different numbers of memory elements and a flat, slowly fading Nakagami channel with m=2 in AWGN.

Results shown in Figure 21 are for m=2. From Figure 21 we see that the effect of Nakagami fading is reduced as the number of memory element increases. From Figure 21, in order to achieve $P_b=10^{-5}$ when m=2, E_b/N_o=13.59 dB is required for K=8 and E_b/N_o=19.12 dB for K=2. The relative E_b/N_o difference that results from increasing K from two to eight is 5.53 dB for m=2. For m=2 and K=2, E_b/N_o=19.12 dB is required.

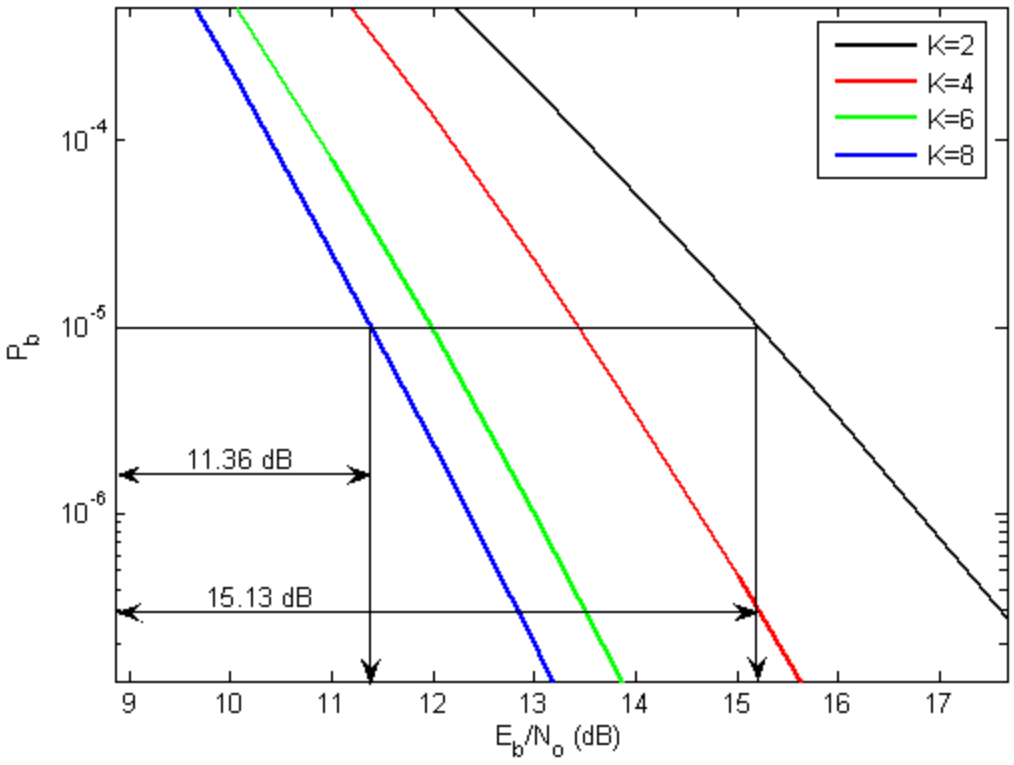

Figure 22. Magnified performance of 8-PSK and r=2/3 convolutionally encoded bits with HDD for different numbers of memory elements and a flat, slowly fading Nakagami channel with m=4 in AWGN.

Results shown in Figure 22 are for m=4. From Figure 22, in order to achieve $P_b=10^{-5}$ when m=4, E_b/N_o=11.36 dB is required for K=8 and E_b/N_o=15.13 dB for K=2. The relative E_b/N_o difference that results from increasing K from two to eight is 3.77 dB for m=4. For m=4 and K=2, E_b/N_o=15.13 dB is required.

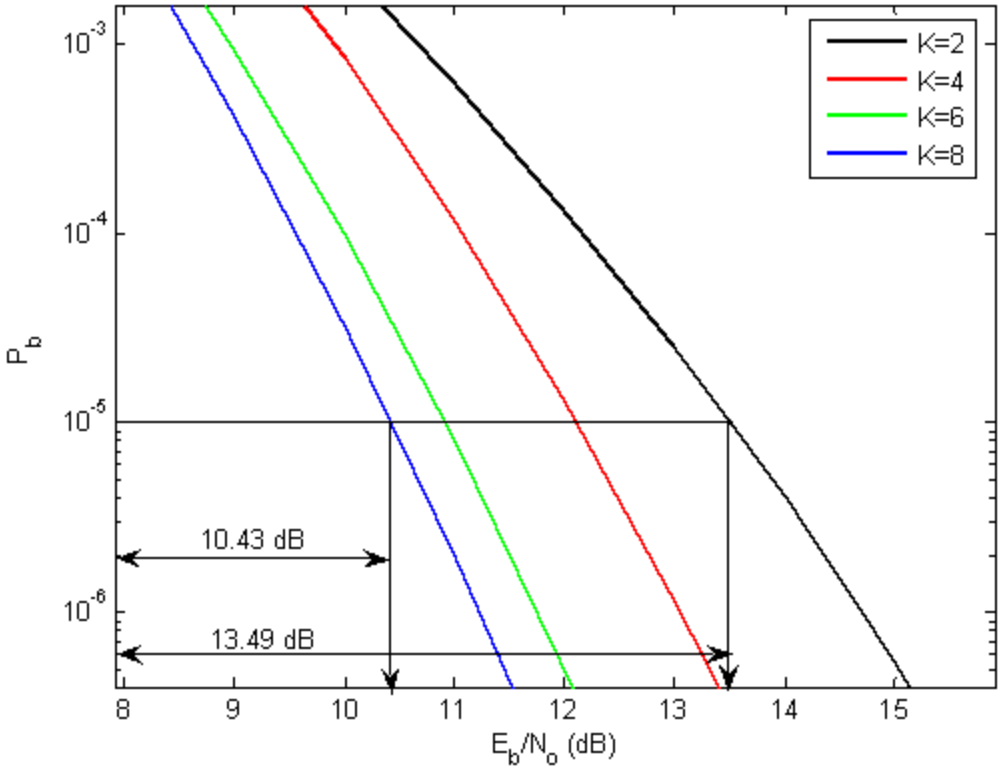

Figure 23. Magnified performance of 8-PSK and r=2/3 convolutionally encoded bits with HDD for different numbers of memory elements and a flat, slowly fading Nakagami channel with m=8 in AWGN.

Results shown in Figure 23 are for m=8. From Figure 23, in order to achieve $P_b=10^{-5}$ when m=8, E_b/N_o=10.43 dB is required for K=8 and E_b/N_o=13.49 dB for K=2. The relative E_b/N_o difference that results from increasing K from two to eight is 3.06 dB for m=8. For m=8 and K=2, E_b/N_o=13.49 dB is required.

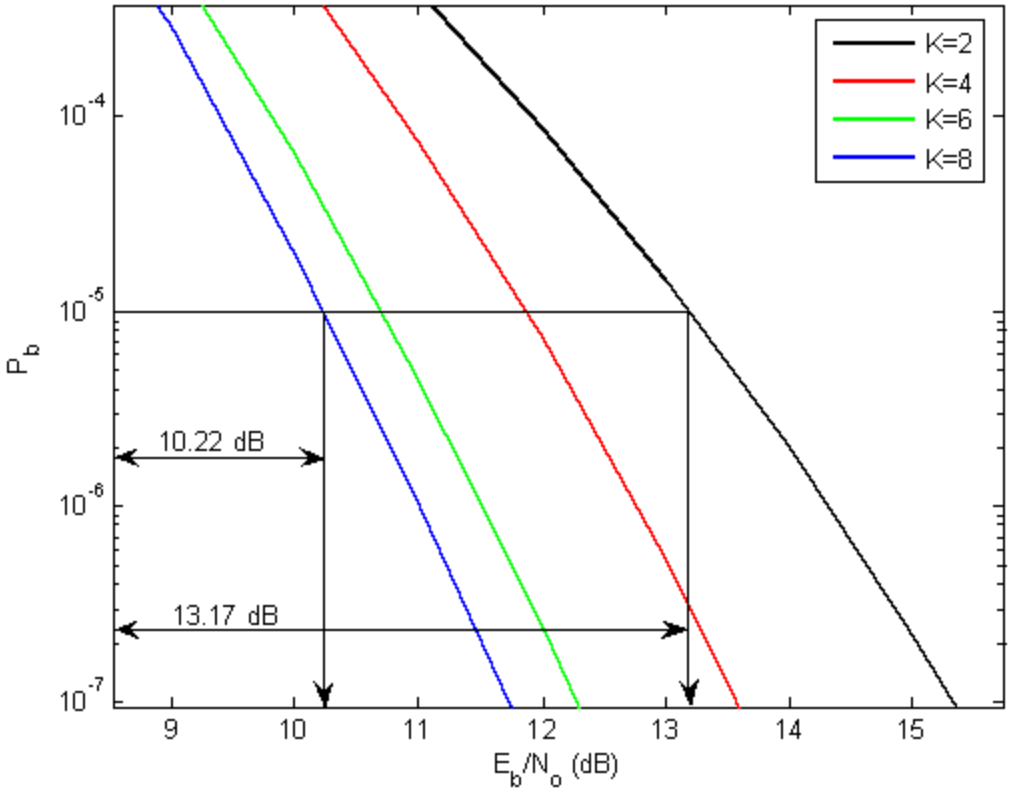

Figure 24. Magnified performance of 8-PSK and r=2/3 convolutionally encoded bits with HDD for different numbers of memory elements and a flat, slowly fading Nakagami channel with m=10 in AWGN.

Finally, the results shown in Figure 24 are for m=10. From Figure 24, in order to achieve $P_b=10^{-5}$ when m=10, E_b/N_o=10.22 dB is required for K=8 and E_b/N_o=13.17 dB for K=2. The relative E_b/N_o difference that results from increasing K from two to eight is 2.95 dB for m=10. For m=10 and K=2, E_b/N_o=13.17 dB is required.

We can increase the Nakagami fading figure m until we reach the no fading boundary where there is no channel fading. Figure 25 shows that when $m>>1$, the performance approaches that obtained with no fading. For K=6, plotted in Figure 25, degradation due to Nakagami fading approaches 24.1 dB, which shows how severe the influence of the Nakagami fading channel is.

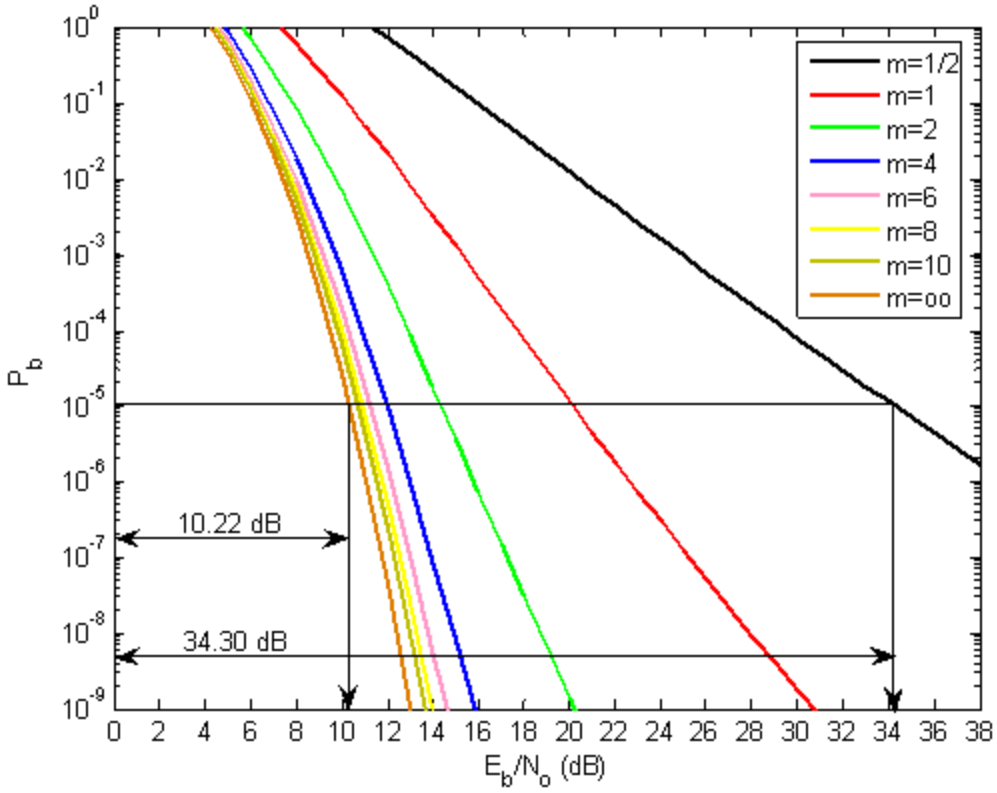

Figure 25. Performance of 8-PSK and r=2/3 convolutionally encoded bits with HDD for K=6 memory elements and a flat, slowly fading Nakagami channel with different m in AWGN.

Table 4 is a summary of the effect of the Nakagami fading channel.

Table 4. Performance results of 8-PSK and r=2/3 convolutional encoding with HDD for a flat, slowly fading Nakagami channel with different m in AWGN.

m	Absolute E_b/N_o for $P_b=10^{-5}$ when K=8	Absolute E_b/N_o for $P_b=10^{-5}$ when K=2	Relative degradation for $P_b=10^{-5}$
1/2	31.63 dB	51.47 dB	19.84 dB
1	18.83 dB	28.78 dB	9.95 dB
2	13.59 dB	19.12 dB	5.53 dB
4	11.36 dB	15.13 dB	3.77 dB
8	10.43 dB	13.49 dB	3.06 dB
10	10.22 dB	13.17 dB	2.95 dB

From Table 4, we see that the effect of the Nakagami fading channel decreases as fading figure m increases. The relative degradation for severe fading (m=1/2) is 19.84 dB, while for minimal fading (m=10), it is 2.95 dB. As can be seen, degradation is 16.89 dB less as m increases from 1/2 to ten. Another interesting result is that E_b/N_o required to reach $P_b=10^{-5}$ decreases significantly for K=2 as m increases. For m=1/2, E_b/N_o=51.47 dB is required to reach $P_b=10^{-5}$, while for m=10 and the same P_b, E_b/N_o=13.17 dB is required. This is a difference of 38.3 dB. Much better results are obtained relative to K=2 for K=8, especially when m is small. Now the difference in E_b/N_o between m=1/2 and m=10 is 21.41 dB, which is much smaller than for K=2 (38.3 dB). The Nakagami fading channel has the least effect when K=8 as compared to K=2.

4. Probability Bit Error with Hard Decision Decoding for Flat, Slowly Fading Nakagami Channels with both AWGN and PNI

When the channel is modeled as a Nakagami fading channel, then equation (3.8) is a conditional probability, and the unconditional probability of channel bit error is obtained from

$$p = \int_0^\infty \frac{2}{3}\left(\rho Q\left[\sqrt{6r\gamma_I \sin^2\left(\frac{\pi}{M}\right)}\right] f_{\Gamma_b}(\gamma_I) + (1-\rho) Q\left[\sqrt{6r\gamma_b \sin^2\left(\frac{\pi}{M}\right)}\right] f_{\Gamma_b}(\gamma_b)\right) d\gamma_b \qquad (3.19)$$

where

$$\gamma_I = \frac{E_b}{N_o + \frac{N_I}{\rho}} = \frac{a_c{}^2 T_b}{N_o + \frac{N_I}{\rho}} \qquad (3.20)$$

Evaluating equation (3.19) with the help of Gauss' hypergeometric function, which is defined in equation (3.18), we get

$$p = \frac{1}{3}\rho \frac{\Gamma\left(m+\frac{1}{2}\right)\left(\frac{2\sin^2\left(\frac{\pi}{M}\right)\left(\frac{\bar{E}_b}{N_o+\frac{N_I}{\rho}}\right)}{m}\right)^{1/2}}{\sqrt{\pi}\Gamma(m+1)\left(1+\frac{2\sin^2\left(\frac{\pi}{M}\right)\left(\frac{\bar{E}_b}{N_o+\frac{N_I}{\rho}}\right)}{m}\right)^{1/2}} \times_2 F_1\left(1, m+\frac{1}{2}; m+1; \frac{1}{1+\frac{2\sin^2\left(\frac{\pi}{M}\right)}{m}\left(\frac{\bar{E}_b}{N_o+\frac{N_I}{\rho}}\right)}\right) +$$

$$\frac{1}{3}(1-\rho) \frac{\Gamma\left(m+\frac{1}{2}\right)\left(\frac{2\sin^2\left(\frac{\pi}{M}\right)\left(\left(\frac{\bar{E}_b}{N_o}\right)\right)}{m}\right)^{1/2}}{\sqrt{\pi}\Gamma(m+1)\left(1+\frac{2\sin^2\left(\frac{\pi}{M}\right)\left(\frac{\bar{E}_b}{N_o}\right)}{m}\right)^{1/2}} \times_2 F_1\left(1, m+\frac{1}{2}; m+1; \frac{1}{1+\frac{2\sin^2\left(\frac{\pi}{M}\right)}{m}\left(\frac{\bar{E}_b}{N_o}\right)}\right) \qquad (3.21)$$

The results shown in Figure 26 represent the performance of the 8-PSK system with K=2, r=2/3 convolutional encoding for m=1/2 in both AWGN and PNI. All plots are obtained for E_b/N_o=81.14 dB, which results in $P_b=10^{-8}$ when $E_b/N_I>>1$.

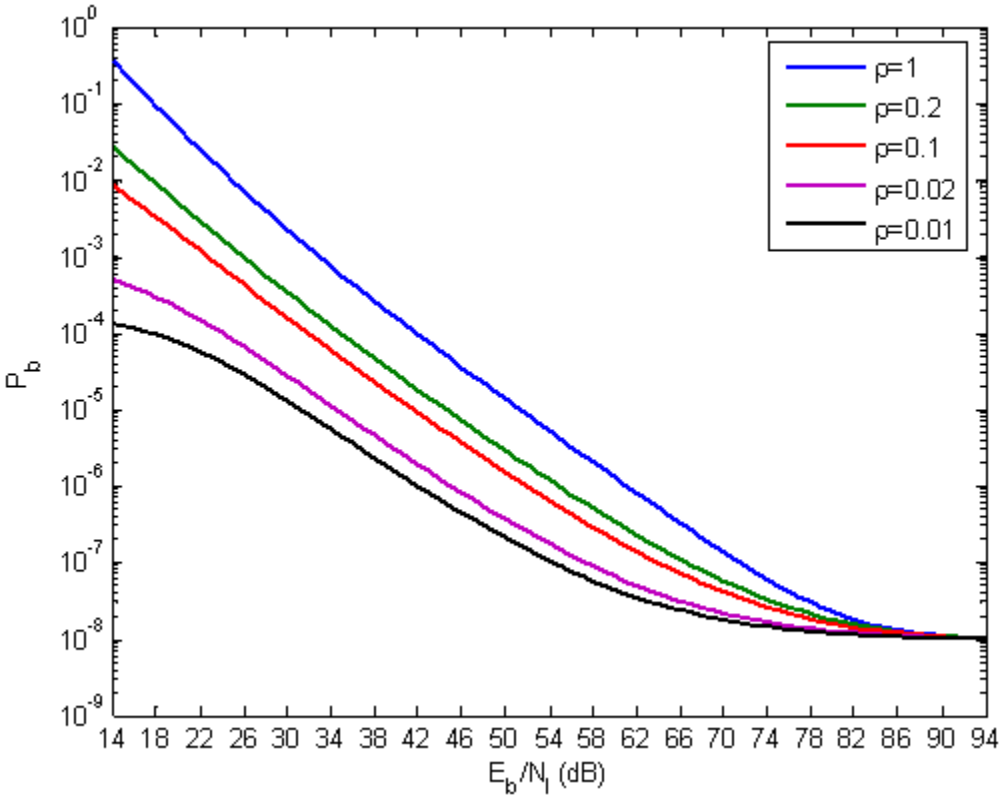

Figure 26. Performance of 8-PSK with K=2, r=2/3 convolutionally encoded bits with HDD for different ρ and a flat, slowly fading Nakagami channel with m=1/2 in both AWGN and PNI.

From Figure 26 we see that when m=1/2, PNI does not degrade performance. This is the opposite of what was found for no channel fading. We see that, regardless of the value of ρ, P_b converges to $P_b=10^{-8}$ as E_b/N_I increases since in that case the interfering signal approaches AWGN.

Figure 27 is a magnified version of Figure 26. For $P_b=10^{-5}$, we need 51.43 dB E_b/N_I for the case of BNI, while 31.29 dB E_b/N_I is required for PNI with ρ=0.01. The relative degradation in E_b/N_I between BNI and PNI for the worst case ρ is zero for K=2, m=1/2, and E_b/N_o=81.14 dB.

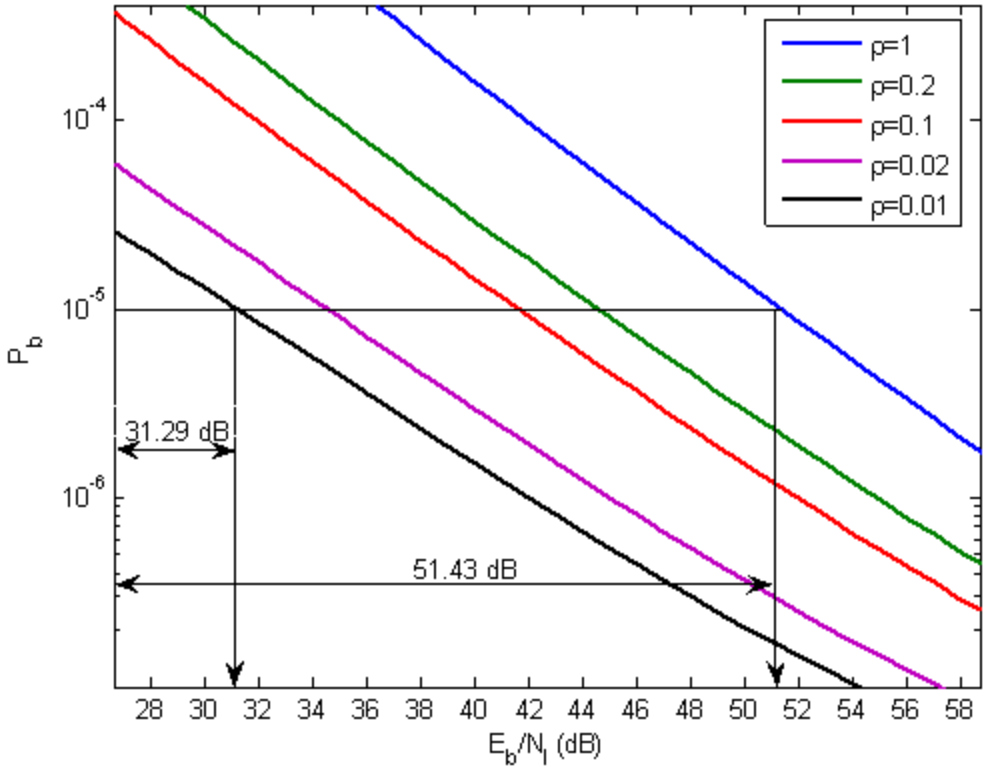

Figure 27. Magnified performance of 8-PSK with K=2, r=2/3 convolutionally encoded bits with HDD for different ρ and a flat, slowly fading Nakagami channel with *m=1/2* in both AWGN and PNI.

For severe Nakagami fading conditions, $1/2 \leq m \leq 1$, PNI is beneficial, and the decrease in E_b/N_I is almost 20.2 dB.

From Figure 28 we see that when m=1, PNI does not degrade performance. For severe Nakagami fading conditions, BNI is slightly more effective than PNI with ρ=0.01 .

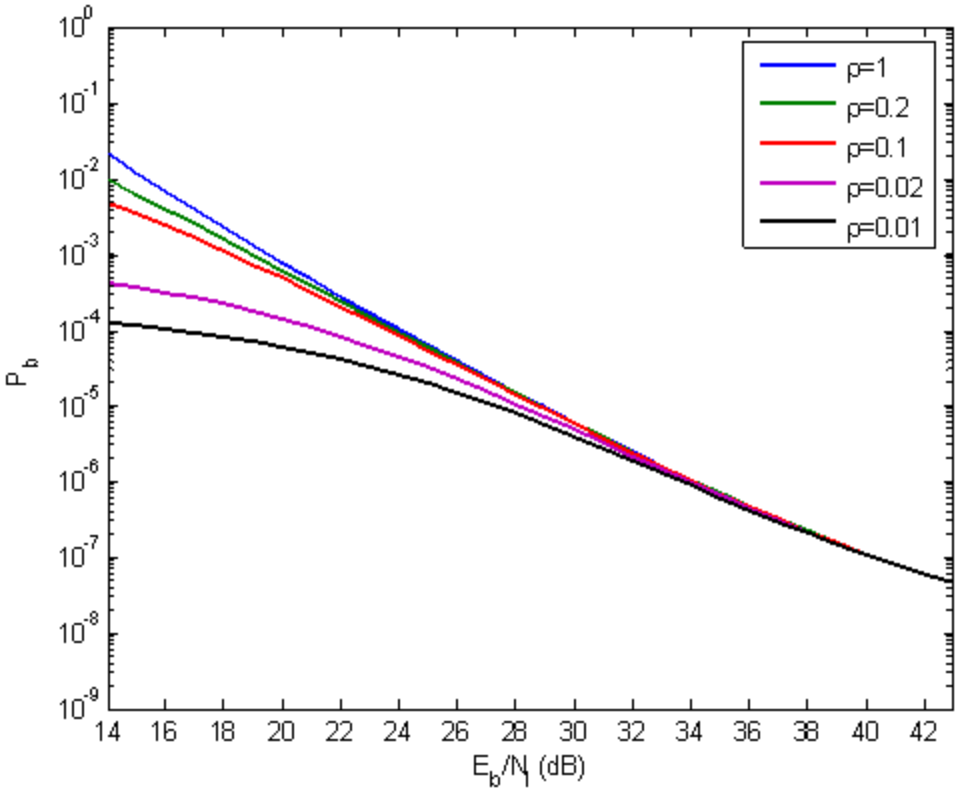

Figure 28. Performance of 8-PSK with K=2, r=2/3 convolutionally encoded bits with HDD for different ρ and a flat, slowly fading Nakagami channel with m=1 in both AWGN and PNI.

From Figure 28 we see that when m=1 (Rayleigh Fading), PNI with ρ=0.01 has almost the same performance as BNI. For m=1/2, the decrease in E_b/N_I is 20.2 dB, but for m=1, the decrease in E_b/N_I is only about 1.6 dB. We can conclude that for Rayleigh fading, PNI and BNI have almost the same effect.

Figure 29 is a magnified version of Figure 28. For $P_b=10^{-5}$, we need E_b/N_I =28.86 dB for BNI, while E_b/N_I=27.28 dB is required for PNI with ρ=0.01. The relative degradation in E_b/N_I between BNI and PNI for the worst case ρ is zero for K=2, m=1, and E_b/N_o=43.58 dB.

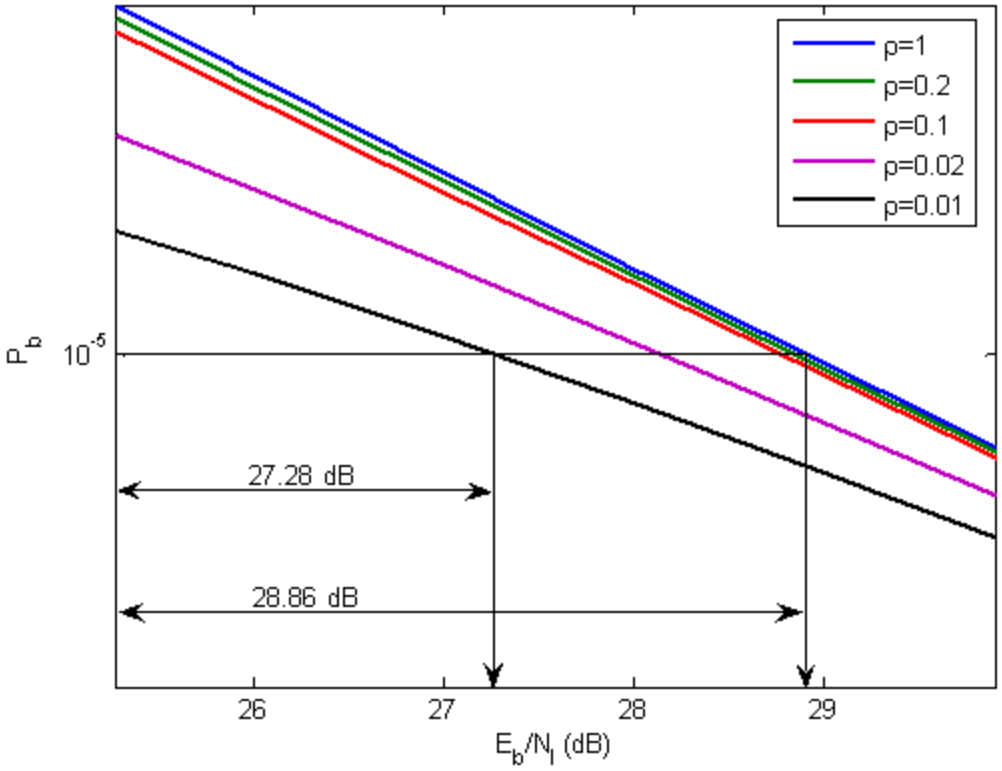

Figure 29. Magnified performance of 8-PSK with K=2, r=2/3 convolutionally encoded bits with HDD for different ρ and a flat, slowly fading Nakagami channel with m=1 in both AWGN and PNI.

Figure 30 shows the performance for m=2. In this situation we have less severe Nakagami fading conditions since m>1. For $P_b=10^{-5}$, we need E_b/N_I=20 dB for BNI, while E_b/N_I=25.69 dB is required for PNI with ρ=0.01 .The relative degradation in E_b/N_I between BNI and PNI for the worst case ρ is 5.69 dB for K=2, m=2, and E_b/N_o=26.77 dB.

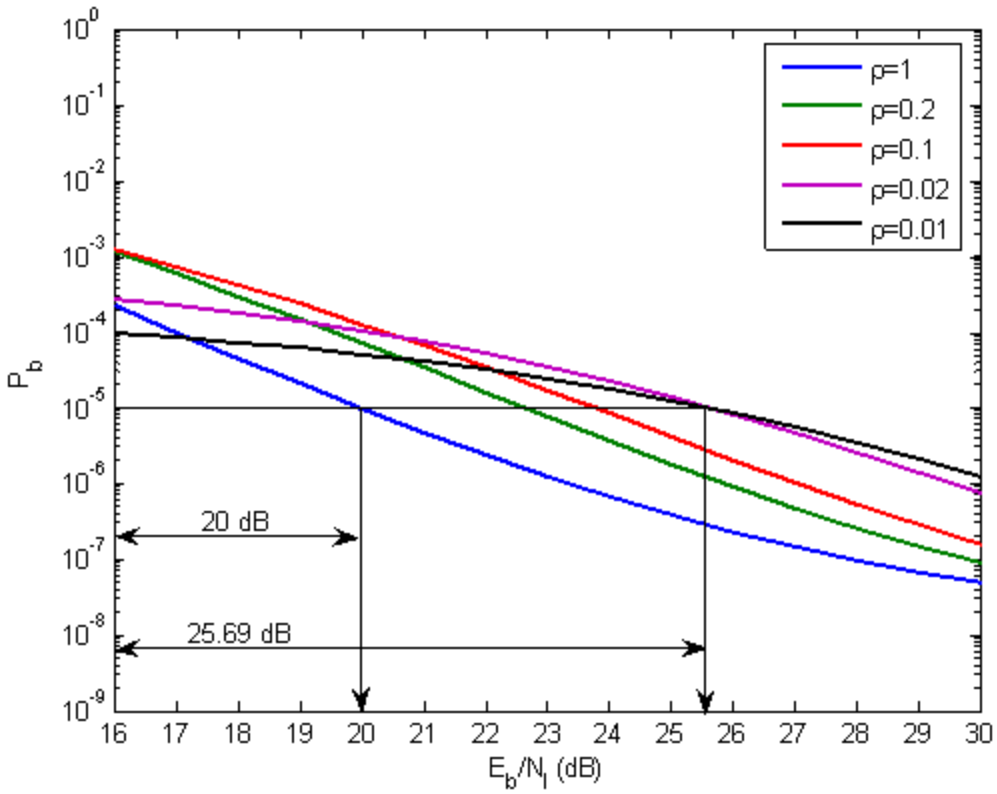

Figure 30. Magnified performance of 8-PSK with K=2, r=2/3 convolutionally encoded bits with HDD for different ρ and a flat, slowly fading Nakagami channel with m=2 in both AWGN and PNI.

Figure 31 shows the performance for m=4. For P_b=10^{-5}, we need E_b/N_I=17.1 dB for BNI, while E_b/N_I=25 dB is required for PNI with ρ=0.01. The relative degradation in E_b/N_I between BNI and PNI for the worst case ρ is 7.9 dB for K=2, m=4, and E_b/N_o=19.71 dB.

A valuable point is that with the increase of the fading figure m when m>1, degradation due to PNI increases. For m=2 the degradation in E_b/N_I is 5.69 dB, while for m=4 the degradation in E_b/N_I is 7.9 dB. The absolute performance in terms of both E_b/N_o and E_b/N_I improves for m>1.

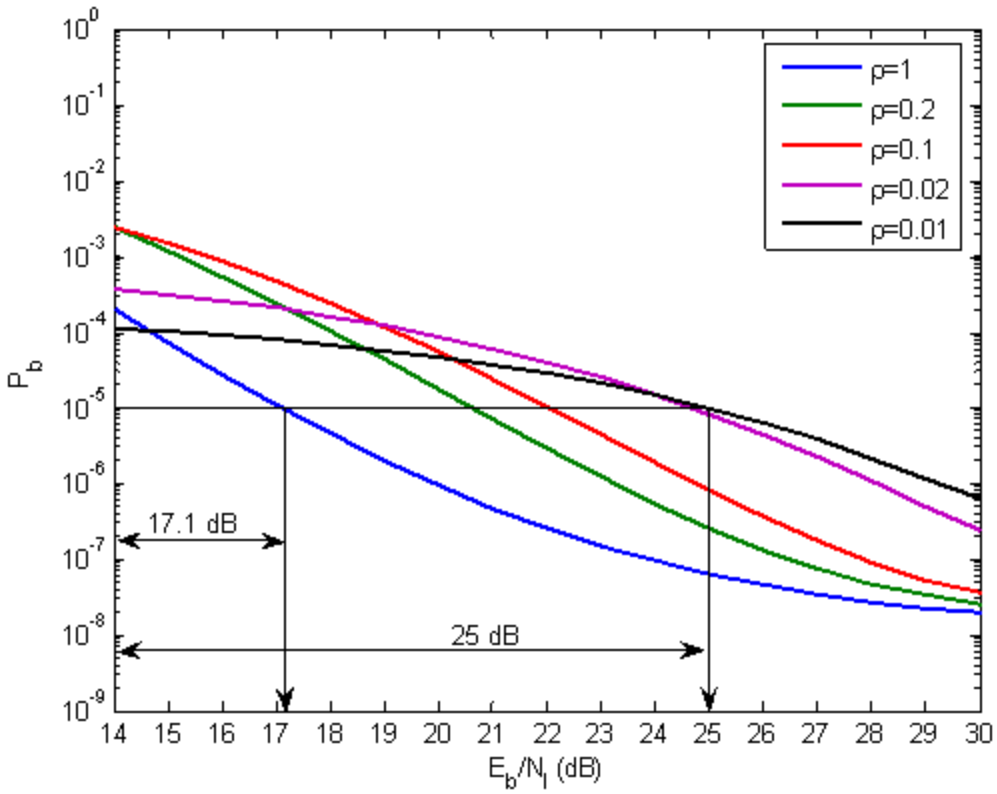

Figure 31. Magnified performance of 8-PSK with K=2, r=2/3 convolutionally encoded bits with HDD for different ρ and a flat, slowly fading Nakagami channel with m=4 in both AWGN and PNI.

Figure 32 shows the performance for m=10. For $P_b=10^{-5}$, we need E_b/N_I=16.24 dB for BNI, while E_b/N_I=24.74 dB is required for PNI with ρ=0.01. The relative degradation in E_b/N_I between BNI and PNI for the worst case ρ is 8.5 dB for K=2, m=10, and E_b/N_o=16.21 dB. The trends previously noted when m>1 continue to be exhibited as m increases.

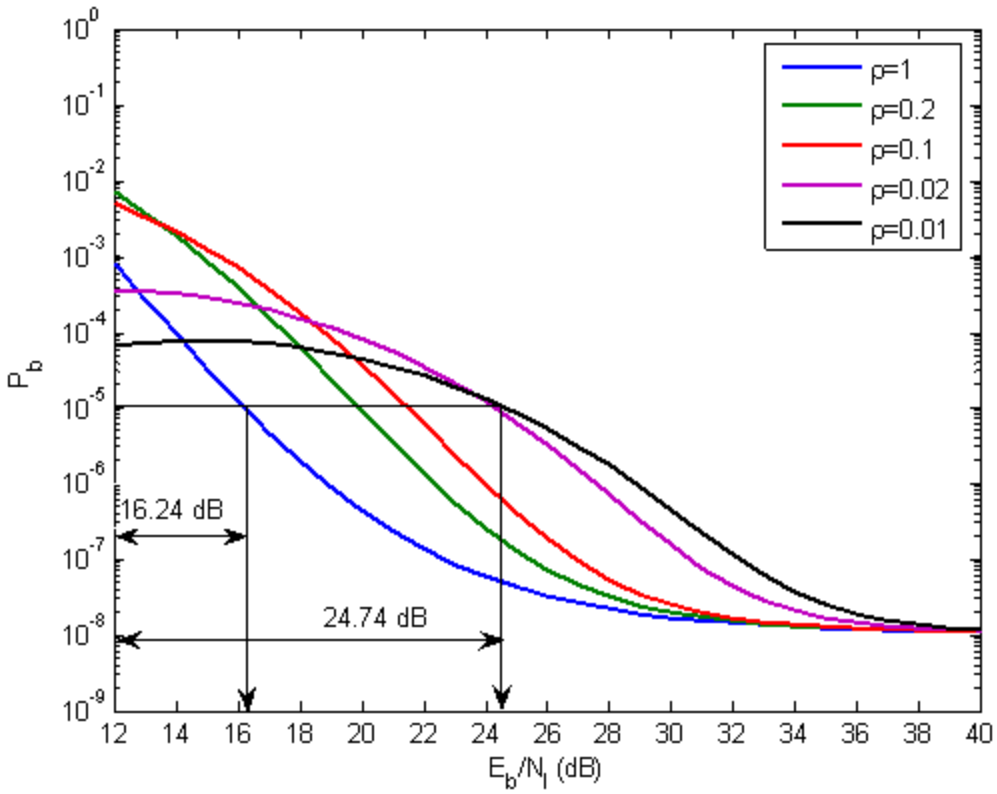

Figure 32. Performance of 8-PSK with K=2, r=2/3 convolutionally encoded bits with HDD for different ρ and a flat, slowly fading Nakagami channel with m=10 in both AWGN and PNI.

Table 5. Performance for 8-PSK with K=2, r=2/3 convolutional encoding and HDD for a flat, slowly fading Nakagami channel in both AWGN and PNI.

m	Required E_b/N_o for $P_b=10^{-8}$	E_b/N_I degradation for $P_b=10^{-5}$	Required E_b/N_I for $P_b=10^{-5}$ for worst case ρ
1/2	81.14 dB	0.0 dB	51.43 dB
1	43.58 dB	0.0 dB	28.86 dB
2	26.77 dB	5.69 dB	25.69 dB
4	19.71 dB	7.9 dB	25 dB
10	16.21 dB	8.5 dB	24.74 dB

Table 5 is a list of the results for 8-PSK with K=2, r=2/3 convolutional encoding and HDD for a flat, slowly fading Nakagami channel. As m increases, performance improves. For K=2, the change in the required E_b/N_o as m changes from 1/2 to 10 is 64.93 dB. Another point is that PNI only degrades the performance when m>1. For 1/2≤ m ≤1, PNI does not degrade performance but actually improves it. For K=2 the maximum increase in the degradation of E_b/N_I is 8.5 dB. Another interesting point is that for m>2, the effect of the Nakagami fading channel does not significantly change the performance of the system with respect to PNI as m increases.

Figures 33-37 repeat the previous figures in this section, but K=8 instead of K=2 (the number of encoder memory elements is greater).

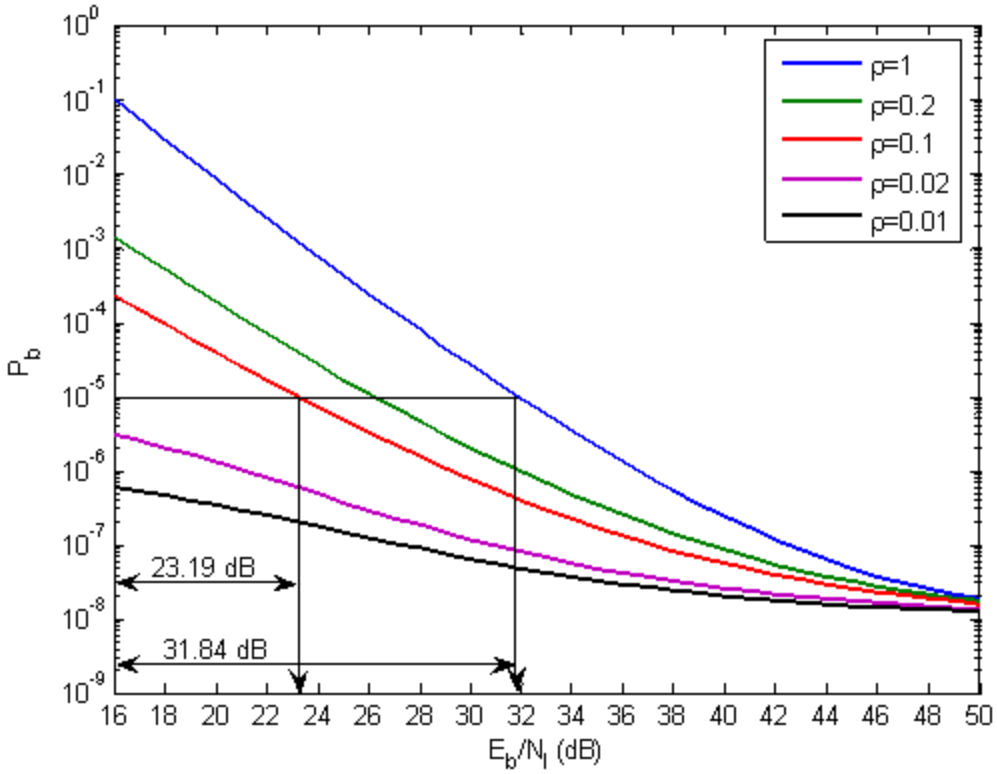

Figure 33. Magnified performance of 8-PSK with K=8, r=2/3 convolutionally encoded bits with HDD for different ρ and a flat, slowly fading Nakagami channel with m=1/2 in both AWGN and PNI when E_b/N_o=45.24 dB.

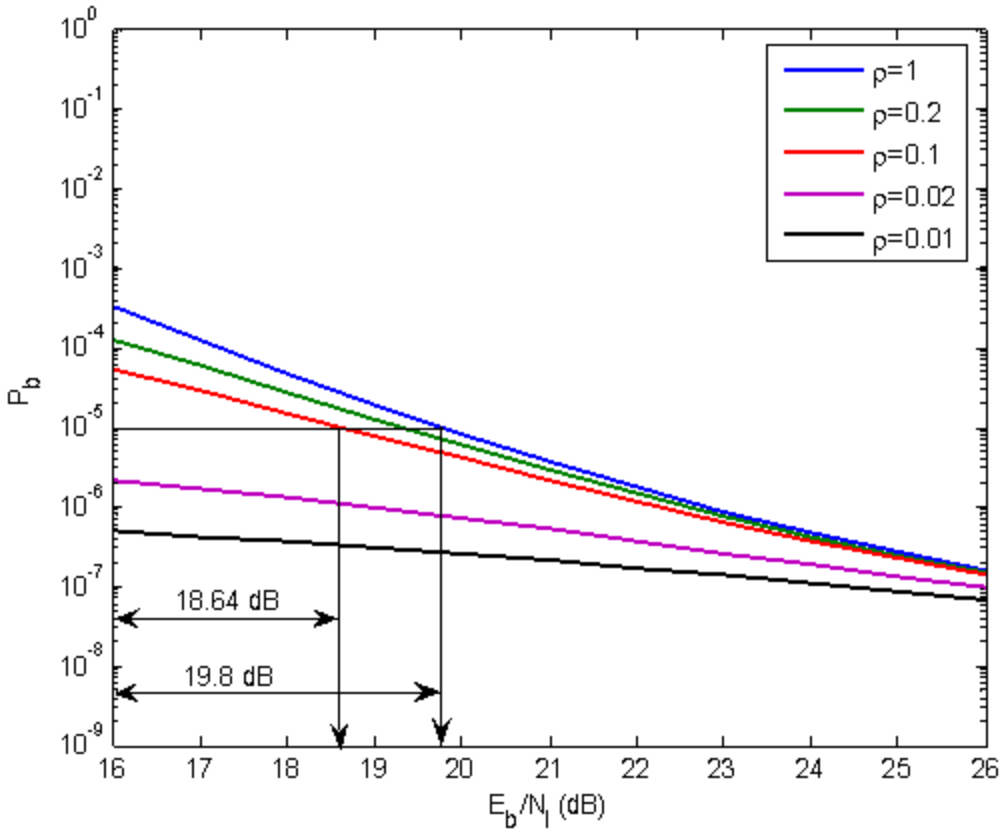

Figure 34. Magnified performance of 8-PSK with K=8, r=2/3 convolutionally encoded bits with HDD for different ρ and a flat, slowly fading Nakagami channel with m=1 in both AWGN and PNI when E_b/N_o=25.82 dB.

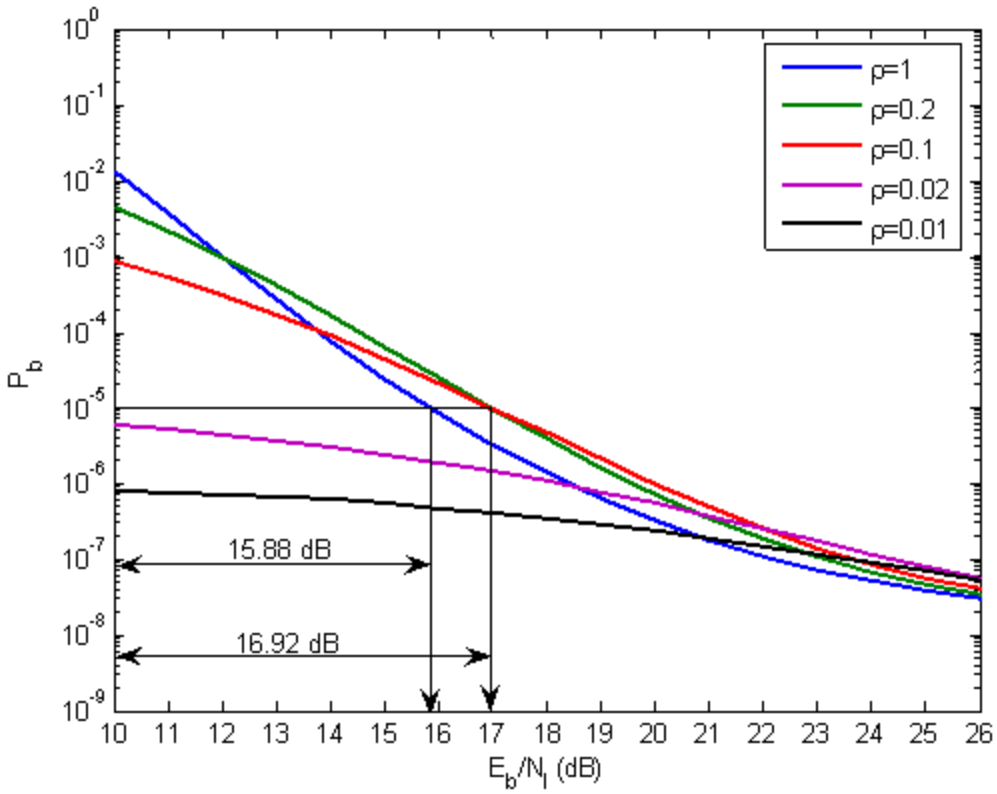

Figure 35. Magnified performance of 8-PSK with K=8, r=2/3 convolutionally encoded bits with HDD for different ρ and a flat, slowly fading Nakagami channel with m=2 in both AWGN and PNI when E_b/N_o=17.46 dB.

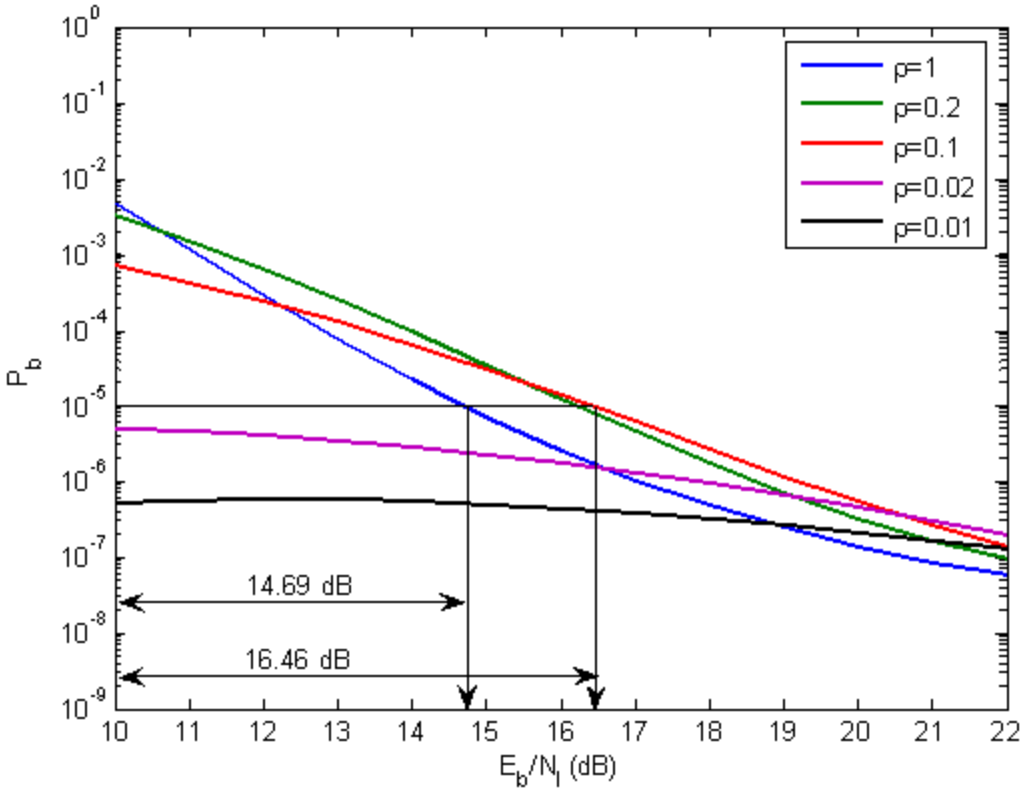

Figure 36. Magnified performance of 8-PSK with K=8, r=2/3 convolutionally encoded bits with HDD for different ρ and a flat, slowly fading Nakagami channel with m=4 in both AWGN and PNI when E_b/N_o=14.13 dB.

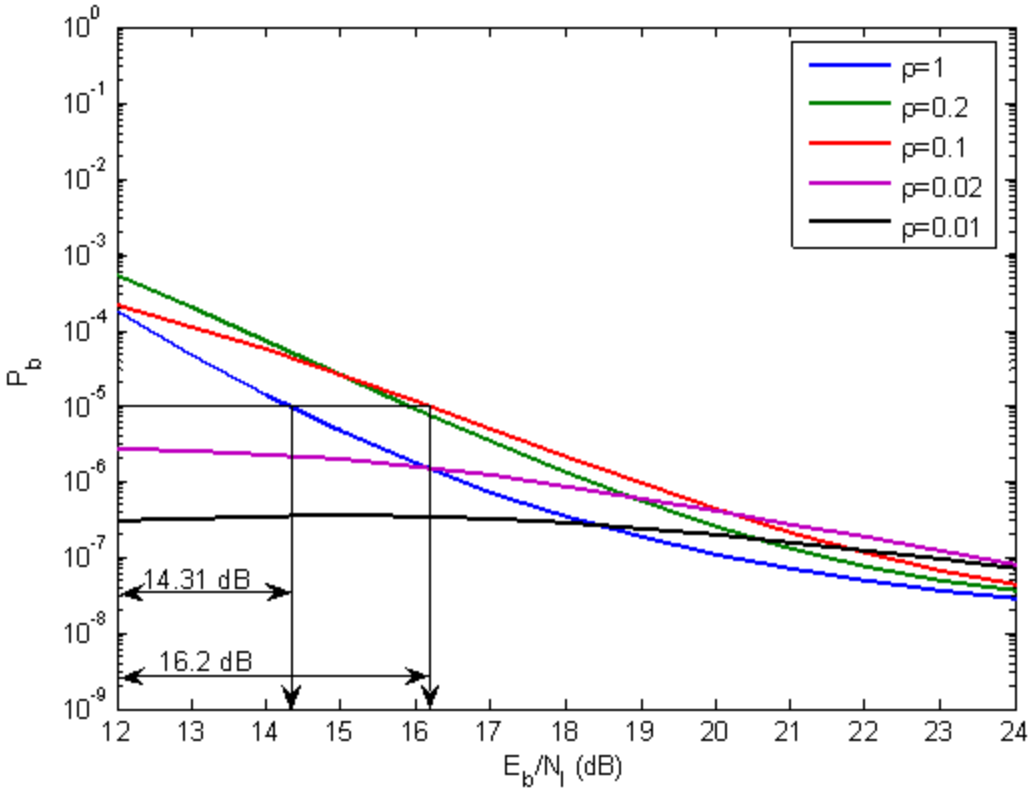

Figure 37. Magnified performance of 8-PSK with K=8, r=2/3 convolutionally encoded bits with HDD for different ρ and a flat, slowly fading Nakagami channel with m=10 in both AWGN and PNI when E_b/N_o=12.41 dB.

Table 6. Performance for 8-PSK with K=8, r=2/3 convolutional encoding and HDD for a flat, slowly fading Nakagami channel in both AWGN and PNI.

m	Required E_b/N_o for $P_b=10^{-8}$	E_b/N_I degradation for $P_b=10^{-5}$	Required E_b/N_I for $P_b=10^{-5}$ for worst case ρ
1/2	45.24 dB	0.0 dB	31.84 dB
1	25.82 dB	0.0 dB	19.8 dB
2	17.46 dB	1.04 dB	16.92 dB
4	14.13 dB	1.77 dB	16.46 dB
10	12.41 dB	1.89 dB	16.2 dB

Table 6 is a list of the performance results for 8-PSK with K=8, r=2/3 convolutional encoding and HDD for a flat, slowly fading Nakagami channel. As m increases, performance improves. For K=8, the change in the required E_b/N_o as m changes from 1/2 to 10 is 32.83 dB. Another point is that PNI only degrades the performance when m>1. For 1/2≤ m ≤1, PNI does not degrade performance but actually improves it. For K=8 the maximum increase in the degradation of E_b/N_I is 1.89 dB. Another interesting point is that for m>2, the effect of the Nakagami fading channel does not significantly change the performance of the system with respect to PNI as m increases.

Comparing Table 5 with Table 6, we see that when K=8, the system performance is significantly better, both in an absolute and a relative sense. This can be also seen in Figures 38-43, where performance is plotted for different m with K as a parameter in each figure. In these figures, only the effect of BNI is considered.

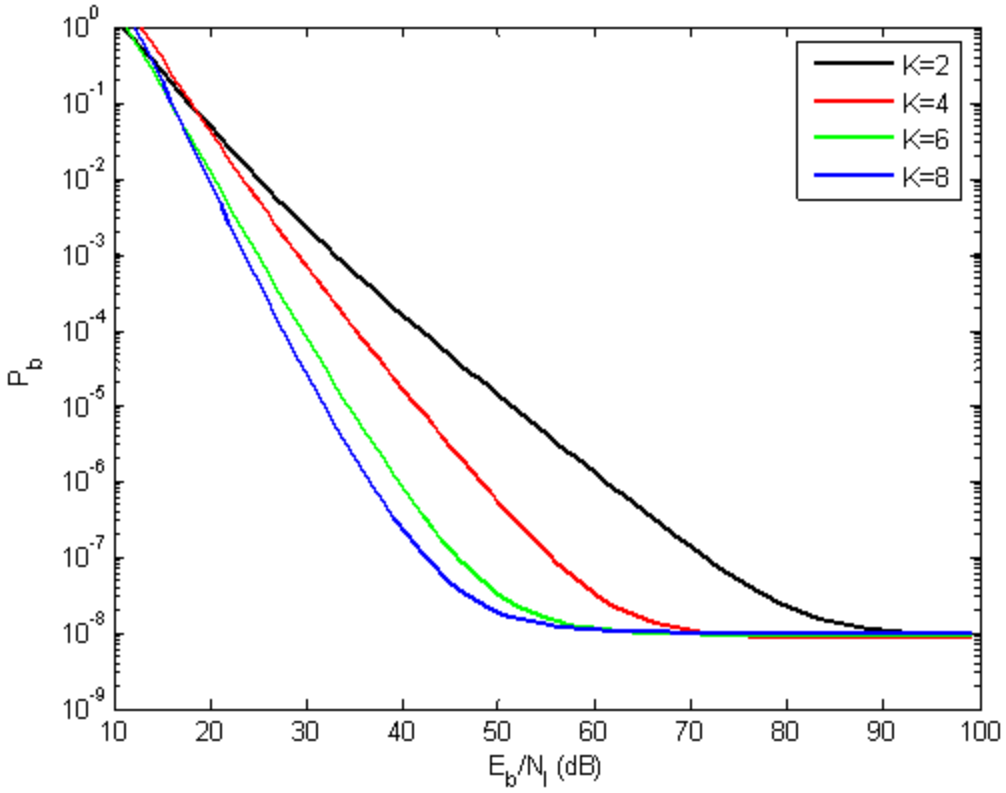

Figure 38. Performance of 8-PSK and r=2/3 convolutionally encoded bits with HDD for different numbers of memory elements and a flat, slowly fading Nakagami channel with m=1/2 in both AWGN and BNI.

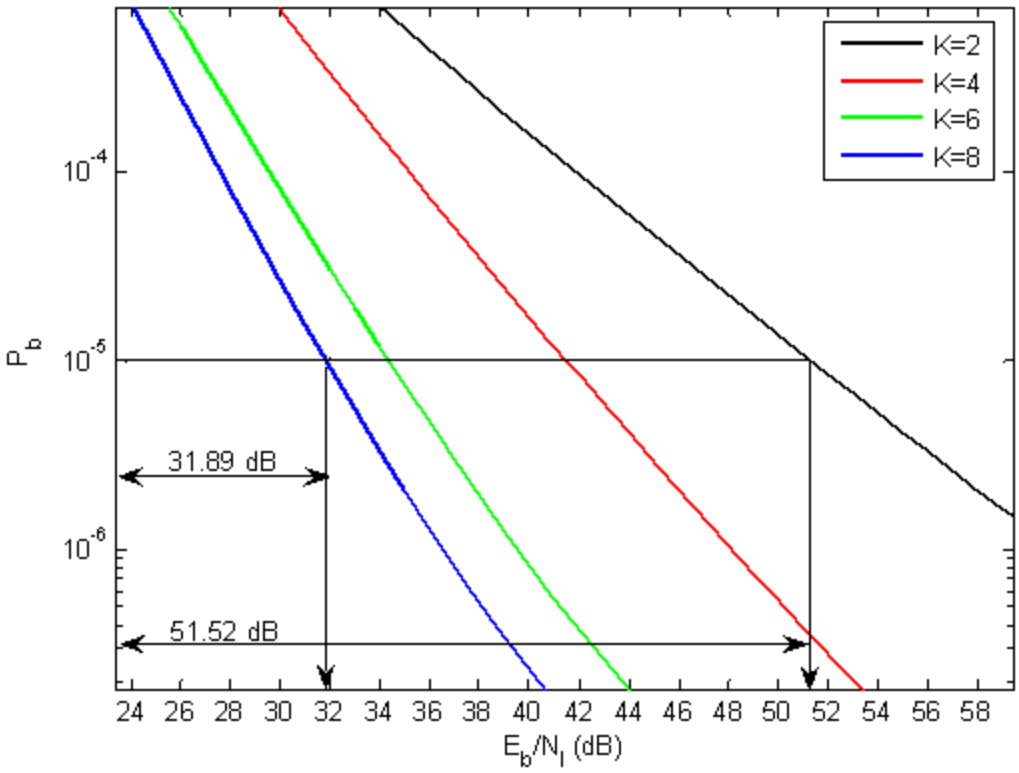

Figure 39. Magnified performance of 8-PSK and r=2/3 convolutionally encoded bits with HDD for different numbers of memory elements and a flat, slowly fading Nakagami channel with m=1/2 in both AWGN and BNI.

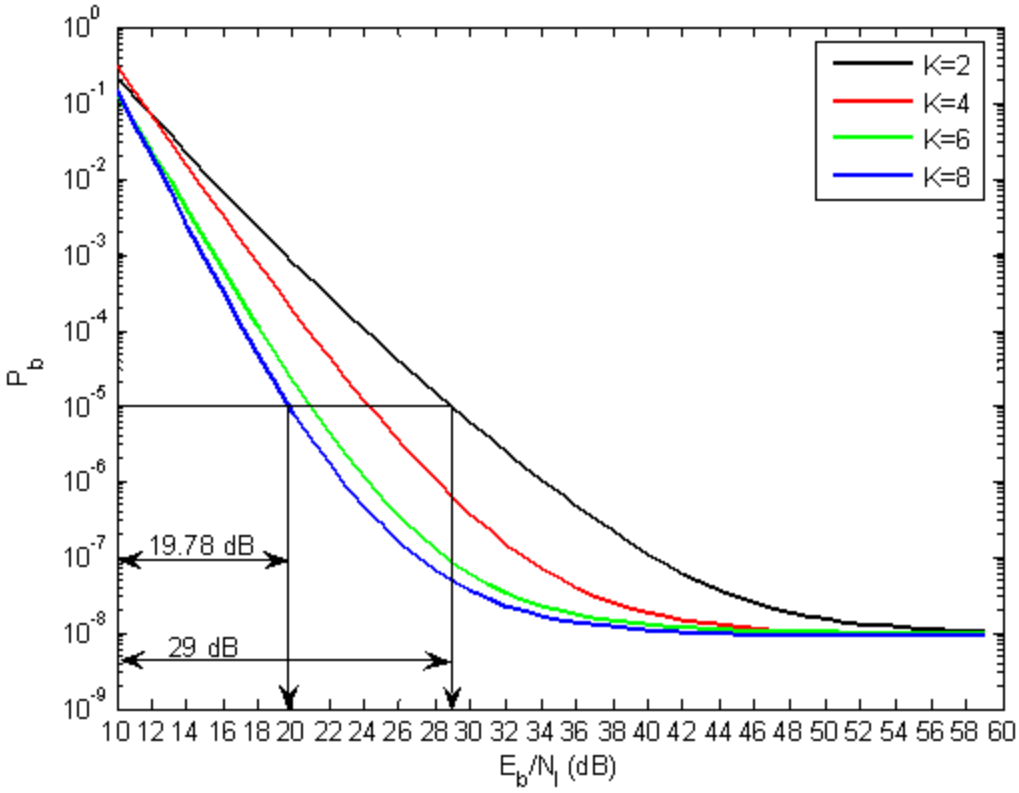

Figure 40. Magnified performance of 8-PSK and r=2/3 convolutionally encoded bits with HDD for different numbers of memory elements and a flat, slowly fading Nakagami channel with m=1 in both AWGN and BNI.

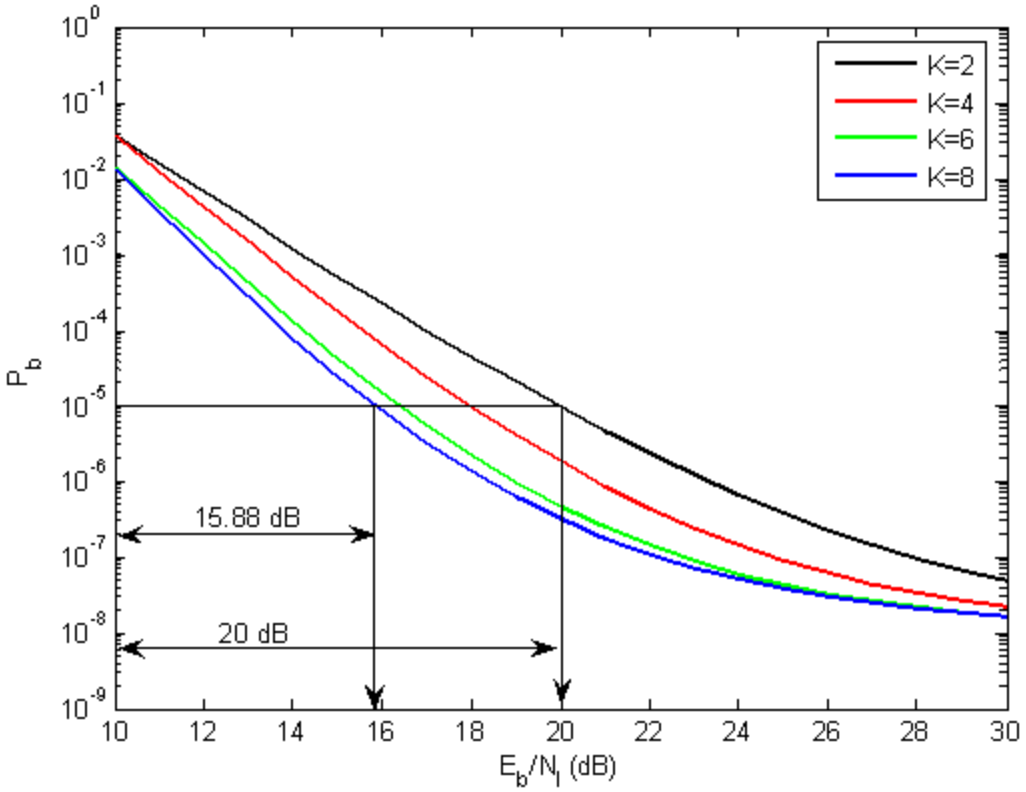

Figure 41. Magnified performance of 8-PSK and r=2/3 convolutionally encoded bits with HDD for different numbers of memory elements and a flat, slowly fading Nakagami channel with m=2 in both AWGN and BNI.

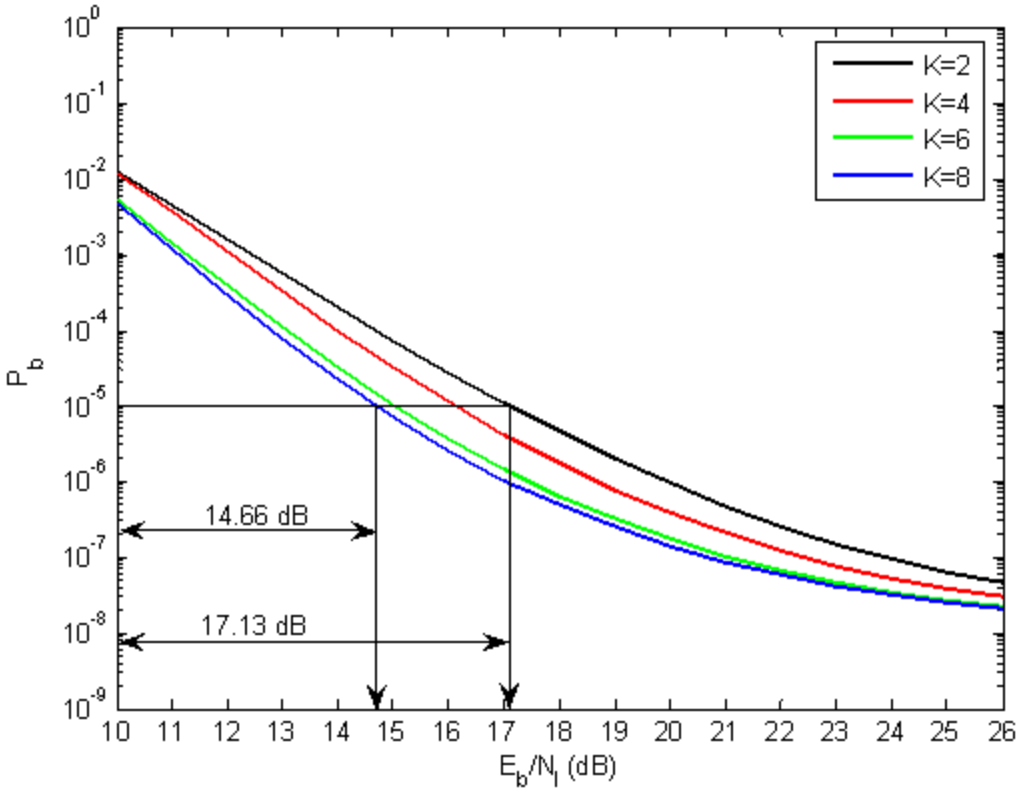

Figure 42. Magnified performance of 8-PSK and r=2/3 convolutionally encoded bits with HDD for different numbers of memory elements and a flat, slowly fading Nakagami channel with m=4 in both AWGN and BNI.

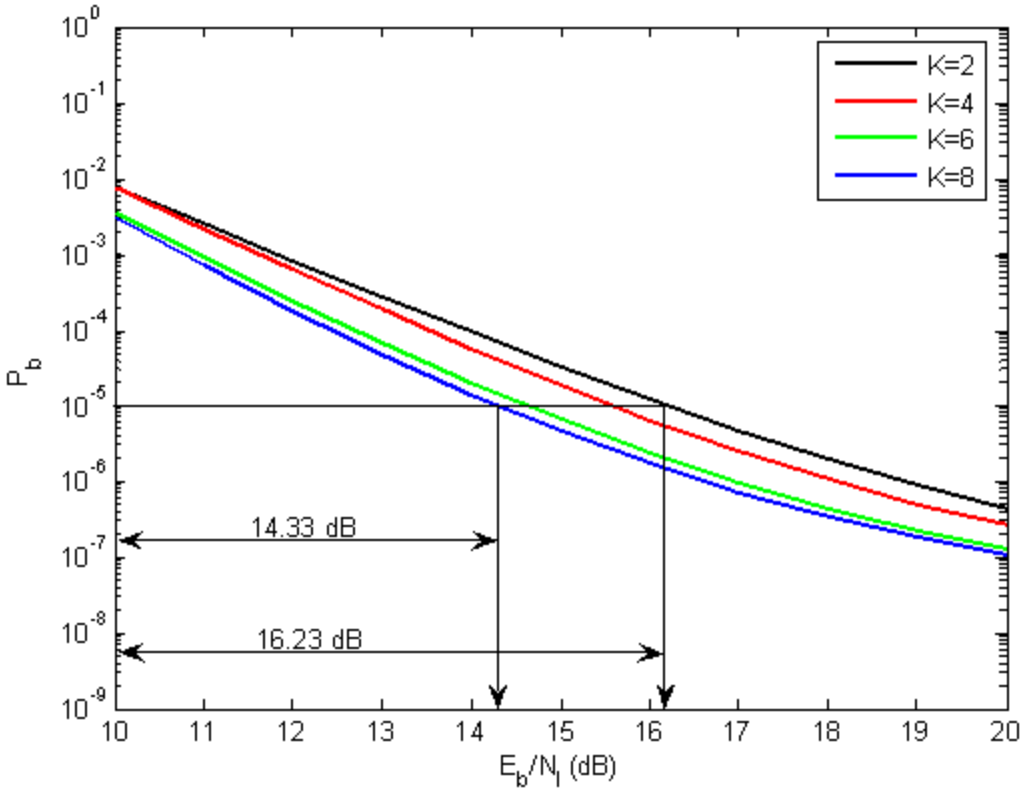

Figure 43. Magnified performance of 8-PSK and r=2/3 convolutionally encoded bits with HDD for different numbers of memory elements and a flat, slowly fading Nakagami channel with m=10 in both AWGN and BNI.

Table 7. Performance results for 8-PSK and r=2/3 convolutional encoding with HDD for a flat, slowly fading Nakagami channel with both AWGN and BNI.

m	Absolute E_b/N_I for $P_b=10^{-5}$ for K=2	Absolute E_b/N_I for $P_b=10^{-5}$ for K=8	Relative change in E_b/N_I for $P_b=10^{-5}$
1/2	51.52 dB	31.89 dB	19.63 dB
1	29 dB	19.78 dB	9.22 dB
2	20 dB	15.88 dB	4.12 dB
4	17.13 dB	14.66 dB	2.47 dB
10	16.23 dB	14.33 dB	1.9 dB

Table 7 is a list of the performance results for 8-PSK and r=2/3 convolutional encoding with HDD for different numbers of memory elements and a flat, slowly fading Nakagami channel with different values of m in both AWGN and BNI.

As m increases, performance improves regardless of K. For K=2, the change in the required E_b/N_I as m increases from 1/2 to 10 is 35.29 dB, while for K=8 the change is 17.56 dB. The relative change in E_b/N_I as m increases from 1/2 to 10 is 17.73 dB. From Table 7, we see that when K=8, the system performance is significantly better in an absolute sense when $m \leq 1$ but is always better to some degree regardless of m.

Figures 44-48 are similar to Figures 38-43, except PNI with ρ=0.2 is considered.

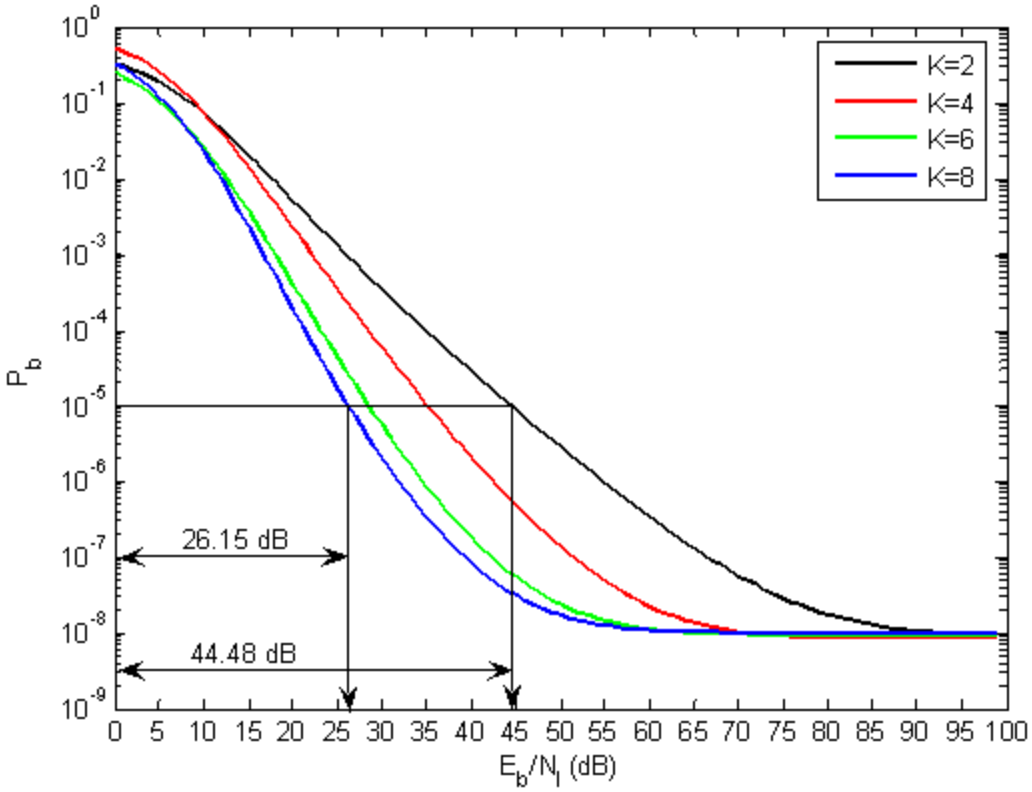

Figure 44. Performance of 8-PSK and r=2/3 convolutionally encoded bits with HDD for different numbers of memory elements and a flat, slowly fading Nakagami channel with m=1/2 in both AWGN and PNI with ρ=0.2.

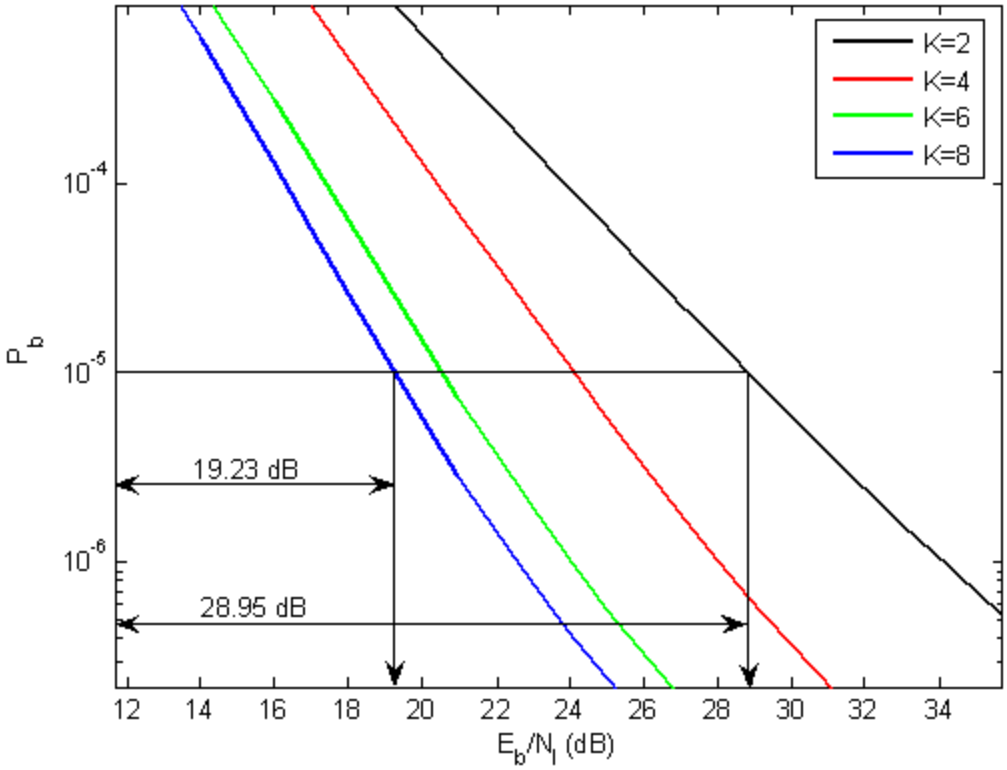

Figure 45. Magnified performance of 8-PSK and r=2/3 convolutionally encoded bits with HDD for different numbers of memory elements and a flat, slowly fading Nakagami channel with m=1 in both AWGN and PNI with ρ=0.2.

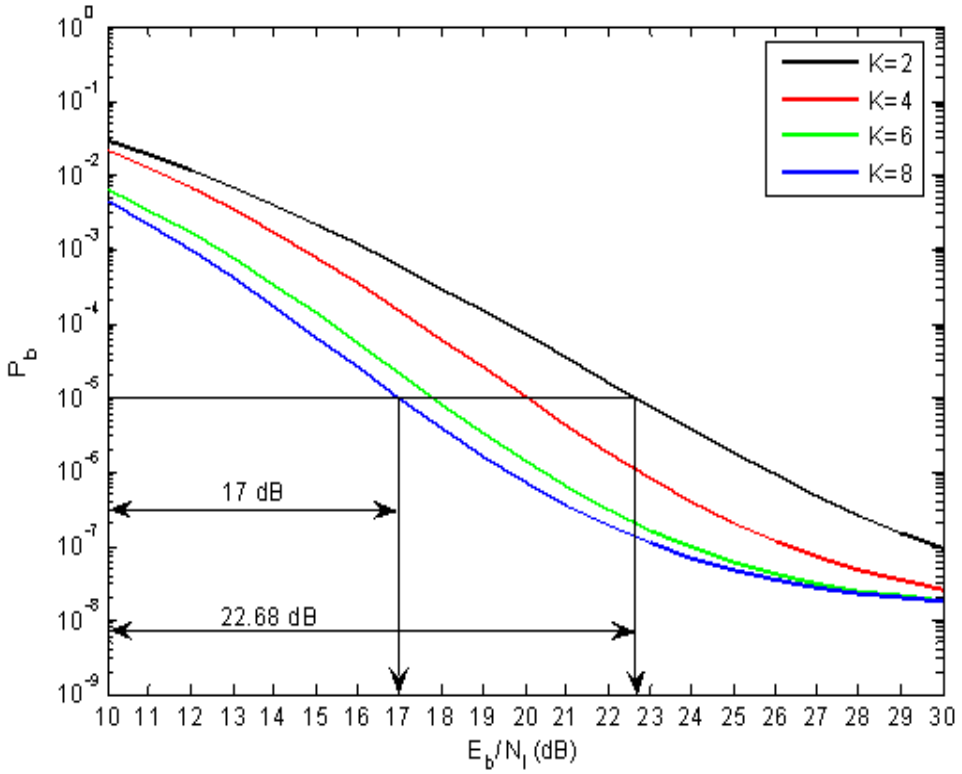

Figure 46. Magnified performance of 8-PSK and r=2/3 convolutionally encoded bits with HDD for different numbers of memory elements and a flat, slowly fading Nakagami channel with m=2 in both AWGN and PNI with ρ=0.2.

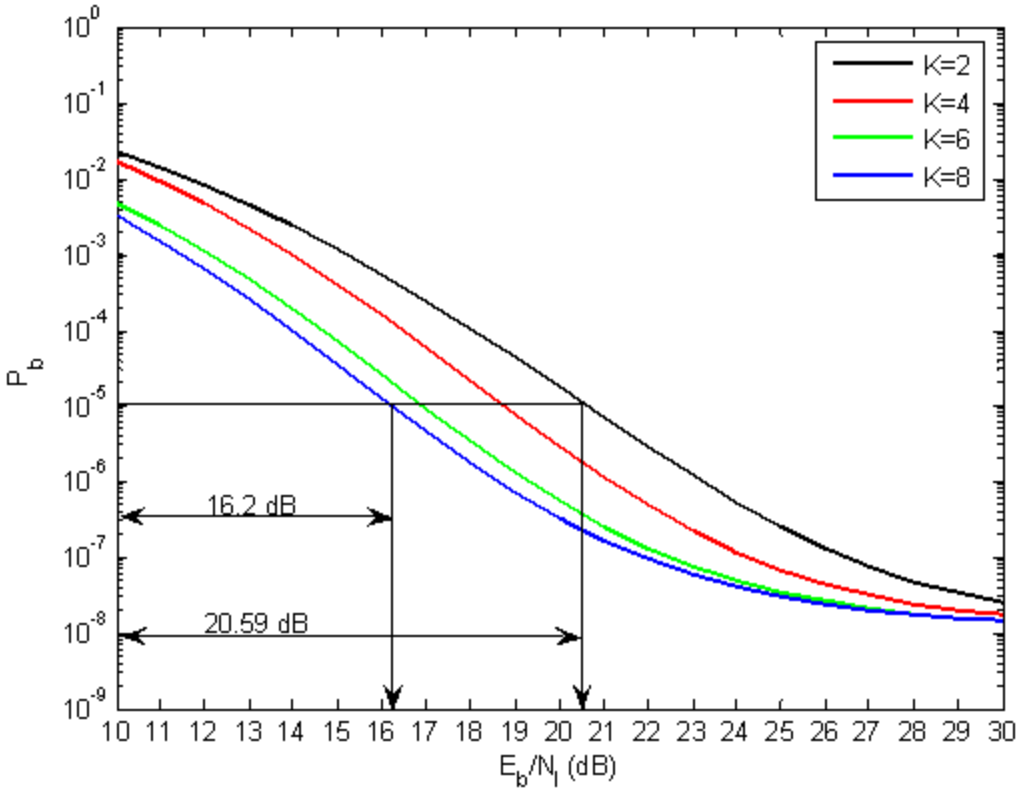

Figure 47. Magnified performance of 8-PSK and r=2/3 convolutionally encoded bits with HDD for different numbers of memory elements and a flat, slowly fading Nakagami channel with m=4 in both AWGN and PNI with ρ=0.2.

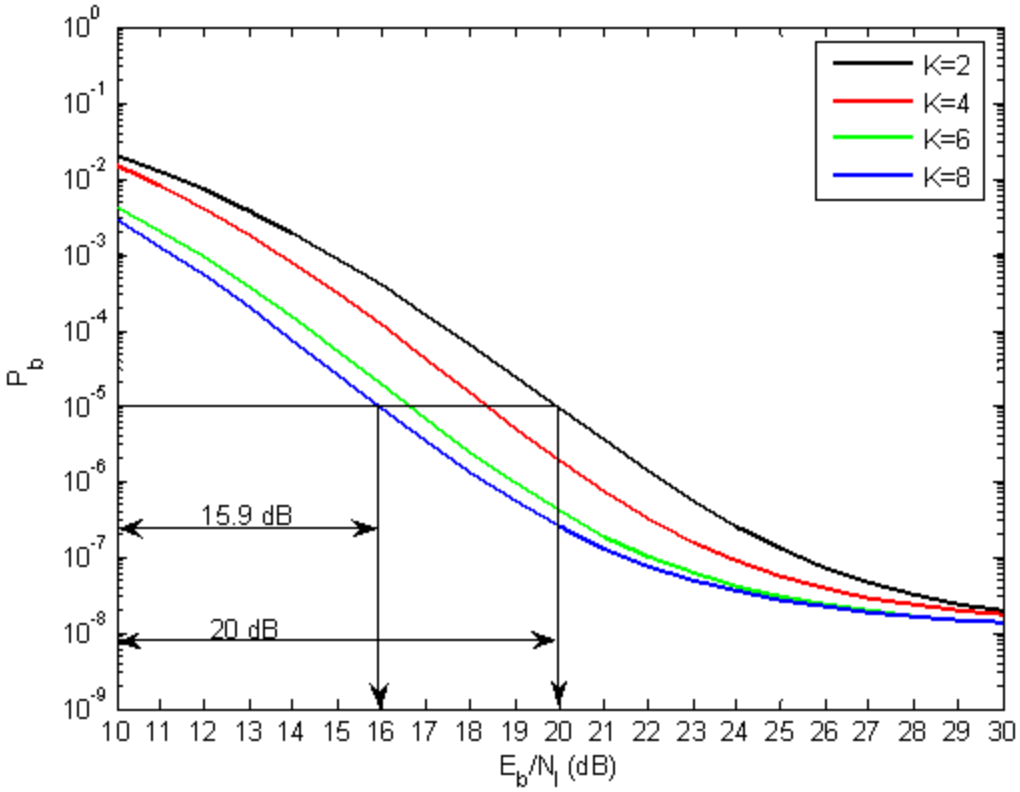

Figure 48. Magnified performance of 8-PSK and r=2/3 convolutionally encoded bits with HDD for different numbers of memory elements and a flat, slowly fading Nakagami channel with m=10 in both AWGN and PNI with ρ=0.2.

Table 8. Performance results for 8-PSK and r=2/3 convolutional encoding with HDD for different numbers of memory elements and a flat, slowly fading Nakagami channel with different values of m in both AWGN and PNI with ρ=0.2.

m	Absolute E_b/N_I for $P_b=10^{-5}$ for K=2	Absolute E_b/N_I for $P_b=10^{-5}$ for K=8	Relative change in E_b/N_I for $P_b=10^{-5}$
1/2	44.48 dB	26.15 dB	18.33 dB
1	28.95 dB	19.23 dB	9.72 dB
2	22.68 dB	17 dB	5.68 dB
4	20.59 dB	16.2 dB	4.39 dB
10	20 dB	15.9 dB	4.1 dB

Table 8 is a list of the performance results for 8-PSK and r=2/3 convolutional encoding with HDD for different numbers of memory elements and a flat, slowly fading Nakagami channel with different values of m in both AWGN and PNI with ρ=0.2.

As m increases, performance improves regardless of K. For K=2, the change in the required E_b/N_I as m increases from 1/2 to 10 is 24.48 dB, while for K=8 the change is 10.25 dB. The relative change in E_b/N_I as m increases from 1/2 to 10 is 14.23 dB. From Table 8, we see that when K=8, the system performance is significantly better in an absolute sense.

In this chapter, the effect of PNI on an 8-PSK, r=2/3 convolutionally encoded signal was examined. In the next chapter, we examine the performance of TCM signals in both AWGN and PNI. In Chapter IV, we examine the probability of sequence error of TCM signals transmitted with either 8-PSK modulation and a rate r=2/3 convolutional encoder or 4-PAM modulation and a rate r=1/2 convolutional encoder.

IV. PERFORMANCE ANALYSIS OF TCM SYSTEMS IN AWGN AND PULSE-NOISE INTERFERENCE.

A. PROBABILITY OF SEQUENCE ERROR OF TCM SIGNALS TRANSMITTED WITH 8-PSK AND A *r*=2/3 CONVOLUTION ENCODER IN AWGN

As previously discussed in Chapter II, parallel paths in the TCM trellis is not generally preferable since, regardless of the complexity of the convolutional encoder, generally the parallel paths result in an error floor beyond which the performance cannot be improved. In order to avoid parallel transitions, we use a generic Ungerboeck encoder where blocks of m information bits are the input of a $r=m/(m+1)$ convolutional encoder. A major disadvantage of $r=m/(m+1)$ convolutional encoders is that for increasing m, decoding complexity increases.

In general, an upper bound on the probability of sequence error is given by equation (2.5), repeated here for convenience:

$$P_E \le P_E(parallel) + Q\left(\sqrt{\frac{E_{sc}d_{free}^2}{2N_0}}\right)\exp\left(\frac{E_{sc}d_{free}^2}{4N_0}\right)\times T(X)\Big|_{X=\exp\left(\frac{-E_{sc}}{4N_0}\right)} \tag{4.1}$$

where $E_{sc} = r(m+1)E_b$, $P_E(parallel)$ is the probability of choosing an incorrect parallel path, the AOWEF $T(X)$ does not account for parallel paths, $A_{d_{free}}$ is the average number of code sequences that have a squared-Euclidean distance d_{free}^2 from the correct sequence, and d_{free}^2 is the minimum squared-Euclidean distance between all pairs of nonparallel sequences.

Equation (4.1) is approximated by

$$P_E \approx P_E(parallel) + A_{d_{free}}Q\left(\sqrt{\frac{E_{sc}d_{free}^2}{2N_0}}\right) \tag{4.2}$$

In this section, m=2 for a r=2/3 convolutional encoder and $E_{sc}=(2/3)(2+1)E_b=2E_b$. For the case of no parallel transitions, from equation (4.2) the probability of sequence error is approximated by

$$P_E \approx A_{d_{free}} Q\left(\sqrt{\frac{E_b d_{free}^2}{N_0}}\right) \tag{4.3}$$

The values of $A_{d_{free}}$ and d_{free}^2 are given in Table 9.

Table 9. Set of optimum TCM code designs for 8-PSK. (After: [4]).

Memory elements	d_{free}^2	$A_{d_{free}}$
2	4	1
3	4.586	2
4	5.172	≈2.3
6	6.343	≈5.3
7	6.586	≈0.5
8	7.515	≈1.5

In Figure 49 we observe probability sequence error for TCM signals transmitted with 8-PSK modulation and a rate r=2/3 convolution encoder in an AWGN environment obtained using equation (4.3).

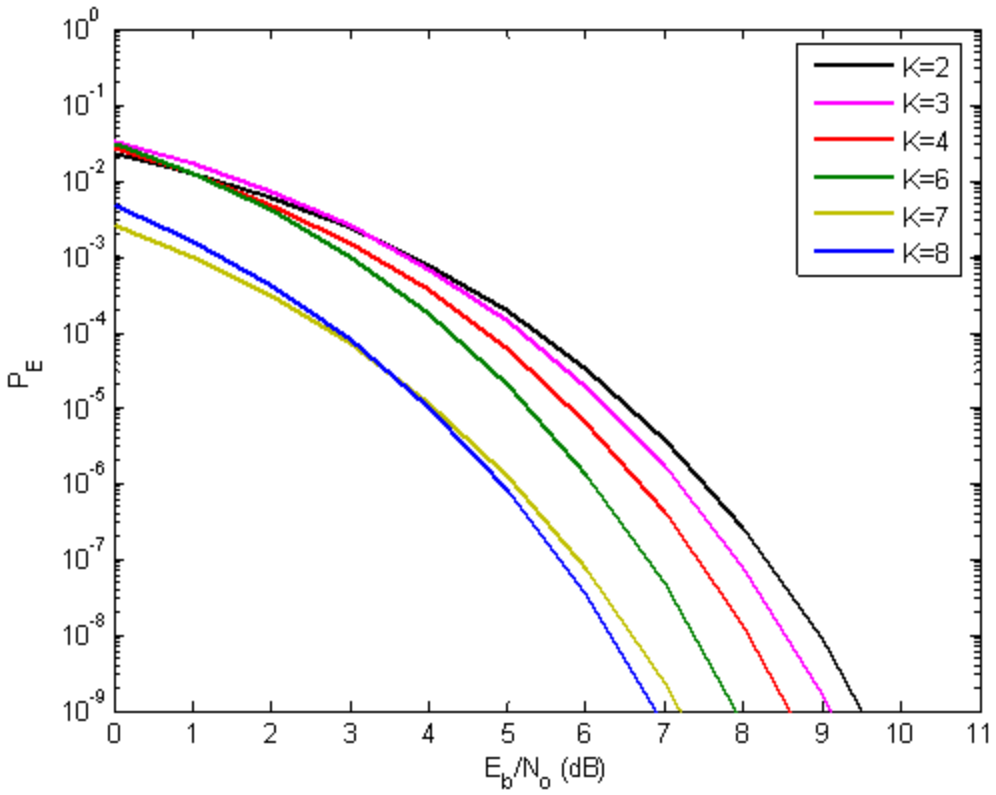

Figure 49. Probability sequence error of TCM signals transmitted with 8-PSK modulation and a rate r=2/3 convolution encoder in AWGN.

From Figure 49, it is clear that the performance of the TCM system improves as the number of memory elements K in the encoder increase. In order to achieve $P_E=10^{-9}$, E_b/N_o=6.89 dB is required for K=8, while for K=2, E_b/N_o=9.52 dB is required. As discussed earlier, the required probability sequence error for most practical applications is $P_E\approx10^{-5}$.

As is shown in Figure 50, which is a magnified version of Figure 49, in order to achieve $P_E=10^{-5}$, E_b/N_o=4.02 dB is required for K=8 and E_b/N_o=6.53 dB is required for K=2. The difference in the E_b/N_o required that results from increasing K from two to eight is 2.51 dB. In order to achieve the same performance for different values of probability sequence error, the encoder with K=8 always requires less E_b/N_o compared to encoders with fewer memory elements.

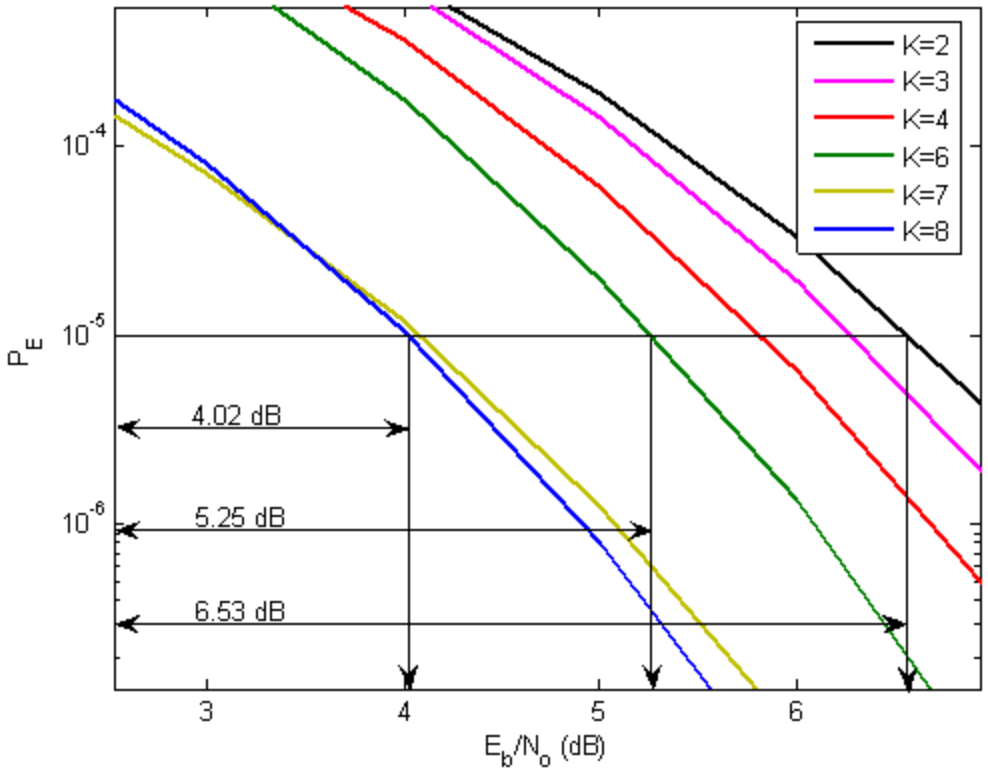

Figure 50. Magnified probability sequence error of TCM signals transmitted with 8-PSK modulation and a rate r=2/3 convolution encoder in AWGN.

In Figure 51 a magnified version of the performance of a non-TCM system with 8-PSK and r=2/3 convolutional encoding, previously shown in Figure 12, is shown. We note at this point that we can use probability of sequence error as a good approximation for the probability of bit error, especially for systems where K is large.

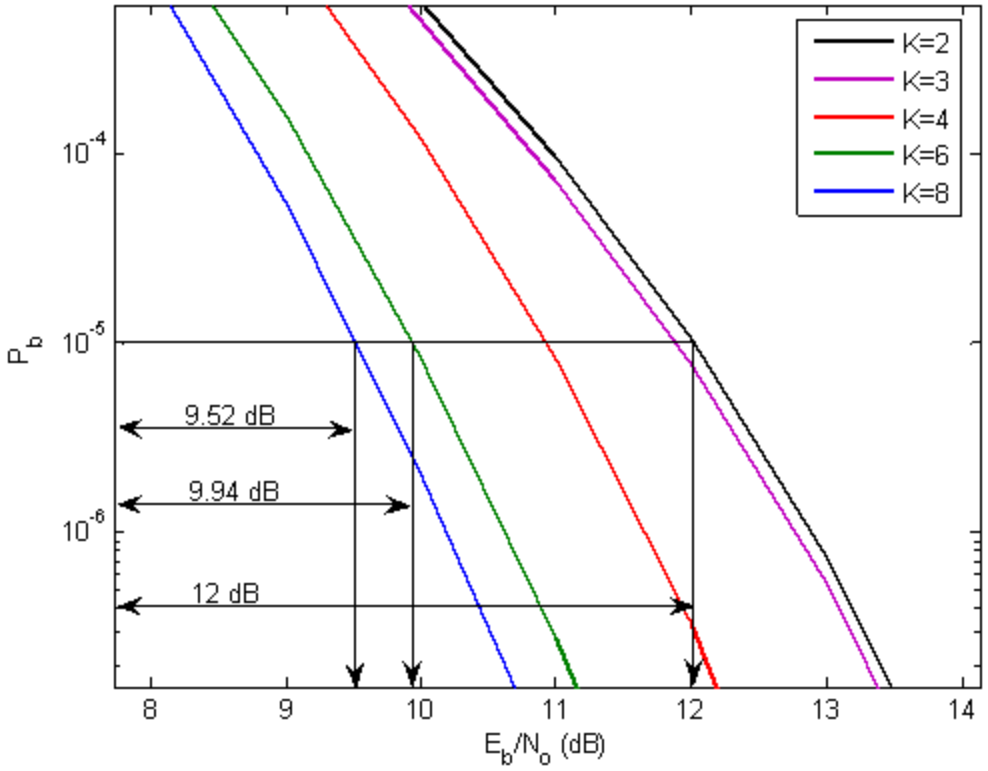

Figure 51. Magnified performance of probability bit error of a non-TCM system with 8-PSK and r=2/3 convolutional encoding in AWGN.

If we compare Figure 50 with Figure 51, we see a clear advantage of TCM signals when they are transmitted with 8-PSK modulation and a rate r=2/3 convolution encoder in an AWGN environment. In order to achieve $P_b=10^{-5}$, E_b/N_o=12 dB is required for K=2 for the non-TCM system with HDD, while E_b/N_o=6.53 dB is required for TCM signals. The improvement due to TCM is almost 5.5 dB. For K=8, E_b/N_o=9.52 dB is required for the non-TCM system with HDD, while E_b/N_o=4.02 dB is required for TCM signals. The improvement in this case due to TCM is again almost 5.5 dB.

B. PROBABILITY OF SEQUENCE ERROR OF TCM SIGNALS TRANSMITTED WITH 4-PAM AND A *r*=1/2 CONVOLUTION ENCODER IN AWGN

We follow the same procedure for obtaining the probability of sequence error as was used in section A when there are no parallel transitions. In this section, m=1 for a

r=1/2 convolutional encoder and E_{sc}=(1/2)(1+1)E_b=E_b. For the case of no parallel transitions, from equation (4.2), the probability of sequence error is approximated by

$$P_E \approx A_{d_{free}} Q\left(\sqrt{\frac{E_b d_{free}^2}{2N_0}}\right) \tag{4.4}$$

The values of $A_{d_{free}}$ and d_{free}^2 are given in Table 10.

Table 10. Set of optimum TCM code designs for 4-PAM. (After: [4]).

Memory elements	d_{free}^2	$A_{d_{free}}$
2	7.2	4
3	8	4
4	8.8	8
6	11.2	36
7	12.8	66

Comparing equations (4.3) and (4.4), we see that for the same d_{free}, TCM with 8-PSK and r=2/3 convolutional encoding has a 3 dB advantage over TCM with 4-PAM and r=1/2 convolutional encoding. In Figure 52 we observe the probability sequence error for TCM signals transmitted with 4-PAM modulation and rate r=1/2 convolution encoding in an AWGN environment obtained using equation (4.4).

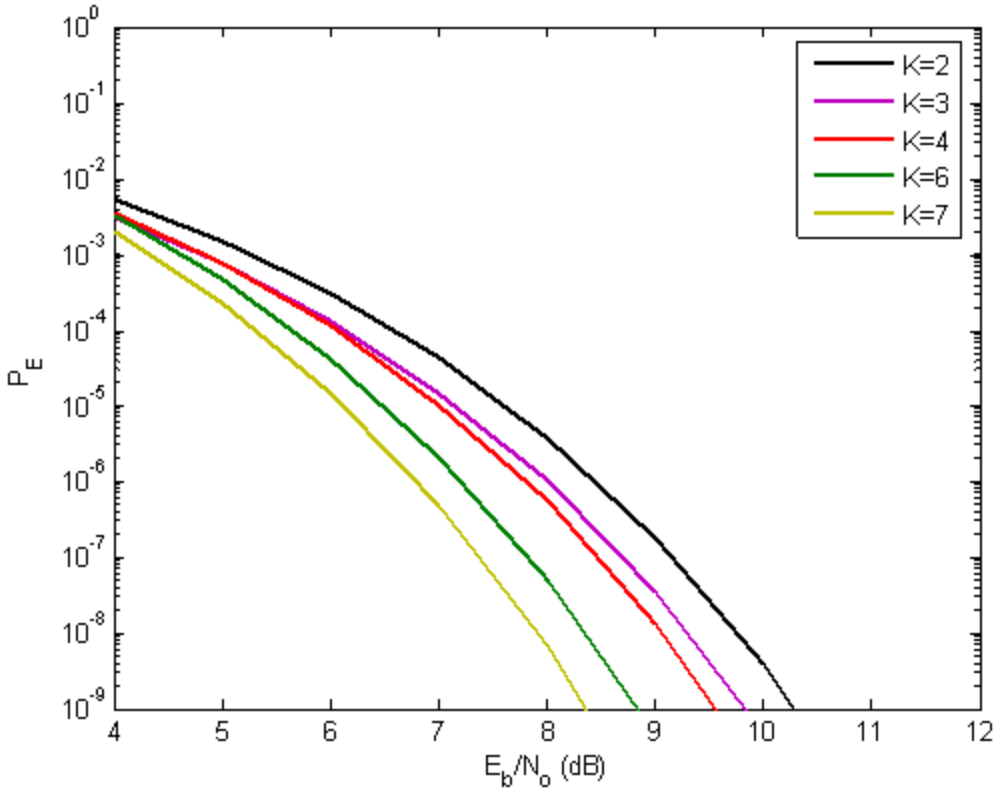

Figure 52. Probability sequence error of TCM signals transmitted with 4-PAM modulation and a rate r=1/2 convolution encoder in AWGN.

From Figure 52, we see that the performance of this TCM system also improves as the number of memory elements of the encoder increase. In order to achieve $P_E=10^{-9}$, E_b/N_o=8.35 dB is required for K=7, while E_b/N_o=10.27 dB is required for K=2.

As is shown in Figure 53, which is a magnified version of Figure 52, in order to achieve $P_E=10^{-5}$, E_b/N_o=6.12 dB is required for K=7 and E_b/N_o=7.59 dB for K=2. The difference in the E_b/N_o required that results from increasing K from two to seven is 1.47 dB.

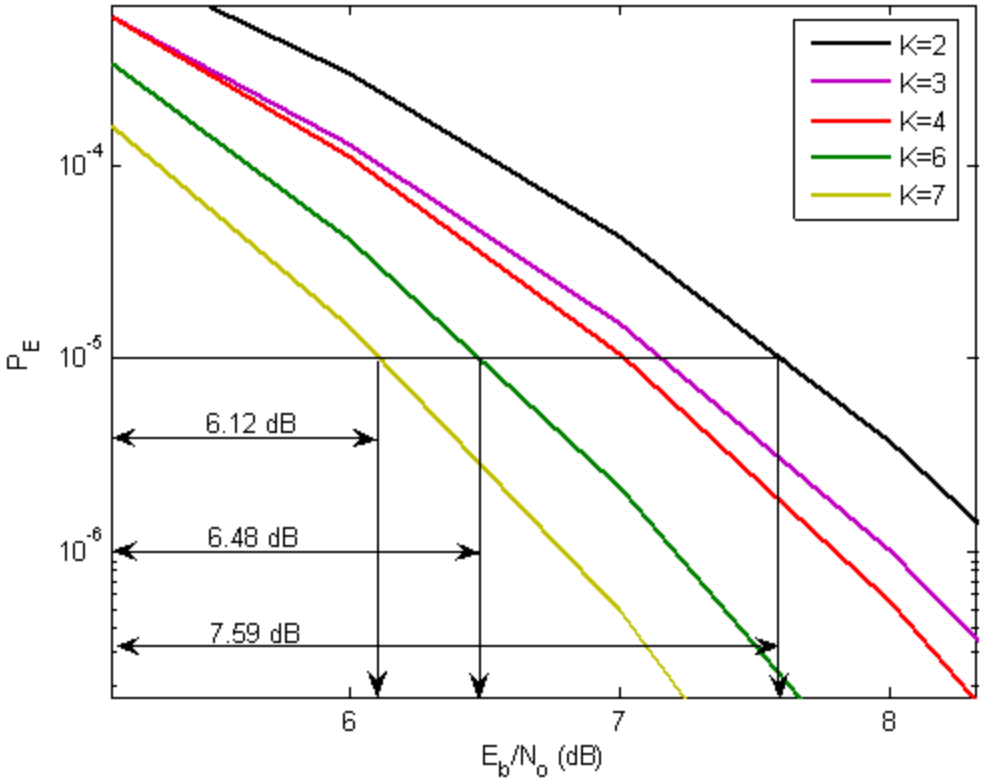

Figure 53. Magnified probability sequence error of TCM signals transmitted with 4-PAM modulation and a rate r=1/2 convolution encoder in AWGN.

If we compare Figure 53 with Figure 50, we see a clear advantage of TCM with 8-PSK modulation and rate r=2/3 convolutional encoding as compared to TCM with 4-PAM modulation and rate r=1/2 convolutional encoding in an AWGN environment. In order to achieve $P_E=10^{-5}$, E_b/N_o=6.53 dB is required for K=2 in the case of 8-PSK with a r=2/3 encoder and E_b/N_o=7.59 dB is required for K=2 for the case of 4-PAM with a r=1/2 encoder. The advantage of the 8-PSK, r=2/3 system is 1.06 dB. For K=6 and $P_E=10^{-5}$, E_b/N_o=5.25 dB is required for the 8-PSK, r=2/3 system and E_b/N_o=6.48 dB is required for the 4-PAM, r=1/2 system. The advantage of the 8-PSK, r=2/3 system is 1.23 dB.

C. PERFORMANCE ANALYSIS OF TCM SIGNALS TRANSMITTING INDEPENDENT DATA ON THE I AND Q CHANNELS IN AWGN

In this section we examine the performance of TCM signals where independent data is transmitted with two 4-PAM, r=1/2 TCM signals, one on the inphase (I) channel and one on the quadrature (Q) channel. TCM signals transmitting data independently on the I and Q channels with two 4-PAM waveforms and r=1/2 convolutional encoding have the same information data rate and channel bandwidth as a TCM signal with r=2/3 convolutional encoding and 8-PSK modulation.

Initially, the two systems are compared for the same number of memory elements. In other words, if the r=2/3 encoder has K memory elements, then each of the r=1/2 encoders in the other system will have K/2 memory elements for a total of K memory elements.

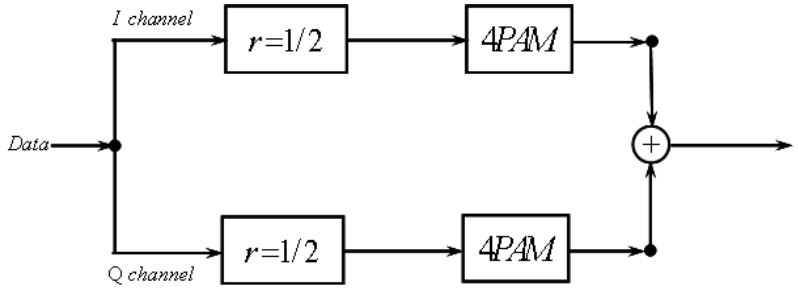

Figure 54. Overview of TCM signals transmitting independent data on the I and Q channels.

Figure 54 is an overview of a system consisting of TCM signals transmitting independent data on the I and Q channels, where each channel is modulated with 4-PAM with Gray mapping. In Gray mapping, adjacent symbols differ in only one bit position. The probability bit error is the same for the I and Q channel, and the overall probability of bit error is equal to the probability of bit error of either the I or the Q channel since the I and Q channels are independent.

1. Probability Bit Error Analysis for K=1

In this subsection we consider a rate r=1/2 convolution encoder with one memory element (K=1), shown in Figure 55. The signal flow graph for Gray mapped 4-PAM/TCM, using Table 1, is shown in Figure 56.

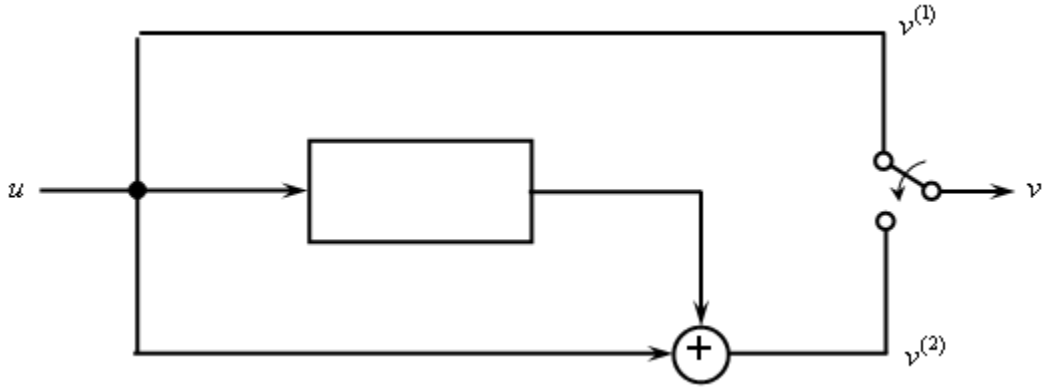

Figure 55. Rate r=1/2, K=1 convolutional encoder.

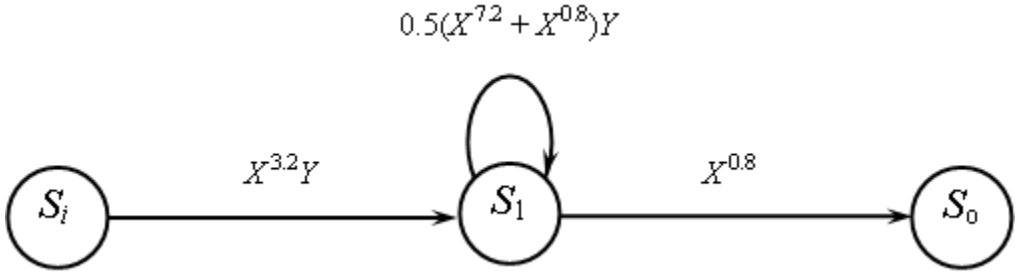

Figure 56. Signal flow graph for r=1/2, K=1 convolutional encoder with Gray mapped 4-PAM/TCM.

Using the transfer function method as in Chapter II, we obtain the AIOWEF for the r=1/2, K=1 convolutional code with Gray mapped 4-PAM/TCM as

$$T_{ave}(X,Y) = \frac{X^4 Y}{1 - \frac{1}{2}X^{0.8}Y - \frac{1}{2}X^{7.2}Y} \tag{4.5}$$

Using the geometric series expansion equation (2.3) in equation (4.5), we obtain the AIOWEF as

$$T_{ave}(X,Y) = X^4Y + \left(\frac{X^{4.8}}{2} + \frac{X^{11.2}}{2}\right)Y^2 + \left(\frac{X^{5.6}}{4} + \frac{X^{12}}{2} + \frac{X^{18.4}}{4}\right)Y^3 + \frac{X^4\ X^{0.8} + X^{7.2}\ ^3}{8}Y^4 + \ldots \tag{4.6}$$

By inspection of equation (4.6), we see that for an arbitrary sequence of code bits there is an average of one path with a squared-Euclidean distance of four associated with one information bit error. Moreover, the AIOWEF implies that there are an average of 1/2 paths with a squared-Euclidean distance of 4.8 associated with two information bit errors, and so on.

In the following analysis, we repeat the steps in Chapter II since the TCM system has no parallel transitions. The probability of bit error is given by equation (2.9) or equation (2.10) and repeated here for convenience:

$$P_b < \frac{1}{m}\sum_{i=1}^{\infty} B_{d_i} Q\left(\sqrt{\frac{E_{sc}d_i^2}{2N_0}}\right) \tag{4.7}$$

$$P_b < \frac{1}{m} Q\left(\sqrt{\frac{E_{sc}d_{free}^2}{2N_0}}\right)\exp\left(\frac{E_{sc}d_{free}^2}{4N_0}\right) \times \left.\frac{\partial T_{ave}(X,Y)}{\partial Y}\right|_{X=\exp\left(\frac{-E_{sc}}{4N_0}\right),Y=1} \tag{4.8}$$

where $E_{sc} = r(m+1)E_b$, B_{d_i} is the total number of information bit errors on all error paths that have a Euclidean distance d_i from the correct path, and $d_1^2 = d_{free}^2$. We need only the first term in the infinite series when $E_b/N_o >> 1$. From equation (4.7) with m=1 and r=1/2,

$$P_b \approx B_{d_{free}} Q\left(\sqrt{\frac{E_b d_{free}^2}{2N_0}}\right) \tag{4.9}$$

In order to calculate the $B_{d_i}s$ from the AIOWEF, we apply the same procedure as for convolutional codes. The result is given by equation (2.12), which is repeated for convenience:

$$\left.\frac{\partial T_{ave}(X,Y)}{\partial Y}\right|_{Y=1} = \sum_{i=1}^{\infty} B_{d_i} X^{d_i^2} \tag{4.10}$$

From equations (4.6), we get

$$\left.\frac{\partial T_{ave}(X,Y)}{\partial Y}\right|_{Y=1} = X^4 + X^{4.8} + X^{11.2} + \frac{3X^{5.6}}{4} + \frac{3X^{12}}{2} + \frac{3X^{18.4}}{4} + \frac{X^4 \quad X^{0.8} + X^{7.2\ \ 3}}{2} + \ldots \tag{4.11}$$

If we rearrange the terms of equation (4.11), we get

$$\left.\frac{\partial T_{ave}(X,Y)}{\partial Y}\right|_{Y=1} = X^4 + X^{4.8} + \frac{3}{4}X^{5.6} + \frac{X^{6.4}}{2} + \frac{5X^{7.2}}{16} + \frac{6X^8}{32} + X^{11.2} + \frac{3}{2}X^{12} + \ldots \tag{4.12}$$

which can be compared with equation (4.10) to get the $B_{d_i}s$. The upper bound on the probability of bit error is now obtained by combining equation (4.7) and the $B_{d_i}s$ obtained from equation (4.12) to get

$$P_b < Q\left(\sqrt{\frac{2E_b}{N_0}}\right) + Q\left(\sqrt{\frac{2.4E_b}{N_0}}\right) + 0.75Q\left(\sqrt{\frac{2.8E_b}{N_0}}\right) + 0.5Q\left(\sqrt{\frac{3.2E_b}{N_0}}\right) + 0.3125Q\left(\sqrt{\frac{3.6E_b}{N_0}}\right) + 0.1875Q\left(\sqrt{\frac{4E_b}{N_0}}\right) + Q\left(\sqrt{\frac{5.6E_b}{N_0}}\right) + 1.5Q\left(\sqrt{\frac{6E_b}{N_0}}\right) + \ldots \tag{4.13}$$

2. Probability Bit Error Analysis for K=2

In this subsection we consider a rate r=1/2 convolution encoder with two memory elements (K=2), shown in Figure 57. The error trellis of the convolutional encoder is shown in Figure 58.

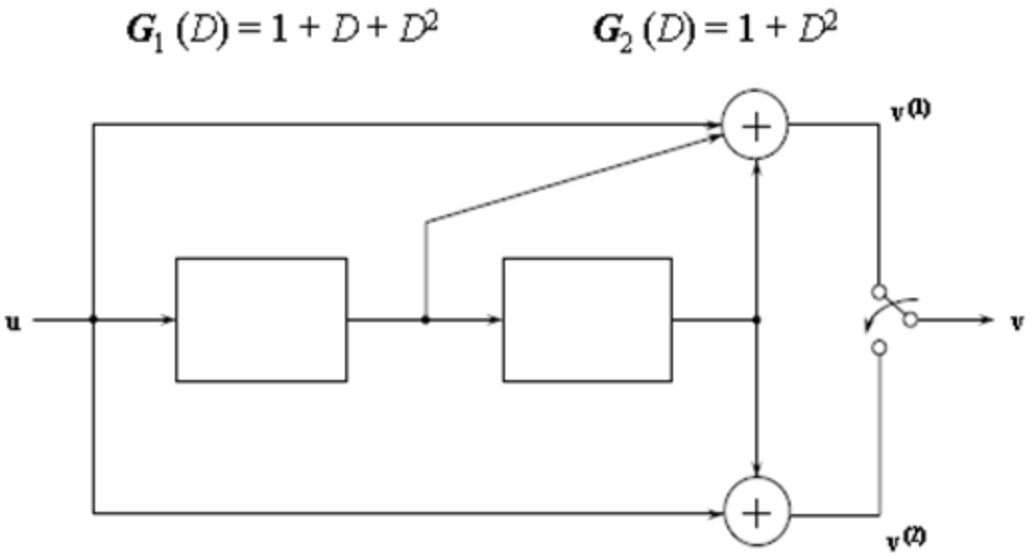

Figure 57. Rate r=1/2, K=2 convolutional encoder. (From: [5]).

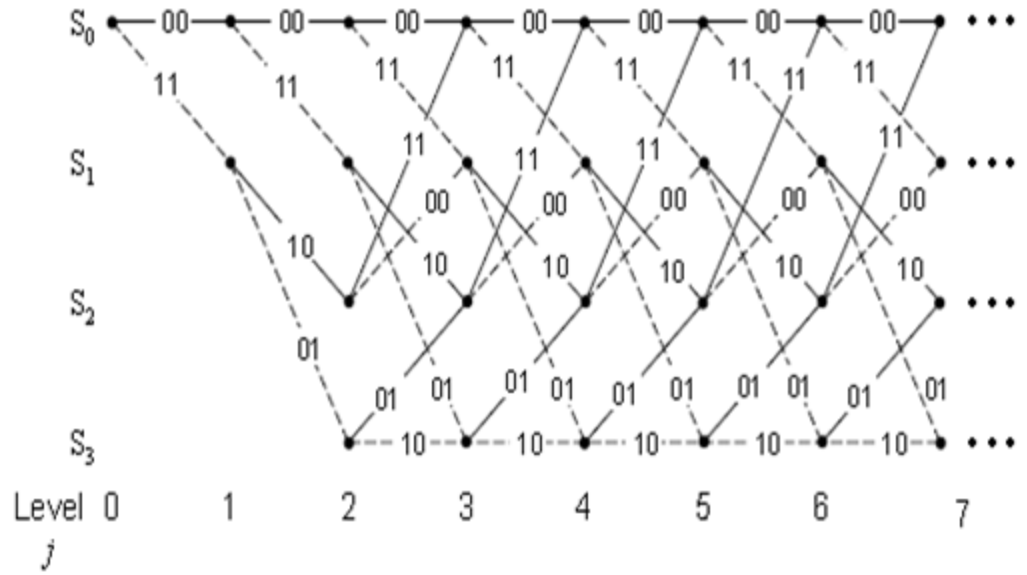

Figure 58. Error trellis for r=1/2, K=2 convolutional encoder. (From: [5]).

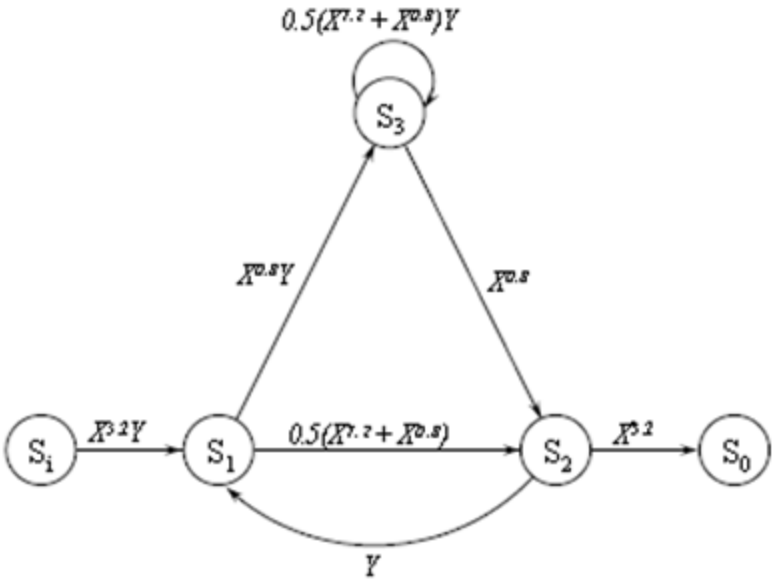

Figure 59. Signal flow graph for r=1/2, K=2 convolutional encoder with Gray mapped 4-PAM/TCM. (From: [5]).

The signal flow graph for Gray mapped 4-PAM/TCM was derived from the error trellis of the encoder using Table 1 and is shown in Figure 59.

The upper bound on the probability bit error for a TCM system with a r=1/2, K=2 convolutional encoder in conjunction with 4-PAM modulation with Gray mapping was derived in Chapter II as an example. The upper bound is given by equation (2.15) and repeated for convenience:

$$P_b < 0.5Q\left(\sqrt{\frac{3.6E_b}{N_0}}\right) + 2.5Q\left(\sqrt{\frac{4E_b}{N_0}}\right) + 4.875Q\left(\sqrt{\frac{4.4E_b}{N_0}}\right) + 8.25Q\left(\sqrt{\frac{4.8E_b}{N_0}}\right) + \ldots \quad (4.14)$$

3. Probability Bit Error Analysis for K=3

In this subsection we consider a rate r=1/2 convolution encoder with three memory elements (K=3), shown in Figure 60. The signal flow graph for Gray mapped 4-PAM/TCM, using Table 1, is shown in Figure 61.

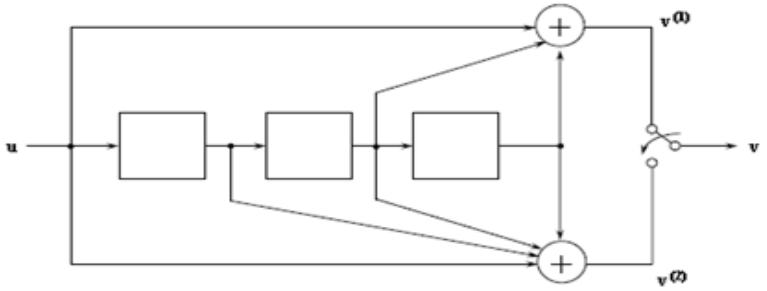

Figure 60. Rate $r=1/2$, K=3 convolutional encoder.

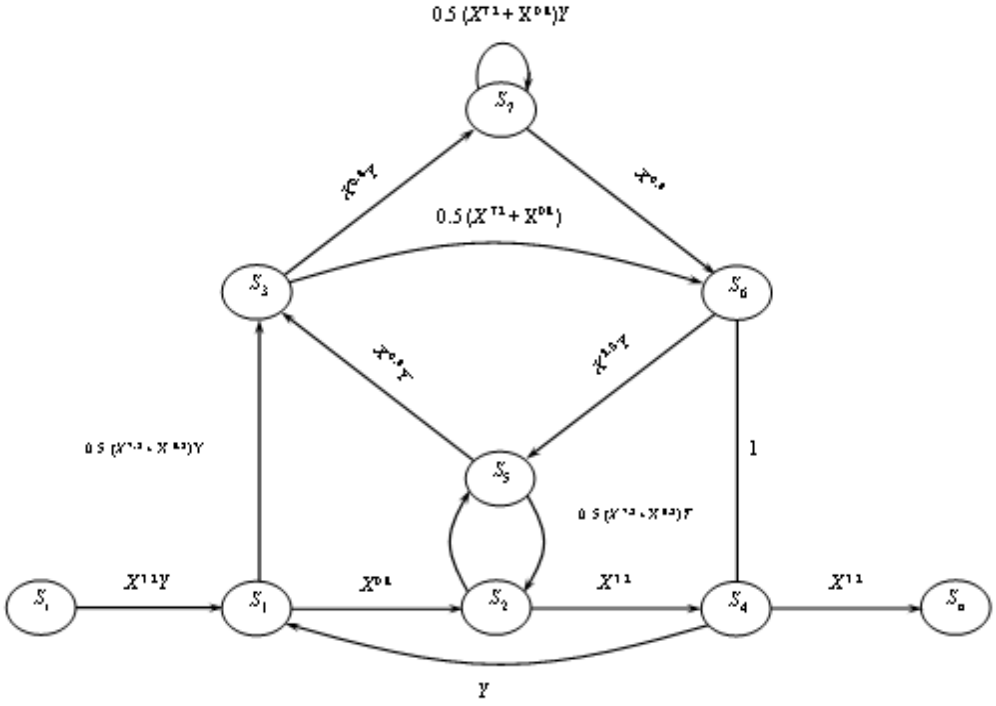

Figure 61. Signal flow graph for $r=1/2$, K=3 convolutional encoder with Gray mapped 4-PAM/TCM.

Using the transfer function method and with the assistance of the geometric series expansion from equation (2.3), we calculate the AIOWEF as

$$T_{ave}(X,Y) = \frac{1}{4}X^{8}Y^{2} + X^{8.8}Y^{3} + \frac{25}{16}X^{9.6}Y^{4} + X^{10.4}Y + \frac{3}{2}X^{10.4}Y^{5} + \ldots \qquad (4.15)$$

By inspection of equation (4.15) we see that for an arbitrary sequence of code bits there are an average of 1/4 code paths with a squared-Euclidean distance of eight associated with two information bit errors. Moreover, equation (4.15) implies that there is one code path with a squared-Euclidean distance of 8.8 associated with three information bit errors, and so on for higher powers of X.

In order to calculate the $B_{d_i}s$ from equation (4.15), we use equation (4.10). Taking the derivative with respect to Y of equation (4.15), we get

$$\left.\frac{\partial T_{ave}(X,Y)}{\partial Y}\right|_{Y=1} = \frac{X^8}{2} + 3X^{8.8} + 6.25X^{9.6} + 8.5X^{10.4} + \ldots \qquad (4.16)$$

Combining equations (4.7) and (4.16), we obtain the upper bound

$$P_b < 0.5Q\left(\sqrt{\frac{4E_b}{N_0}}\right) + 3Q\left(\sqrt{\frac{4.4E_b}{N_0}}\right) + 6.25Q\left(\sqrt{\frac{4.8E_b}{N_0}}\right) + 8.5Q\left(\sqrt{\frac{5.2E_b}{N_0}}\right) + \ldots \qquad (4.17)$$

where the first term is sufficient when $E_b/N_o >> 1$.

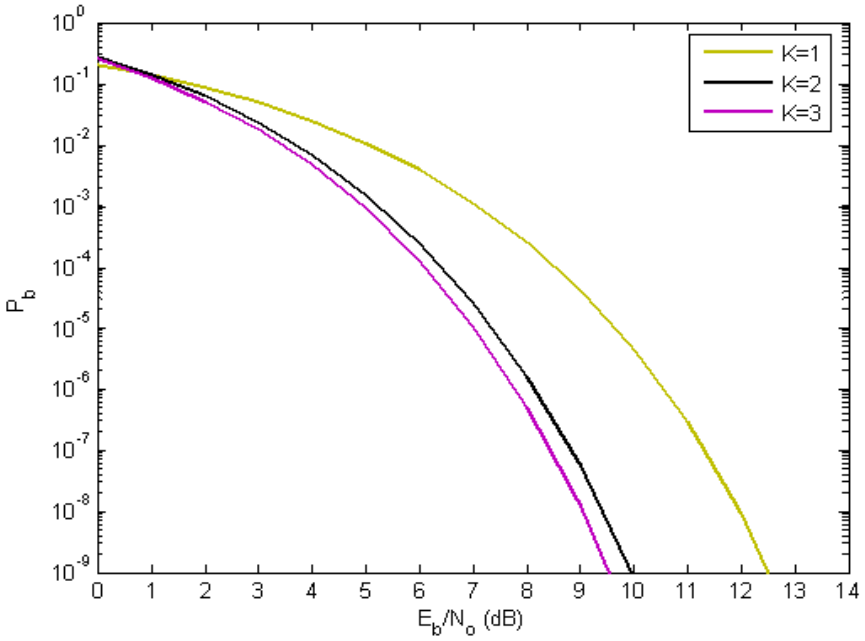

Figure 62. Probability bit error of TCM signals transmitting data independently on the I and Q channels each modulated with 4-PAM waveforms encoded with a rate r=1/2 convolutional code for K=1, 2 and 3 in AWGN.

In Figure 62 we observe the performance of probability bit error of TCM signals transmitting data independently on the I and Q channels, each modulated with 4-PAM waveforms encoded with a rate r=1/2 convolution code for K=1, 2 and 3 in AWGN. As expected, the performance of the system improves as the number of memory elements increases. Figure 63 is a magnified version of Figure 62. We see that in order to achieve $P_b=10^{-5}$, E_b/N_o=9.66 dB is required for K=1, E_b/N_o=7.35 dB for K=2, and E_b/N_o=7.01 dB for K=3. The relative difference in E_b/N_o between K=1 and K=3 is 2.65 dB.

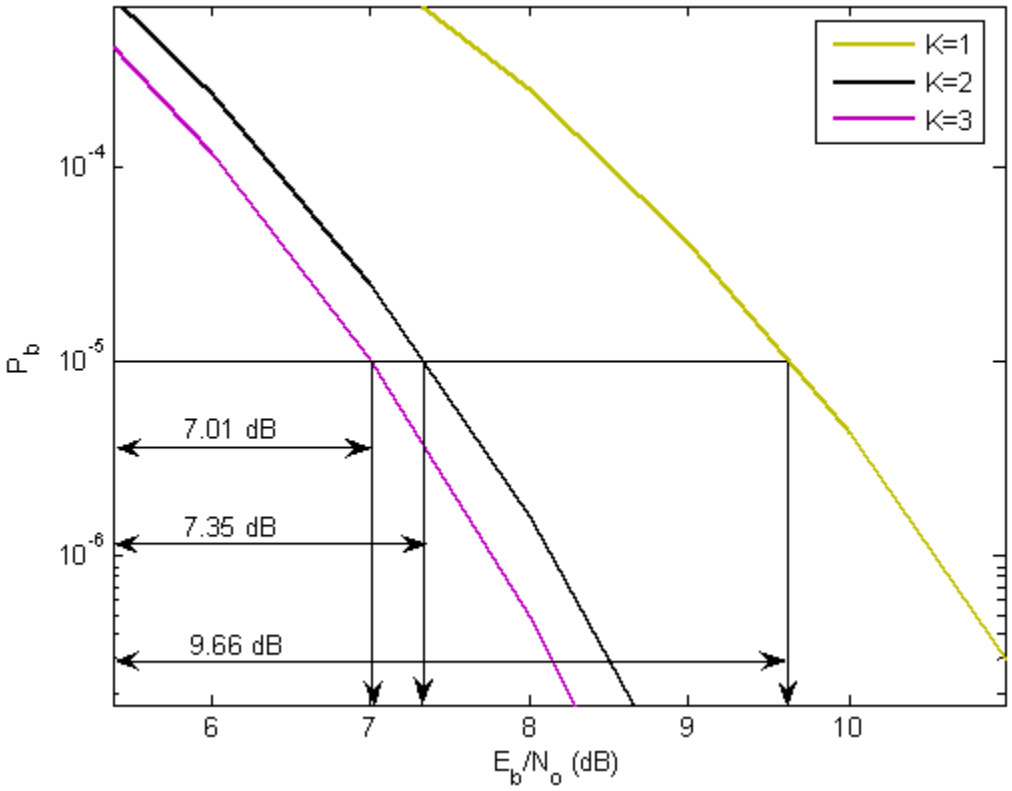

Figure 63. Magnified probability bit error of TCM signals transmitting data independently on the I and Q channels, each modulated with 4-PAM waveforms encoded with a rate r=1/2 convolutional code for K=1, 2 and 3 in AWGN.

D. PERFORMANCE ANALYSIS OF TCM SIGNALS WITH 8-PSK MODULATION AND A RATE *r*=2/3 CONVOLUTION ENCODER IN AWGN

1. Probability Bit Error Analysis for K=1

In this case we use natural mapping with 8-PSK modulation in conjunction with a r=2/3 convolutional encoder. The 8-PSK constellation with natural mapping is shown in Figure 64. Natural mapping of 8-PSK clearly has a uniform pattern.

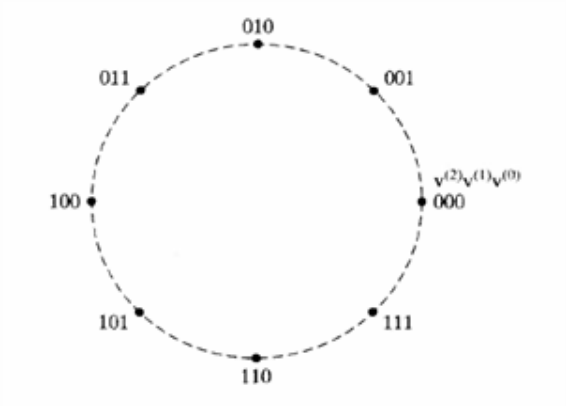

Figure 64. Natural mapping 8-PSK constellation. (From: [4]).

The error vectors and the squared-Euclidean distances for natural-mapped 8-PSK are listed in Table 11 [4].

Table 11. Error vectors and squared-Euclidean distance for 8-PSK with natural mapping. (After: [4]).

e	$\Delta_e^2(X)$
000	X^0
001	$X^{0.586}$
010	X^2
011	$\frac{1}{2}X^{0.586}+\frac{1}{2}X^{3.414}$
100	X^4

101	$X^{3.414}$
110	X^{2}
111	$\frac{1}{2}X^{0.586}+\frac{1}{2}X^{3.414}$

The rate r=2/3 convolution encoder with one memory element (K=1) is shown in Figure 65, and the state diagram, obtained using Figure 65 and Table 11, is shown in Figure 66.

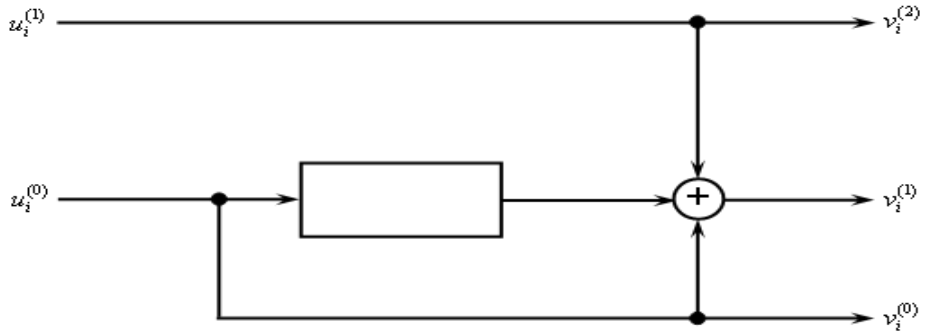

Figure 65. Rate r=2/3, K=1 convolutional encoder.

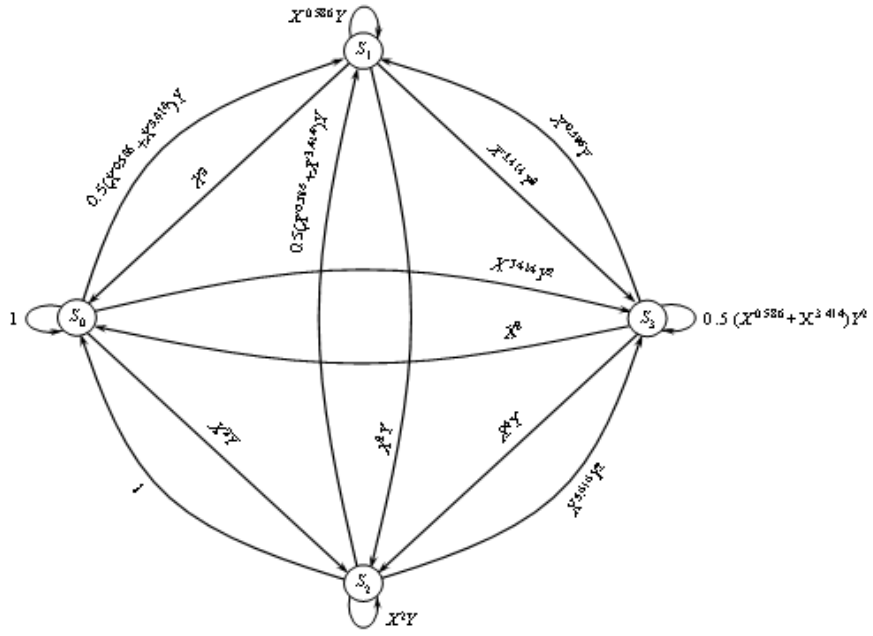

Figure 66. State diagram for r=2/3, K=1 convolutional encoder for TCM with 8-PSK and natural mapping.

From Figure 66, we can obtain the signal flow graph, which in turn allows us to calculate the AIOWEF :

$$T_{ave}(X,Y) = X^2Y + \frac{1}{2}X^{2.586}Y + \frac{1}{2}X^{2.586}Y^2 + \frac{1}{2}X^{3.172}Y^2 + \frac{1}{2}X^{3.172}Y^3 + \ldots \quad (4.18)$$

By inspection of equation (4.18), we see that for an arbitrary sequence of code bits there is an average of one path with a squared-Euclidean distance of two and an average of 1/2 paths with a squared-Euclidean distance of 2.586, both associated with one information bit error. Moreover, equation (4.18) implies that there are an average of 1/2 paths with a squared-Euclidean distance of 2.586 and an average of 1/2 paths with a squared-Euclidean distance of 3.172, both associated with two information bit errors, and so on for higher powers of *X*.

Taking the derivative of equation (4.18) with respect to *Y*, we get

$$\left.\frac{\partial T_{ave}(X,Y)}{\partial Y}\right|_{Y=1} = X^2 + \frac{1}{2}X^{2.586} + X^{2.586} + X^{3.172} + \frac{3}{2}X^{3.172} + \ldots \quad (4.19)$$

which can be simplified to

$$\left.\frac{\partial T_{ave}(X,Y)}{\partial Y}\right|_{Y=1} = X^2 + \frac{3}{2}X^{2.586} + \frac{5}{2}X^{3.172} + \ldots \quad (4.20)$$

Comparing equations (4.20) and (4.10) and using the result in equation (4.7), we get

$$P_b < 0.5Q\left(\sqrt{\frac{2E_b}{N_0}}\right) + 0.75Q\left(\sqrt{\frac{2.586E_b}{N_0}}\right) + 1.25Q\left(\sqrt{\frac{3.172E_b}{N_0}}\right) + \ldots \quad (4.21)$$

which can be approximated using only the first term when $E_b/N_o >> 1$.

2. Probability Bit Error Analysis for K=2

In this case we use the rate $r=2/3$ convolution encoder with two memory elements (K=2) which shown in Figure 67. The state diagram is obtained with the assistance of Table 11 and shown in Figure 68.

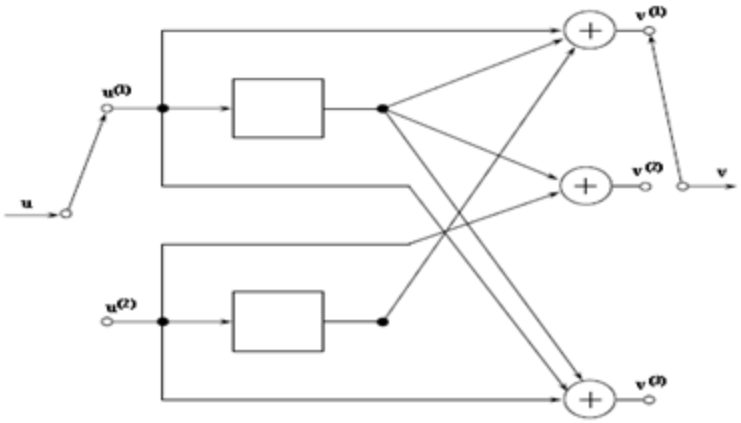

Figure 67. Rate $r=2/3$, K=2 convolutional encoder.

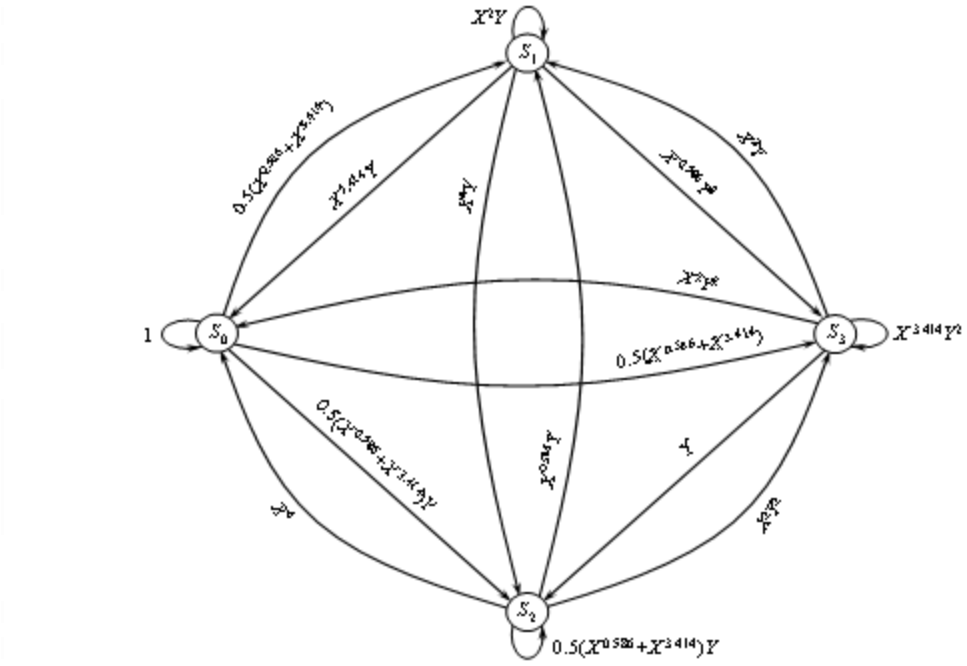

Figure 68. State diagram for $r=2/3$, K=2 convolutional encoder for TCM with 8-PSK and natural mapping.

As with K=1, we use Figure 68 to obtain the AIOWEF :

$$T_{ave}(X,Y) = \frac{1}{4}X^{1.758}Y^2 + \frac{1}{8}X^{2.344}Y^3 + \frac{1}{4}X^{2.344}Y^4 + \frac{1}{2}X^{2.586}Y^2 + \frac{1}{2}X^{3.172}Y^4 + \frac{1}{4}X^{3.172}Y^3 + \ldots \tag{4.22}$$

By inspection of equation (4.22) we see that for an arbitrary sequence of code bits there are an average of 1/4 paths with a squared-Euclidean distance of 1.758 and an average of 1/2 paths with a squared-Euclidean distance of 2.586, both associated with two information bit errors. Moreover, equation (4.22) implies that there are an average of 1/8 paths with a squared-Euclidean distance of 2.344 and an average of 1/4 paths with a squared-Euclidean distance of 3.172, both associated with three information bit errors, and so on.

From equation (4.22),

$$\left.\frac{\partial T_{ave}(X,Y)}{\partial Y}\right|_{Y=1} = \frac{1}{2}X^{1.758} + \frac{11}{8}X^{2.344} + X^{2.586} + \frac{11}{4}X^{3.172} + \ldots \qquad (4.23)$$

Comparing equations (4.23) and (4.10) and using the result in equation (4.7), we get

$$P_b < 0.25Q\left(\sqrt{\frac{1.758E_b}{N_0}}\right) + 0.6875Q\left(\sqrt{\frac{2.344E_b}{N_0}}\right) + 0.5Q\left(\sqrt{\frac{2.586E_b}{N_0}}\right) + 1.375Q\left(\sqrt{\frac{3.172E_b}{N_0}}\right)\ldots \qquad (4.24)$$

which can be approximated by the first term for $E_b/No >> 1$.

3. Probability Bit Error Analysis for K=3

In this case we use the rate r=2/3 convolution encoder with three memory elements (K=3) shown in Figure 69. The error trellis is obtained with the assistance of Table 11 and shown in Figure 70.

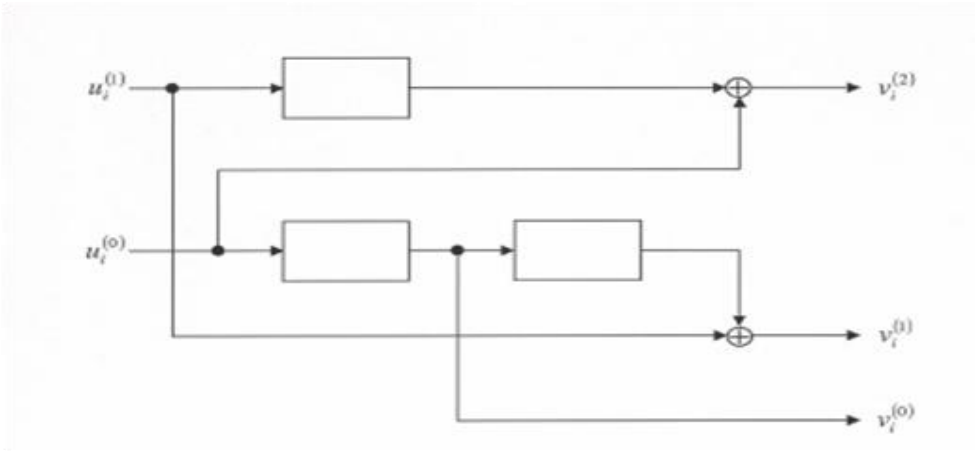

Figure 69. Rate r=2/3, K=3 convolutional encoder. (From: [5]).

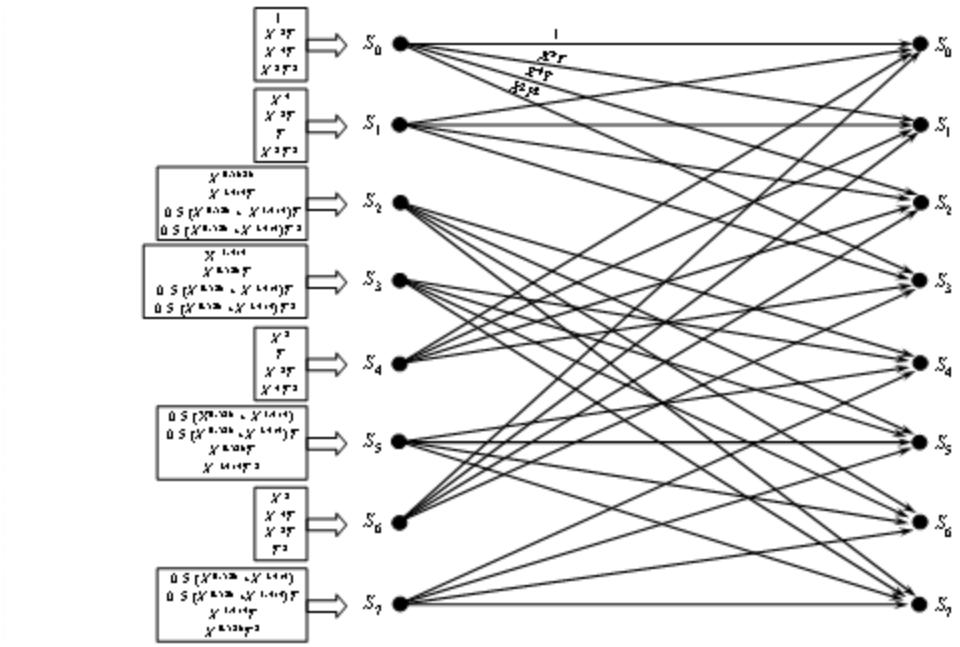

Figure 70. Error trellis for r=2/3, K=3 convolutional encoder for TCM with 8-PSK and natural mapping.

As before, we can now obtain the AIOWEF :

$$T_{ave}(X,Y) = X^{4.586}Y^2 + \frac{1}{2}X^{4.586}Y^3 + \frac{1}{2}X^{4.586}Y^3 + \ldots \qquad (4.25)$$

By inspection of equation (4.25), we see that for an arbitrary sequence of code bits there is an average of one path with a squared-Euclidean distance of 4.586 associated with two information bit errors. Moreover, equation (4.25) implies that there are an average of one code path with a squared-Euclidean distance of 4.586 associated with three information bit errors, and so on.

From equation (4.25), we derive

$$\left.\frac{\partial T_{ave}(X,Y)}{\partial Y}\right|_{Y=1} = 2X^{4.586} + \frac{3}{2}X^{4.586} + \frac{3}{2}X^{4.586}\ldots \qquad (4.26)$$

Comparing equations (4.26) and (4.10) and using the result in equation (4.7), we get

$$P_b \approx 2.5Q\left(\sqrt{\frac{4.586E_b}{N_0}}\right) \tag{4.27}$$

where only the first term is shown since it dominates the series for $E_b/No>>1$.

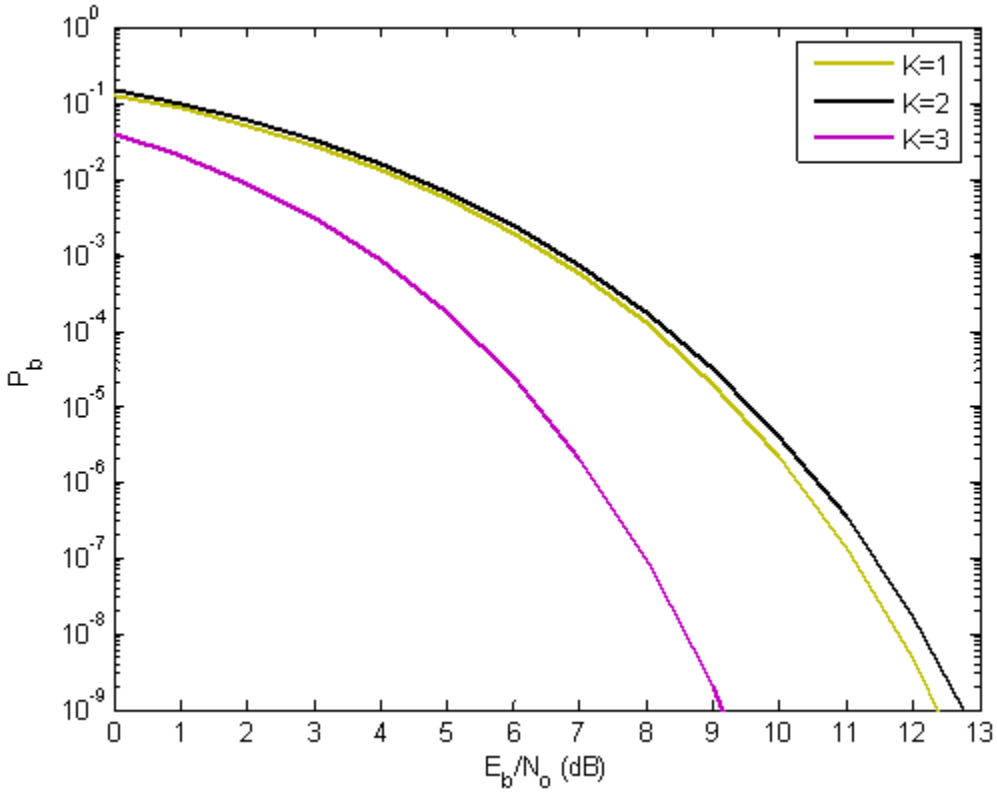

Figure 71. Probability bit error of TCM signals with 8-PSK and r=2/3 convolution encoding with K=1, 2, and 3 in AWGN.

In Figure 71 we observe the probability bit error of TCM signals with 8-PSK and r=2/3 convolution encoding with K=1, 2 and 3 in AWGN. An interesting result is that performance is better with K=1 than with K=2. As the number of memory elements increases (K≥3), performance improves. Figure 72 is a magnified version of Figure 71, and from this figure we see that, in order to achieve $P_b=10^{-5}$, E_b/N_o=9.27 dB is required for K=1, E_b/N_o=9.54 dB for K=2, and E_b/N_o=6.34 dB for K=3. The relative difference in E_b/N_o between K=1 and K=3 is 3.2 dB.

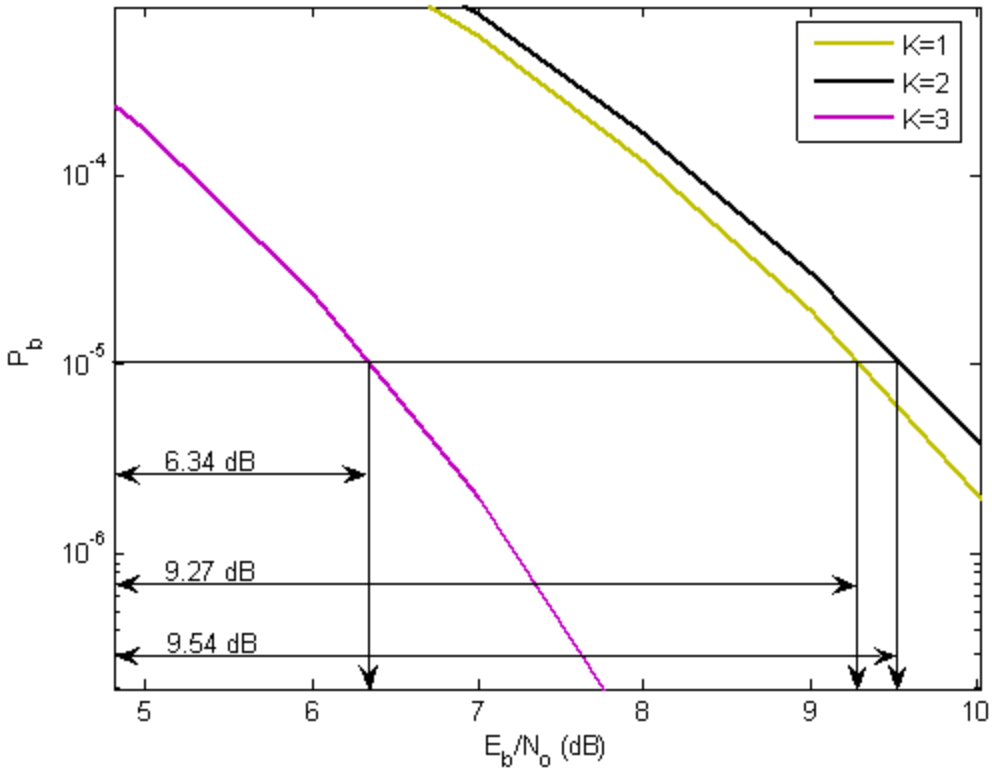

Figure 72. Magnified probability bit error of TCM signals with 8-PSK and r=2/3 convolution encoding with K=1, 2, and 3 in AWGN.

If we compare Figure 72 with Figure 63, we observe that, with the exception of K=2, TCM signals with 8-PSK and r=2/3 convolution encoding is superior in AWGN.

For K=1 and $P_b=10^{-5}$, E_b/N_o=9.66 dB is required for TCM signals transmitted independently on the I and Q channels and modulated with 4-PAM and r=1/2 convolution encoding, while E_b/N_o=9.27 dB is required for TCM with 8-PSK and r=2/3 convolution encoding. The relative difference in E_b/N_o is 0.39 dB for K=1. For K=2, E_b/N_o=7.35 dB is required for the first case and E_b/N_o=9.54 dB is required for the second case. The relative difference in E_b/N_o is -2.19 dB. When the number of memory elements increases to K=3, E_b/N_o=7.01 dB is required for the first case and E_b/N_o=6.34 dB is required for the second case. The relative difference in E_b/N_o is 0.67 dB.

Table 12 is an overview of the preceding results.

Table 12. Probability bit error of TCM with different modulation and code rates in AWGN when $P_b=10^{-5}$.

K	E_b/N_o for TCM with 4-PAM and r=1/2 encoding	E_b/N_o for TCM with 8-PSK and r=2/3 encoding	E_b/N_o difference
1	9.66 dB	9.27 dB	0.39 dB
2	7.35 dB	9.54 dB	-2.19 dB
3	7.01 dB	6.34 dB	0.67 dB

We first compare the two systems under consideration when the two TCM systems have the same number of memory elements. In other words, if the r=2/3 encoder has K memory elements, then each of the r=1/2 encoders has K/2 memory elements for a total of K memory elements. Second, we compare the two different TCM systems when the r=2/3 encoder has K memory elements and each of the r=1/2 encoders has K memory elements for a total of 2K memory elements. In Table 12 the relative difference in E_b/N_o calculated for $P_b=10^{-5}$ is based on the second way of comparison where the r=1/2 encoders have a memory element advantage.

If we compare the performance of the two TCM systems for K=3, we see from Table 12 that TCM with 8-PSK and r=2/3 convolutional encoding has a slightly better performance of 0.67 dB. In this case the improvement in coding gain can be sacrificed in order to reduce decoding complexity. For K=2 we combine better coding gain (2.19 dB) and reduced decoding complexity.

Using the first way of comparison, we see that for K=2, TCM with 8-PSK and r=2/3 convolutional encoding has a slightly better performance (0.12 dB).

Generally, if we consider both coding gain improvement and decoding complexity, TCM signals transmitting data independently on the I and Q channels, each modulated with 4-PAM and r=1/2 TCM, are preferred since the coding gain disadvantage, when it exists, is insignificant (a maximum of 0.67 dB) compared to the advantage of decreased decoding complexity.

Table 13 is a review of the probability of sequence error results from Figure 50 and Figure 53. The overall performance as the number of memory elements increases is much better for the TCM system with r=2/3 convolutional encoding and 8-PSK.

Table 13. Probability sequence error of TCM signals with different modulation and code rates in AWGN when $P_E = 10^{-5}$.

K	E_b/N_o for TCM with 4-PAM and r=1/2 encoding	E_b/N_o for TCM with 8-PSK and r=2/3 encoding	E_b/N_o difference
2	7.59 dB	6.53 dB	1.06 dB
3	7.13 dB	6.25 dB	0.88 dB
4	7.01 dB	5.81 dB	1.2 dB
6	6.48 dB	5.25 dB	1.23 dB
7	6.12 dB	4.08 dB	2.04 dB
8		4.02 dB	

In Table 13 the relative E_b/N_o difference for $P_E = 10^{-5}$ is based on the second way of comparison where the r=1/2 encoder has a memory element advantage. As we can see the maximum relative E_b/N_o difference for $P_E = 10^{-5}$ is 2.04 dB.

When the two TCM systems are compared for the same number of memory elements, TCM with 8-PSK and r=2/3 convolutional encoding is superior. From Table 13, we see that if each of the r=1/2 encoders in the 4-PAM system has K=2 memory elements for a total of K=4, then E_b/N_o=7.59 dB is required, but only E_b/N_o=5.81 dB is required for 8-PSK, r=2/3 TCM. The relative E_b/N_o difference is 1.78 dB. If each of the r=1/2 encoders in the 4-PAM system has K=3 memory elements for a total of K=6, then E_b/N_o=7.13 dB is required, but only E_b/N_o=5.25 dB is required for 8-PSK, r=2/3 TCM. The relative E_b/N_o difference is 1.88 dB. Finally, if each of the r=1/2 encoders in the 4-

PAM system has K=4 memory elements for a total of K=8, then E_b/N_o=7.01 dB is required, but only E_b/N_o=4.02 dB is required for 8-PSK, r=2/3 TCM. The relative E_b/N_o difference is 2.99 dB.

From the previous performance results of probability of sequence error we derive that as K increases we can not sacrifice the coding gain advantage for the reduced decoding complexity because the maximum relative E_b/N_o difference value is 2.99 dB which is a significant improvement.

E. PERFORMANCE ANALYSIS OF TCM SIGNALS IN PNI

For TCM systems with no parallel transitions in the error trellis, the probability of bit error when only AWGN is present can be upper bounded by [4]

$$P_b < \frac{1}{m}\sum_{i=1}^{\infty} B_{d_i^2} Q\left(\sqrt{\frac{E_{s_c} d_i^2}{2N_0}}\right) \tag{4.28}$$

where m is the number of information bits per code symbol, $E_{sc} = r(m+1)E_b$, $B_{d_i^2}$ is the total number of information bit ones on all error paths that are a squared-Euclidean distance d_i^2 from the all-zero error path, and $d_1^2 = d_{free}^2$.

In order to calculate the $B_{d_i^2}s$ from the average input-output weight enumerating function (AIOWEF), we use a procedure analogous to that used for conventional convolutional codes. The relationship is given by [4]

$$\left.\frac{\partial T_{ave}(X,Y)}{\partial Y}\right|_{Y=1} = \sum_{i=1}^{\infty} B_{d_i^2} X^{d_i^2} \tag{4.29}$$

where $T_{ave}(X,Y)$ is the AIOWEF.

For a TCM system in a PNI environment, in order to calculate the probability of bit error, each path through the trellis must be treated independently. Bits that are received may be affected differently by the channel since some are affected only by AWGN while some are affected by both AWGN and PNI. The PSD of AWGN is N_o, and the PSD of barrage noise interference is N_I. For PNI, the interference PSD is N_I/ρ, where

ρ is the fraction of the time the PNI is on. The total noise PSD due to AWGN plus PNI at the receiver is

$$N_T = \begin{cases} N_o & \text{with probability } (1-\rho) \\ N_o + \dfrac{N_I}{\rho} & \text{with probability } \rho \end{cases} \tag{4.30}$$

We define the average probability $P_{d_i^2,l_k}$ of selecting a code sequence of l_k branches that have a squared-Euclidean distance d_i^2 from the correct code sequence as

$$P_{d_i^2,l_k} = \sum_{i=0}^{l_k} \binom{l_k}{i} \rho^i (1-\rho)^{l_k - i} P_{d_i^2,l_k}(i) \tag{4.31}$$

where $P_{d_i^2,l_k}(i)$ is the conditional probability that i of the l_k branches are affected by both AWGN and PNI while the remaining (l_k-i) branches are affected only by AWGN.
Now the probability of bit error is upper bounded by

$$P_b < \frac{1}{m} \sum_{i=1}^{\infty} \frac{1}{\lambda_{d_i^2}} \sum_{l_k = l_{\min}}^{\infty} \sum_{k=1}^{\infty} B_{d_i^2,l_k} P_{d_i^2,l_k} \tag{4.32}$$

where $B_{d_i^2,l_k}$ is the total number of information bit ones on the k^{th} error path consisting of l_k branches that are a squared- Euclidean distance of d_i^2 from the all-zero error path, and $\lambda_{d_i^2}$ is the total number of error paths that are a squared- Euclidean distance of d_i^2 from the all-zero error path regardless of length. When PNI is not present, it is clear that equation (4.32) simplifies to equation (4.28) as expected. A tight upper bound on equation (4.32) is obtained from

$$P_b < \frac{1}{m} \sum_{i=1}^{\infty} \frac{B_{d_i^2}}{\lambda_{d_i^2}} \sum_{l_k = l_{\min}}^{\infty} \sum_{k=1}^{\infty} P_{d_i^2,l_k} \tag{4.33}$$

Since the probability of bit error P_b depends on the particular code sequence transmitted, we cannot derive a general formula which applies to each case but must evaluate it independently for different TCM systems with different codes and code rates.

F. PERFORMANCE ANALYSIS OF TCM SIGNALS TRANSMITTED INDEPENDENTLY ON THE I AND Q CHANNELS IN AWGN AND PNI

In this section we examine the performance of TCM signals transmitted independently on the I and Q channels. Each TCM signal is modulated with 4-PAM and encoded with a rate r=1/2 convolution code. The effect of varying the number of encoder memory elements is examined for both AWGN and PNI. This system has the same spectral efficiency as TCM with 8-PSK modulation and r=2/3 encoding. For TCM signals implemented with 4-PAM modulation and r=1/2 convolutional encoding, m=1, and $E_{sc}=E_b$ since r=1/2.

1. Probability Bit Error Analysis for K=1

We first obtain P_b for TCM with the rate r=1/2 convolution encoder with one memory element (K=1) shown in Figure 55. The corresponding signal flow graph for Gray mapped 4-PAM/TCM is shown in Figure 56. From the signal flow graph shown in Figure 56, we derived the AIOWEF in part C of Chapter IV, and obtained

$$T_{ave}(X,Y) = X^4Y + \left(\frac{X^{4.8}}{2} + \frac{X^{11.2}}{2}\right)Y^2 + \left(\frac{X^{5.6}}{4} + \frac{X^{12}}{2} + \frac{X^{18.4}}{4}\right)Y^3 + \frac{X^4\left(X^{0.8} + X^{7.2}\right)^3}{8}Y^4 + \ldots \quad (4.34)$$

Comparing

$$\left.\frac{\partial T_{ave}(X,Y)}{\partial Y}\right|_{Y=1} = X^4 + X^{4.8} + \frac{3}{4}X^{5.6} + \frac{X^{6.4}}{2} + \frac{5X^{7.2}}{16} + \frac{6X^8}{32} + X^{11.2} + \frac{3}{2}X^{12} + \ldots \quad (4.35)$$

with equation (4.29), we obtain the squared-Euclidean distance and the total information weight for all paths having the same squared-Euclidean distance. For example, from Figure 56 the minimum squared-Euclidean distance corresponds to path $S_i - S_1 - S_o$, d^2_{free}=4, and λ_4=1. The average information weight of this path is B_4=1. There is only one path $S_i - S_1 - S_1 - S_o$ with a squared-Euclidean distance d^2=4.8, so $\lambda_{4.8}$=1 and the total average information weight is $B_{4.8}$=1. Similarly there is only one path $S_i - S_1 - S_1 - S_1 - S_o$ with a squared-Euclidean distance d^2=5.6, so $\lambda_{5.6}$=1 and the total

average information weight is $B_{5.6}$=3/4. Applying a similar procedure, we can obtain the squared-Euclidean distance and total information weight of each path on the signal flow graph.

Using the first three terms in the outer summation of equation (4.33), we obtain

$$P_b \approx B_4 P_{4,2_1} + B_{4.8} P_{4.8,3_1} + B_{5.6} P_{5.6,4_1} + \ldots \tag{4.36}$$

From equation (4.31) we get

$$\begin{aligned} P_{4,2_1} &= \binom{2}{0}(1-\rho)^2 Q\left(\sqrt{\frac{E_b}{N_0}\frac{4}{2}}\right) \\ &+ \binom{2}{1}\rho(1-\rho)\left[\frac{1}{2}Q\left(\sqrt{\frac{E_b}{2}\left(\frac{0.8}{N_0}+\frac{3.2}{N_T}\right)}\right)+\frac{1}{2}Q\left(\sqrt{\frac{E_b}{2}\left(\frac{3.2}{N_0}+\frac{0.8}{N_T}\right)}\right)\right] \\ &+ \binom{2}{2}\rho^2 Q\left(\sqrt{\frac{E_b}{N_T}\frac{4}{2}}\right) \end{aligned} \tag{4.37}$$

and

$$\begin{aligned} P_{4.8,3_1} &= \binom{3}{0}(1-\rho)^3 Q\left(\sqrt{\frac{E_b}{N_0}\frac{4.8}{2}}\right) \\ &+ \binom{3}{1}\rho(1-\rho)^2\left[\frac{1}{3}Q\left(\sqrt{\frac{E_b}{2}\left(\frac{1.6}{N_0}+\frac{3.2}{N_T}\right)}\right)+\frac{2}{3}Q\left(\sqrt{\frac{E_b}{2}\left(\frac{4}{N_0}+\frac{0.8}{N_T}\right)}\right)\right] \\ &+ \binom{3}{2}\rho^2(1-\rho)\left[\frac{2}{3}Q\left(\sqrt{\frac{E_b}{2}\left(\frac{0.8}{N_0}+\frac{4}{N_T}\right)}\right)+\frac{1}{3}Q\left(\sqrt{\frac{E_b}{2}\left(\frac{3.2}{N_0}+\frac{1.6}{N_T}\right)}\right)\right] \\ &+ \binom{3}{3}\rho^3 Q\left(\sqrt{\frac{E_b}{N_T}\frac{4.8}{2}}\right) \end{aligned} \tag{4.38}$$

and

$$
\begin{aligned}
P_{5.6,4_1} &= \binom{4}{0}(1-\rho)^4 Q\left(\sqrt{\frac{E_b}{N_0}\frac{5.6}{2}}\right) \\
&+ \binom{4}{1}\rho(1-\rho)^3\left[\frac{1}{2}Q\left(\sqrt{\frac{E_b}{2}\left(\frac{4.8}{N_0}+\frac{0.8}{N_T}\right)}\right)+\frac{1}{4}Q\left(\sqrt{\frac{E_b}{2}\left(\frac{2.4}{N_0}+\frac{3.2}{N_T}\right)}\right)+\frac{1}{4}Q\left(\sqrt{\frac{E_b}{2}\left(\frac{4.8}{N_0}+\frac{0.8}{N_T}\right)}\right)\right] \\
&+ \binom{4}{2}\rho^2(1-\rho)^2\left[\frac{1}{3}Q\left(\sqrt{\frac{E_b}{2}\left(\frac{1.6}{N_0}+\frac{4}{N_T}\right)}\right)+\frac{1}{2}Q\left(\sqrt{\frac{E_b}{2}\left(\frac{4}{N_0}+\frac{1.6}{N_T}\right)}\right)+\frac{1}{6}Q\left(\sqrt{\frac{E_b}{2}\left(\frac{1.6}{N_0}+\frac{4}{N_T}\right)}\right)\right] \\
&+ \binom{4}{3}\rho^3(1-\rho)\left[\frac{3}{4}Q\left(\sqrt{\frac{E_b}{2}\left(\frac{0.8}{N_0}+\frac{4.8}{N_T}\right)}\right)+\frac{1}{4}Q\left(\sqrt{\frac{E_b}{2}\left(\frac{3.2}{N_0}+\frac{2.4}{N_T}\right)}\right)\right] \\
&+ \binom{4}{4}\rho^4 Q\left(\sqrt{\frac{E_b}{N_T}\frac{5.6}{2}}\right)
\end{aligned}
\tag{4.39}
$$

The performance of TCM signals transmitting on the I and Q channels with 4-PAM and rate r=1/2 convolution encoding in both AWGN and PNI for K=1 is shown in Figure 73. The results in Figure 73 are obtained for E_b/N_o=12 dB, which results in $P_b=10^{-8}$ when $E_b/N_I>>1$. As can be seen, PNI degrades system performance much more than BNI except for $E_b/N_I>>1$ when performance is dominated by E_b/N_o.

Figure 74 is a magnified version of Figure 73, and from Figure 74 we see that in order to achieve $P_b=10^{-5}$, which is a practical performance target for many digital communications systems, we require E_b/N_I=13.5 dB for BNI, while E_b/N_I=24.24 dB is required for PNI with ρ=0.01. The relative degradation in E_b/N_I between BNI and PNI for the worst case ρ is 10.74 dB for K=1 and E_b/N_o=12 dB.

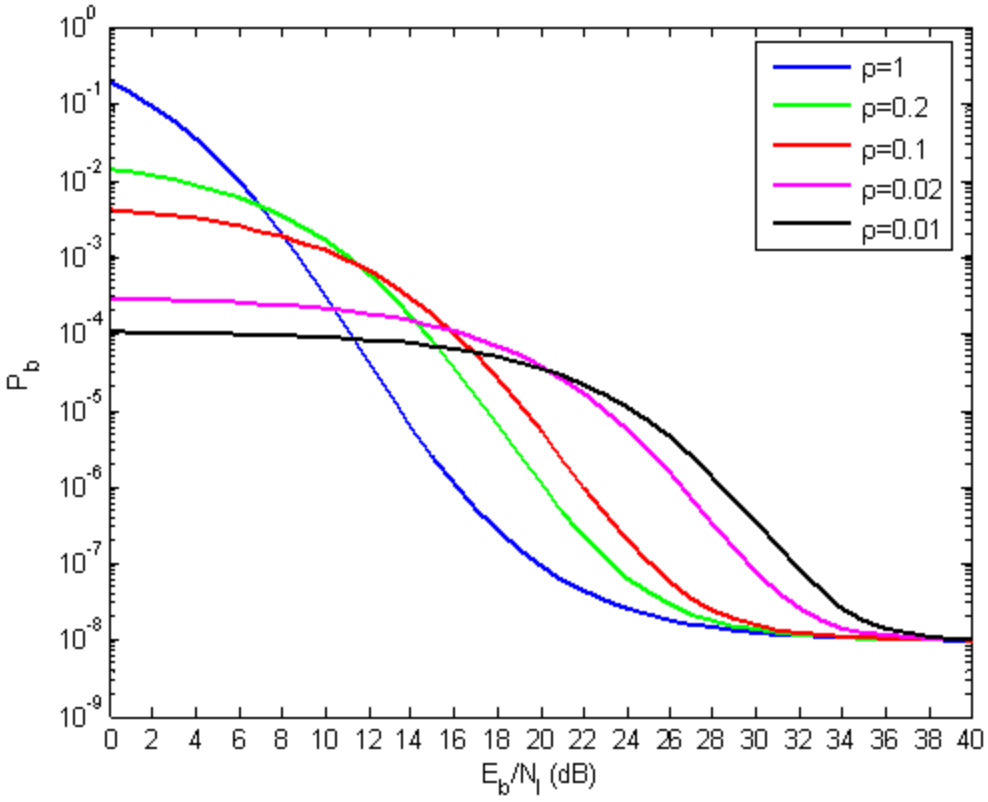

Figure 73. Probability bit error of TCM signals transmitting data independently on the I and Q channels, each modulated with 4-PAM waveforms encoded with a rate r=1/2 convolutional code for K=1 in both AWGN and PNI.

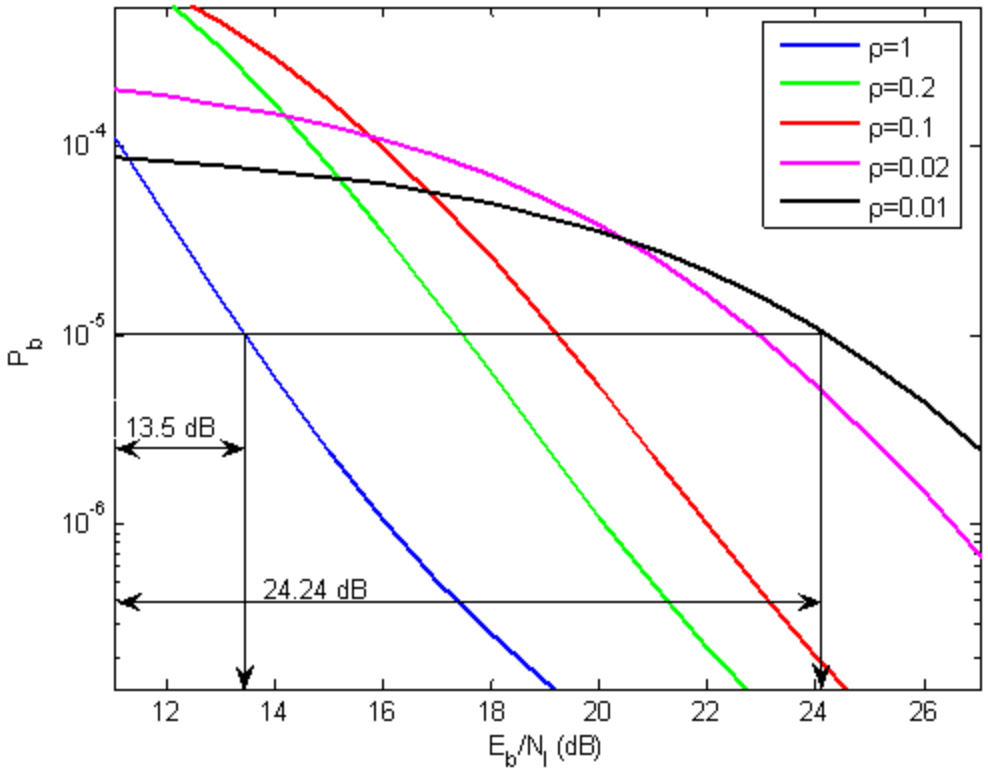

Figure 74. Magnified probability bit error of TCM signals transmitting data independently on the I and Q channels, each modulated with 4-PAM waveforms encoded with a rate r=1/2 convolution code for K=1 in both AWGN and PNI.

2. Probability Bit Error Analysis for K=2

In this subsection we obtain P_b for the TCM system with the r=1/2 convolutional encoder with two memory elements (K=2) shown in Figure 57. The corresponding signal flow graph for Gray mapped 4-PAM/TCM is shown in Figure 59.

Equation (2.14) from part F of Chapter II is

$$\left.\frac{\partial T_{ave}(X,Y)}{\partial Y}\right|_{Y=1} = \frac{X^{7.2}}{2} + \frac{5X^{8.0}}{2} + \frac{39X^{8.8}}{8} + \frac{33X^{9.6}}{4} + \ldots \qquad (4.40)$$

Comparing equation (4.40) with equation (4.29), we obtain the squared-Euclidean distance and the total information weight for all paths having the same squared-Euclidean distance. For example, from Figure 59 the minimum squared-Euclidean distance

corresponds to path $S_i - S_1 - S_2 - S_o$, d^2_{free}=7.2, and $\lambda_{7.2}$=1. The average information weight of this path is $B_{7.2}$=1/2. There are two paths with a squared-Euclidean distance d^2=8, so λ_8=2, and the total average information weight is B_8=5/2. The first path, $S_i - S_1 - S_3 - S_2 - S_o$, has four branches, and the second path, $S_i - S_1 - S_2 - S_1 - S_2 - S_o$, has five branches. As a result, the average probability $P_{d_i^2, l_k}$ for these two paths cannot be calculated in the same way. Applying a similar procedure, we can obtain the squared-Euclidean distance and total information weight of each path on the signal flow graph.

Using the first two terms in the outer summation of equation (4.33), we obtain

$$P_b \approx B_{7.2} P_{7.2,3_1} + \frac{1}{2} B_8 P_{8,4_1} + \frac{1}{2} B_8 P_{8,5_1} + \ldots \tag{4.41}$$

From equation (4.31), we get

$$\begin{aligned} P_{7.2,3_1} &= \binom{3}{0}(1-\rho)^3 Q\left(\sqrt{\frac{E_b}{N_0}\frac{7.2}{2}}\right) \\ &+ \binom{3}{1}\rho(1-\rho)^2\left[\frac{1}{3}Q\left(\sqrt{\frac{E_b}{2}\left(\frac{6.4}{N_0}+\frac{0.8}{N_T}\right)}\right)+\frac{2}{3}Q\left(\sqrt{\frac{E_b}{2}\left(\frac{4}{N_0}+\frac{3.2}{N_T}\right)}\right)\right] \\ &+ \binom{3}{3}\rho^2(1-\rho)\left[\frac{1}{3}Q\left(\sqrt{\frac{E_b}{2}\left(\frac{0.8}{N_0}+\frac{6.4}{N_T}\right)}\right)+\frac{2}{3}Q\left(\sqrt{\frac{E_b}{2}\left(\frac{3.2}{N_0}+\frac{4}{N_T}\right)}\right)\right] \\ &+ \binom{3}{3}\rho^3 Q\left(\sqrt{\frac{E_b}{N_T}\frac{7.2}{2}}\right) \end{aligned} \tag{4.42}$$

and

$$
\begin{aligned}
P_{8,4_1} &= \binom{4}{0}(1-\rho)^4 Q\left(\sqrt{\frac{E_b}{N_0}\frac{8}{2}}\right) \\
&+ \binom{4}{1}\rho(1-\rho)^3\left[\frac{1}{2}Q\left(\sqrt{\frac{E_b}{2}\left(\frac{7.2}{N_0}+\frac{0.8}{N_T}\right)}\right)+\frac{1}{2}Q\left(\sqrt{\frac{E_b}{2}\left(\frac{4.8}{N_0}+\frac{3.2}{N_T}\right)}\right)\right] \\
&+ \binom{4}{2}\rho^2(1-\rho)^2\left[\frac{4}{6}Q\left(\sqrt{\frac{E_b}{2}\left(\frac{4}{N_0}+\frac{4}{N_T}\right)}\right)+\frac{1}{6}Q\left(\sqrt{\frac{E_b}{2}\left(\frac{1.6}{N_0}+\frac{6.4}{N_T}\right)}\right)+\frac{1}{6}Q\left(\sqrt{\frac{E_b}{2}\left(\frac{6.4}{N_0}+\frac{1.6}{N_T}\right)}\right)\right] \\
&+ \binom{4}{3}\rho^3(1-\rho)\left[\frac{1}{2}Q\left(\sqrt{\frac{E_b}{2}\left(\frac{0.8}{N_0}+\frac{7.2}{N_T}\right)}\right)+\frac{1}{2}Q\left(\sqrt{\frac{E_b}{2}\left(\frac{3.2}{N_0}+\frac{4.8}{N_T}\right)}\right)\right] \\
&+ \binom{4}{4}\rho^4 Q\left(\sqrt{\frac{E_b}{N_T}\frac{8}{2}}\right)
\end{aligned}
\tag{4.43}
$$

and

$$
\begin{aligned}
P_{8,5_1} &= \binom{5}{0}(1-\rho)^5 Q\left(\sqrt{\frac{E_b}{N_0}\frac{8}{2}}\right) \\
&+ \binom{5}{1}\rho(1-\rho)^4\left[\frac{2}{5}Q\left(\sqrt{\frac{E_b}{2}\left(\frac{4.8}{N_0}+\frac{3.2}{N_T}\right)}\right)+\frac{2}{5}Q\left(\sqrt{\frac{E_b}{2}\left(\frac{7.2}{N_0}+\frac{0.8}{N_T}\right)}\right)+\frac{1}{5}Q\left(\sqrt{\frac{E_b}{2}\left(\frac{8}{N_0}\right)}\right)\right] \\
&+ \binom{5}{2}\rho^2(1-\rho)^3\left[\begin{array}{l}\frac{4}{10}Q\left(\sqrt{\frac{E_b}{2}\left(\frac{4}{N_0}+\frac{4}{N_T}\right)}\right)+\frac{2}{10}Q\left(\sqrt{\frac{E_b}{2}\left(\frac{4.8}{N_0}+\frac{3.2}{N_T}\right)}\right)+\frac{1}{10}Q\left(\sqrt{\frac{E_b}{2}\left(\frac{1.6}{N_0}+\frac{6.4}{N_T}\right)}\right) \\ +\frac{1}{10}Q\left(\sqrt{\frac{E_b}{2}\left(\frac{6.4}{N_0}+\frac{1.6}{N_T}\right)}\right)+\frac{2}{10}Q\left(\sqrt{\frac{E_b}{2}\left(\frac{7.2}{N_0}+\frac{0.8}{N_T}\right)}\right)\end{array}\right] \\
&+ \binom{5}{3}\rho^3(1-\rho)^2\left[\begin{array}{l}\frac{1}{10}Q\left(\sqrt{\frac{E_b}{2}\left(\frac{6.4}{N_0}+\frac{1.6}{N_T}\right)}\right)+\frac{1}{10}Q\left(\sqrt{\frac{E_b}{2}\left(\frac{1.6}{N_0}+\frac{6.4}{N_T}\right)}\right)+\frac{2}{10}Q\left(\sqrt{\frac{E_b}{2}\left(\frac{0.8}{N_0}+\frac{7.2}{N_T}\right)}\right) \\ +\frac{4}{10}Q\left(\sqrt{\frac{E_b}{2}\left(\frac{4}{N_0}+\frac{4}{N_T}\right)}\right)+\frac{2}{10}Q\left(\sqrt{\frac{E_b}{2}\left(\frac{3.2}{N_0}+\frac{4.8}{N_T}\right)}\right)\end{array}\right] \\
&+ \binom{5}{4}\rho^4(1-\rho)\left[\frac{2}{5}Q\left(\sqrt{\frac{E_b}{2}\left(\frac{3.2}{N_0}+\frac{4.8}{N_T}\right)}\right)+\frac{2}{5}Q\left(\sqrt{\frac{E_b}{2}\left(\frac{0.8}{N_0}+\frac{7.2}{N_T}\right)}\right)+\frac{1}{5}Q\left(\sqrt{\frac{E_b}{2}\left(\frac{8}{N_T}\right)}\right)\right] \\
&+ \binom{5}{5}\rho^5 Q\left(\sqrt{\frac{E_b}{N_T}\frac{8}{2}}\right)
\end{aligned}
\tag{4.44}
$$

The performance with K=2 is shown in Figures 75 and 76. The results in Figure 75 and 76 are obtained for E_b/N_o=9.4 dB, which results in $P_b=10^{-8}$ when $E_b/N_I>>1$. As can be seen, PNI degrades system performance much more than BNI except for $E_b/N_I>>1$, when performance is dominated by E_b/N_o.

For $P_b=10^{-5}$, we require E_b/N_I=11.12 dB for BNI, while E_b/N_I=14.44 dB is required for PNI with ρ=0.1. The relative degradation in E_b/N_I between BNI and PNI for the worst case ρ is 3.32 dB for K=2 and E_b/N_o=9.4 dB.

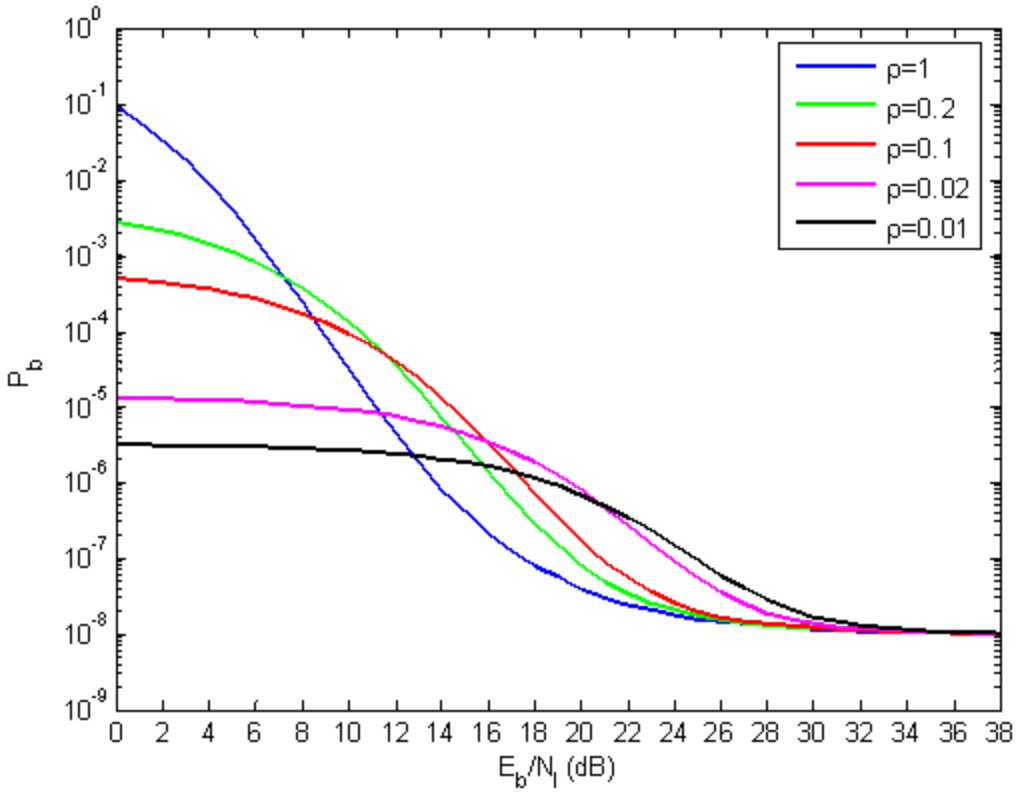

Figure 75. Probability bit error of TCM signals transmitting data independently on the I and Q channels, each modulated with 4-PAM waveforms encoded with a rate r=1/2 convolution code for K=2 in both AWGN and PNI.

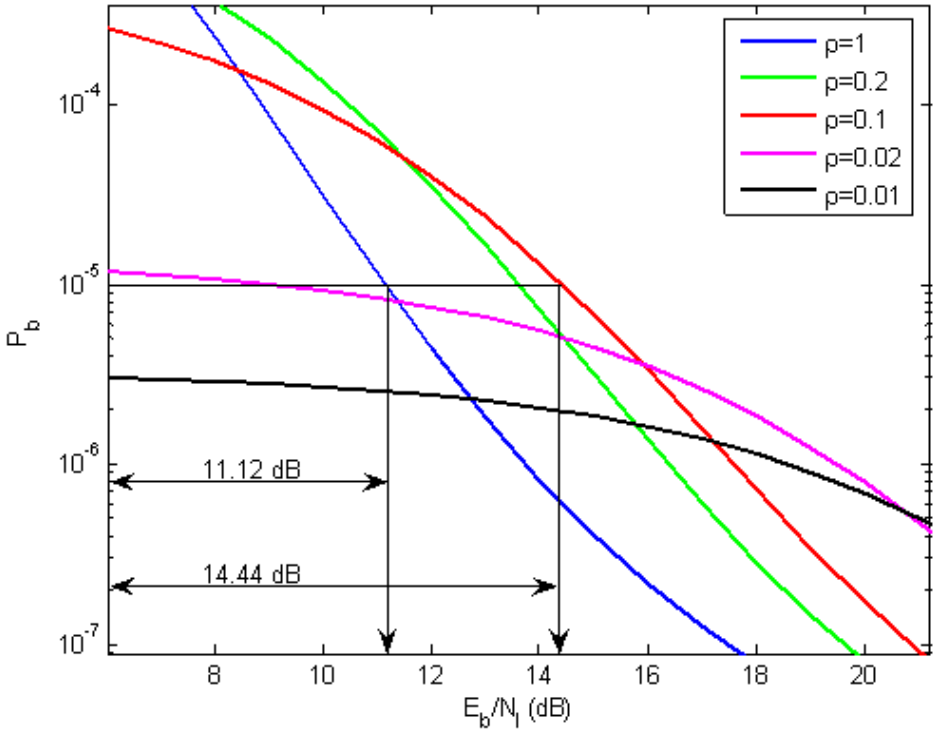

Figure 76. Magnified probability bit error of TCM signals transmitting data independently on the I and Q channels, each modulated with 4-PAM waveforms encoded with a rate r=1/2 convolution code for K=2 in both AWGN and PNI.

3. Probability Bit Error Analysis for K=3

In this subsection we obtain P_b for the TCM system with the r=1/2 convolutional encoder with three memory elements (K=3) shown in Figure 60. The corresponding signal flow graph for Gray mapped 4-PAM/TCM is shown in Figure 61.

Equation (4.16) from part C of Chapter IV is

$$\left.\frac{\partial T_{ave}(X,Y)}{\partial Y}\right|_{Y=1} = \frac{X^8}{2} + 3X^{8.8} + 6.25X^{9.6} + 8.5X^{10.4} + \ldots \qquad (4.45)$$

Comparing equation (4.45) with equation (4.29), we obtain the squared-Euclidean distance and the total information weight for all paths having the same squared-Euclidean distance. For example, from Figure 61 the minimum squared-Euclidean distance

corresponds to path $S_i - S_1 - S_3 - S_6 - S_4 - S_o$, d^2_{free}=8, and λ_8=1. The average information weight of this path is B_8=1/2. There are two paths with a squared-Euclidean distance d^2=8.8, so $\lambda_{8.8}$=2, and the total average information weight is $B_{8.8}$=3. The first path, $S_i - S_1 - S_3 - S_7 - S_6 - S_4 - S_o$, has six branches, and the second path, $S_i - S_1 - S_2 - S_5 - S_3 - S_6 - S_4 - S_o$, has seven branches. As a result, the average probability $P_{d_i^2, l_k}$ for these two paths cannot be calculated in the same way. Applying a similar procedure, we can obtain the squared-Euclidean distance and total information weight of each path on the signal flow graph.

Using the first two terms in the outer summation of equation (4.33), we obtain

$$P_b \approx B_8 P_{8,5_1} + \frac{1}{2} B_{8.8} P_{8.8,6_1} + \frac{1}{2} B_{8.8} P_{8.8,7_1} + \ldots \tag{4.46}$$

From equation (4.31) we get

$$\begin{aligned}
P_{8,5_1} = {} & \binom{5}{0}(1-\rho)^5 Q\left(\sqrt{\frac{E_b}{N_0}\frac{8}{2}}\right) \\
& + \binom{5}{1}\rho(1-\rho)^4\left[\frac{2}{5}Q\left(\sqrt{\frac{E_b}{2}\left(\frac{4.8}{N_0}+\frac{3.2}{N_T}\right)}\right)+\frac{2}{5}Q\left(\sqrt{\frac{E_b}{2}\left(\frac{7.2}{N_0}+\frac{0.8}{N_T}\right)}\right)+\frac{1}{5}Q\left(\sqrt{\frac{E_b}{2}\left(\frac{8}{N_0}\right)}\right)\right] \\
& + \binom{5}{2}\rho^2(1-\rho)^3\left[\begin{array}{l}\frac{4}{10}Q\left(\sqrt{\frac{E_b}{2}\left(\frac{4}{N_0}+\frac{4}{N_T}\right)}\right)+\frac{2}{10}Q\left(\sqrt{\frac{E_b}{2}\left(\frac{4.8}{N_0}+\frac{3.2}{N_T}\right)}\right)+\frac{1}{10}Q\left(\sqrt{\frac{E_b}{2}\left(\frac{1.6}{N_0}+\frac{6.4}{N_T}\right)}\right) \\ +\frac{1}{10}Q\left(\sqrt{\frac{E_b}{2}\left(\frac{6.4}{N_0}+\frac{1.6}{N_T}\right)}\right)+\frac{2}{10}Q\left(\sqrt{\frac{E_b}{2}\left(\frac{7.2}{N_0}+\frac{0.8}{N_T}\right)}\right)\end{array}\right] \\
& + \binom{5}{3}\rho^3(1-\rho)^2\left[\begin{array}{l}\frac{1}{10}Q\left(\sqrt{\frac{E_b}{2}\left(\frac{6.4}{N_0}+\frac{1.6}{N_T}\right)}\right)+\frac{1}{10}Q\left(\sqrt{\frac{E_b}{2}\left(\frac{1.6}{N_0}+\frac{6.4}{N_T}\right)}\right)+\frac{2}{10}Q\left(\sqrt{\frac{E_b}{2}\left(\frac{0.8}{N_0}+\frac{7.2}{N_T}\right)}\right) \\ +\frac{4}{10}Q\left(\sqrt{\frac{E_b}{2}\left(\frac{4}{N_0}+\frac{4}{N_T}\right)}\right)+\frac{2}{10}Q\left(\sqrt{\frac{E_b}{2}\left(\frac{3.2}{N_0}+\frac{4.8}{N_T}\right)}\right)\end{array}\right] \\
& + \binom{5}{4}\rho^4(1-\rho)\left[\frac{2}{5}Q\left(\sqrt{\frac{E_b}{2}\left(\frac{3.2}{N_0}+\frac{4.8}{N_T}\right)}\right)+\frac{2}{5}Q\left(\sqrt{\frac{E_b}{2}\left(\frac{0.8}{N_0}+\frac{7.2}{N_T}\right)}\right)+\frac{1}{5}Q\left(\sqrt{\frac{E_b}{2}\left(\frac{8}{N_T}\right)}\right)\right] \\
& + \binom{5}{5}\rho^5 Q\left(\sqrt{\frac{E_b}{N_T}\frac{8}{2}}\right)
\end{aligned} \tag{4.47}$$

and

$$
\begin{aligned}
P_{8.8,6_1} &= \binom{6}{0}(1-\rho)^6 Q\left(\sqrt{\frac{E_b}{N_0}\frac{8.8}{2}}\right) \\
&+ \binom{6}{1}\rho(1-\rho)^5\left[\frac{1}{3}Q\left(\sqrt{\frac{E_b}{2}\left(\frac{5.6}{N_0}+\frac{3.2}{N_T}\right)}\right)+\frac{1}{2}Q\left(\sqrt{\frac{E_b}{2}\left(\frac{8}{N_0}+\frac{0.8}{N_T}\right)}\right)+\frac{1}{6}Q\left(\sqrt{\frac{E_b}{2}\left(\frac{8.8}{N_0}\right)}\right)\right] \\
&+ \binom{6}{2}\rho^2(1-\rho)^4\left[\begin{array}{l}\frac{2}{15}Q\left(\sqrt{\frac{E_b}{2}\left(\frac{5.6}{N_0}+\frac{3.2}{N_T}\right)}\right)+\frac{6}{15}Q\left(\sqrt{\frac{E_b}{2}\left(\frac{4.8}{N_0}+\frac{4}{N_T}\right)}\right)+\frac{3}{15}Q\left(\sqrt{\frac{E_b}{2}\left(\frac{8}{N_0}+\frac{0.8}{N_T}\right)}\right) \\ +\frac{3}{15}Q\left(\sqrt{\frac{E_b}{2}\left(\frac{7.2}{N_0}+\frac{1.6}{N_T}\right)}\right)+\frac{1}{15}Q\left(\sqrt{\frac{E_b}{2}\left(\frac{2.4}{N_0}+\frac{6.4}{N_T}\right)}\right)\end{array}\right] \\
&+ \binom{6}{3}\rho^3(1-\rho)^3\left[\begin{array}{l}\frac{3}{20}Q\left(\sqrt{\frac{E_b}{2}\left(\frac{7.2}{N_0}+\frac{1.6}{N_T}\right)}\right)+\frac{1}{20}Q\left(\sqrt{\frac{E_b}{2}\left(\frac{2.4}{N_0}+\frac{6.4}{N_T}\right)}\right)+\frac{6}{20}Q\left(\sqrt{\frac{E_b}{2}\left(\frac{4}{N_0}+\frac{4.8}{N_T}\right)}\right) \\ +\frac{6}{20}Q\left(\sqrt{\frac{E_b}{2}\left(\frac{4.8}{N_0}+\frac{4}{N_T}\right)}\right)+\frac{3}{20}Q\left(\sqrt{\frac{E_b}{2}\left(\frac{1.6}{N_0}+\frac{7.2}{N_T}\right)}\right)+\frac{1}{20}Q\left(\sqrt{\frac{E_b}{2}\left(\frac{6.4}{N_0}+\frac{2.4}{N_T}\right)}\right)\end{array}\right] \\
&+ \binom{6}{4}\rho^4(1-\rho)^2\left[\begin{array}{l}\frac{3}{15}Q\left(\sqrt{\frac{E_b}{2}\left(\frac{0.8}{N_0}+\frac{8}{N_T}\right)}\right)+\frac{6}{15}Q\left(\sqrt{\frac{E_b}{2}\left(\frac{4}{N_0}+\frac{4.8}{N_T}\right)}\right)+\frac{3}{15}Q\left(\sqrt{\frac{E_b}{2}\left(\frac{1.6}{N_0}+\frac{7.2}{N_T}\right)}\right) \\ +\frac{2}{15}Q\left(\sqrt{\frac{E_b}{2}\left(\frac{3.2}{N_0}+\frac{5.6}{N_T}\right)}\right)+\frac{1}{15}Q\left(\sqrt{\frac{E_b}{2}\left(\frac{6.4}{N_0}+\frac{2.4}{N_T}\right)}\right)\end{array}\right] \\
&+ \binom{6}{5}\rho^5(1-\rho)\left[\frac{1}{2}Q\left(\sqrt{\frac{E_b}{2}\left(\frac{0.8}{N_0}+\frac{8}{N_T}\right)}\right)+\frac{1}{3}Q\left(\sqrt{\frac{E_b}{2}\left(\frac{3.2}{N_0}+\frac{5.6}{N_T}\right)}\right)+\frac{1}{6}Q\left(\sqrt{\frac{E_b}{2}\left(\frac{8.8}{N_T}\right)}\right)\right] \\
&+ \binom{6}{6}\rho^6 Q\left(\sqrt{\frac{E_b}{N_T}\frac{8.8}{2}}\right)
\end{aligned}
\tag{4.48}
$$

and

$$
\begin{aligned}
P_{8.8,7_1} &= \binom{7}{0}(1-\rho)^7 Q\left(\sqrt{\frac{E_b}{N_0}\frac{8.8}{2}}\right) \\
&+\binom{7}{1}\rho(1-\rho)^6\left[\frac{2}{7}Q\left(\sqrt{\frac{E_b}{2}\left(\frac{5.6}{N_0}+\frac{3.2}{N_T}\right)}\right)+\frac{3}{7}Q\left(\sqrt{\frac{E_b}{2}\left(\frac{8}{N_0}+\frac{0.8}{N_T}\right)}\right)+\frac{2}{7}Q\left(\sqrt{\frac{E_b}{2}\left(\frac{8.8}{N_0}\right)}\right)\right] \\
&+\binom{7}{2}\rho^2(1-\rho)^5\left[\begin{array}{l}\frac{4}{21}Q\left(\sqrt{\frac{E_b}{2}\left(\frac{5.6}{N_0}+\frac{3.2}{N_T}\right)}\right)+\frac{6}{21}Q\left(\sqrt{\frac{E_b}{2}\left(\frac{4.8}{N_0}+\frac{4}{N_T}\right)}\right)+\frac{5}{21}Q\left(\sqrt{\frac{E_b}{2}\left(\frac{8}{N_0}+\frac{0.8}{N_T}\right)}\right) \\ +\frac{4}{21}Q\left(\sqrt{\frac{E_b}{2}\left(\frac{7.2}{N_0}+\frac{1.6}{N_T}\right)}\right)+\frac{1}{21}Q\left(\sqrt{\frac{E_b}{2}\left(\frac{2.4}{N_0}+\frac{6.4}{N_T}\right)}\right)+\frac{1}{21}Q\left(\sqrt{\frac{E_b}{2}\left(\frac{8.8}{N_0}\right)}\right)\end{array}\right] \\
&+\binom{7}{3}\rho^3(1-\rho)^4\left[\begin{array}{l}\frac{12}{35}Q\left(\sqrt{\frac{E_b}{2}\left(\frac{4.8}{N_0}+\frac{4}{N_T}\right)}\right)+\frac{6}{35}Q\left(\sqrt{\frac{E_b}{2}\left(\frac{4}{N_0}+\frac{4.8}{N_T}\right)}\right)+\frac{6}{35}Q\left(\sqrt{\frac{E_b}{2}\left(\frac{7.2}{N_0}+\frac{1.6}{N_T}\right)}\right) \\ +\frac{3}{35}Q\left(\sqrt{\frac{E_b}{2}\left(\frac{1.6}{N_0}+\frac{7.2}{N_T}\right)}\right)+\frac{3}{35}Q\left(\sqrt{\frac{E_b}{2}\left(\frac{8}{N_0}+\frac{0.8}{N_T}\right)}\right)+\frac{2}{35}Q\left(\sqrt{\frac{E_b}{2}\left(\frac{5.6}{N_0}+\frac{3.2}{N_T}\right)}\right) \\ +\frac{1}{35}Q\left(\sqrt{\frac{E_b}{2}\left(\frac{6.4}{N_0}+\frac{2.4}{N_T}\right)}\right)+\frac{1}{35}Q\left(\sqrt{\frac{E_b}{2}\left(\frac{2.4}{N_0}+\frac{6.4}{N_T}\right)}\right)\end{array}\right] \\
&+\binom{7}{4}\rho^4(1-\rho)^3\left[\begin{array}{l}\frac{12}{35}Q\left(\sqrt{\frac{E_b}{2}\left(\frac{4}{N_0}+\frac{4.8}{N_T}\right)}\right)+\frac{6}{35}Q\left(\sqrt{\frac{E_b}{2}\left(\frac{4.8}{N_0}+\frac{4}{N_T}\right)}\right)+\frac{6}{35}Q\left(\sqrt{\frac{E_b}{2}\left(\frac{1.6}{N_0}+\frac{7.2}{N_T}\right)}\right) \\ +\frac{3}{35}Q\left(\sqrt{\frac{E_b}{2}\left(\frac{7.2}{N_0}+\frac{1.6}{N_T}\right)}\right)+\frac{2}{35}Q\left(\sqrt{\frac{E_b}{2}\left(\frac{6.4}{N_0}+\frac{2.4}{N_T}\right)}\right)+\frac{2}{35}Q\left(\sqrt{\frac{E_b}{2}\left(\frac{3.2}{N_0}+\frac{5.6}{N_T}\right)}\right) \\ +\frac{3}{35}Q\left(\sqrt{\frac{E_b}{2}\left(\frac{0.8}{N_0}+\frac{8}{N_T}\right)}\right)+\frac{1}{35}Q\left(\sqrt{\frac{E_b}{2}\left(\frac{2.4}{N_0}+\frac{6.4}{N_T}\right)}\right)\end{array}\right] \\
&+\binom{7}{5}\rho^5(1-\rho)^2\left[\begin{array}{l}\frac{4}{21}Q\left(\sqrt{\frac{E_b}{2}\left(\frac{3.2}{N_0}+\frac{5.6}{N_T}\right)}\right)+\frac{6}{21}Q\left(\sqrt{\frac{E_b}{2}\left(\frac{4}{N_0}+\frac{4.8}{N_T}\right)}\right)+\frac{6}{21}Q\left(\sqrt{\frac{E_b}{2}\left(\frac{0.8}{N_0}+\frac{8}{N_T}\right)}\right) \\ +\frac{1}{21}Q\left(\sqrt{\frac{E_b}{2}\left(\frac{6.4}{N_0}+\frac{2.4}{N_T}\right)}\right)+\frac{3}{21}Q\left(\sqrt{\frac{E_b}{2}\left(\frac{1.6}{N_0}+\frac{7.2}{N_T}\right)}\right)+\frac{1}{21}Q\left(\sqrt{\frac{E_b}{2}\left(\frac{8.8}{N_T}\right)}\right)\end{array}\right] \\
&+\binom{7}{6}\rho^6(1-\rho)\left[\frac{2}{7}Q\left(\sqrt{\frac{E_b}{2}\left(\frac{8.8}{N_T}\right)}\right)+\frac{2}{7}Q\left(\sqrt{\frac{E_b}{2}\left(\frac{3.2}{N_0}+\frac{5.6}{N_T}\right)}\right)+\frac{3}{7}Q\left(\sqrt{\frac{E_b}{2}\left(\frac{0.8}{N_0}+\frac{8}{N_T}\right)}\right)\right] \\
&+\binom{7}{7}\rho^7 Q\left(\sqrt{\frac{E_b}{N_T}\frac{8.8}{2}}\right)
\end{aligned}
\tag{4.49}
$$

The performance with K=3 is shown in Figures 77 and 78. The results in Figures 77 and 78 are obtained for E_b/N_o=9 dB, which results in $P_b=10^{-8}$ with $E_b/N_I>>1$. As can be seen, PNI degrades system performance much more than BNI except for $E_b/N_I>>1$, when performance is dominated by E_b/N_o.

For P_b=10^{-5}, we need E_b/N_I=10.8 dB for BNI, while E_b/N_I=12.45 dB is required for PNI with ρ=0.1 .The relative degradation in E_b/N_I between BNI and PNI for the worst case ρ is 1.65 dB for K=3 and E_b/N_o=9 dB.

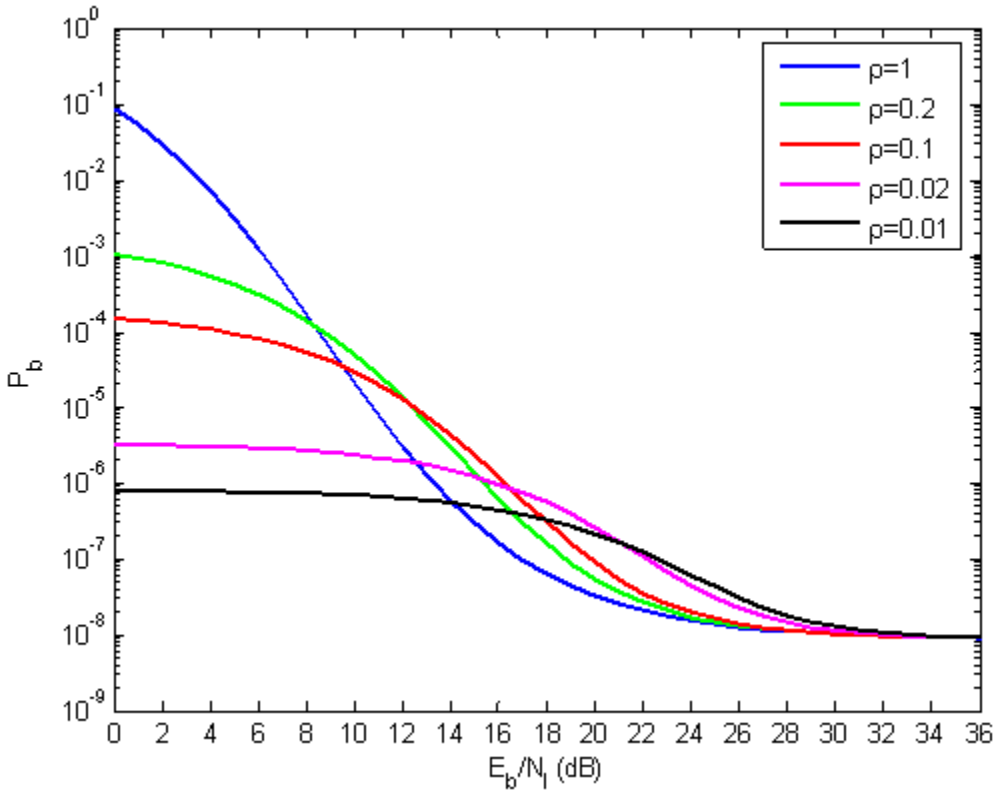

Figure 77. Probability bit error of TCM signals transmitting data independently on the I and Q channels, each modulated with 4-PAM waveforms encoded with a rate r=1/2 convolution code for K=3 in both AWGN and PNI.

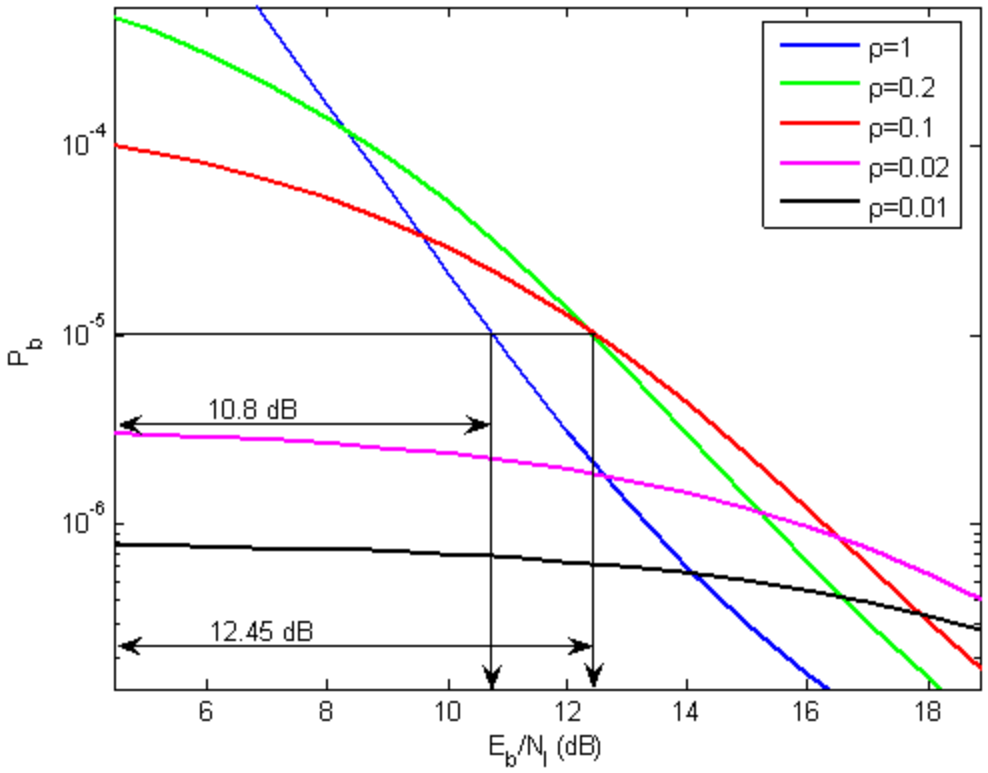

Figure 78. Magnified probability bit error of TCM signals transmitting data independently on the I and Q channels, each modulated with 4-PAM waveforms encoded with a rate r=1/2 convolution code for K=3 in both AWGN and PNI.

Table 14. Performance of TCM signals transmitted independently on the I and Q channels, each with 4-PAM, r=1/2 TCM in both AWGN and PNI.

K	Absolute E_b/N_I for $P_b=10^{-5}$ and ρ=1	Absolute E_b/N_I for $P_b=10^{-5}$ and worst case ρ	Relative E_b/N_I degradation for $P_b=10^{-5}$
1	13.5 dB	24.24 dB	10.74 dB
2	11.12 dB	14.44 dB	3.32 dB
3	10.8 dB	12.45 dB	1.65 dB

From Table 14, we see that the relative degradation in E_b/N_I between BNI and PNI for the worst case ρ is 10.74 dB for K=1 and E_b/N_o=12 dB, 3.32 dB for K=2 and E_b/N_o=9.4

dB, and 1.65 dB for K=3 and E_b/N_o=9 dB. From these results we see that as the number of encoder memory elements increases, the performance of the TCM system improves both in an absolute sense, the E_b/N_I and E_b/N_o required to achieve $P_b=10^{-5}$ both decrease as K increases, and in a relative sense since the TCM system has greater resistance to PNI, the difference in E_b/N_I between BNI and PNI with worst case ρ for $P_b=10^{-5}$ is reduced as K increases.

G. PERFORMANCE ANALYSIS OF TCM SIGNALS WITH 8-PSK MODULATION AND A *r*=2/3 CONVOLUTIONAL ENCODING IN AWGN AND PNI

In this section we examine the performance of TCM signals implemented with 8-PSK modulation and encoded with a r=2/3 convolutional encoder. The effect of varying the number of encoder memory elements is examined for both AWGN and PNI. This system has the same spectral efficiency as TCM system implemented with 4-PAM modulation and r=1/2 convolutional encoding. In this case, m=2 for a r=2/3 convolutional encoder, and $E_{sc}=r(m+1)E_b=2E_b$. There are no parallel transitions, so equation (4.33) can be used.

1. Probability Bit Error Analysis for K=1

In this subsection we obtain P_b for the TCM system with the r=2/3 convolutional encoder with one memory element (K=1) shown in Figure 65. The corresponding state diagram for natural mapped 8-PSK/TCM is shown in Figure 66.

Equation (4.20) from part D of Chapter IV is

$$\left.\frac{\partial T_{ave}(X,Y)}{\partial Y}\right|_{Y=1} = X^2 + \frac{3}{2}X^{2.586} + \frac{5}{2}X^{3.172} + \ldots \qquad (4.50)$$

Comparing equation (4.50) with equation (4.29), we obtain the squared-Euclidean distance and the total information weight for all paths having the same squared-Euclidean distance. From Figure 66 the minimum squared-Euclidean distance corresponds to path $S_0 - S_2 - S_o$, d^2_{free}=2, and λ_2=1. The average information weight of this path is B_2=1. Continuing, we find that two paths, $S_0 - S_1 - S_o$ and $S_0 - S_1 - S_2 - S_o$, have a squared-

Euclidean distance d^2=2.586, and $\lambda_{2.586}$=2. The corresponding average information weight is $B_{2.586}$=3/2. The first path, $S_0 - S_1 - S_o$, has two branches, and the second path, $S_0 - S_1 - S_2 - S_o$, has three branches. As a result, the average probability $P_{d_i^2, l_k}$ for these two paths cannot be calculated in the same way. Applying a similar procedure, we can obtain the squared-Euclidean distance and total information weight of each path on the state diagram.

Using the first two terms in the outer summation of equation (4.33), we obtain

$$P_b \approx B_2 P_{2,2_1} + \frac{1}{2} B_{2.586} P_{2.586,2_1} + \frac{1}{2} B_{2.586} P_{2.586,3_1} + \ldots \tag{4.51}$$

From equation (4.31), we get

$$\begin{aligned} P_{2,2_1} &= \binom{2}{0}(1-\rho)^2 \frac{1}{2} Q\left(\sqrt{\frac{E_b}{N_0} 2}\right) \\ &+ \binom{2}{1}\rho(1-\rho)\frac{1}{2}\left[\frac{1}{2} Q\left(\sqrt{\frac{E_b}{2}\left(\frac{2}{N_T}\right)}\right) + \frac{1}{2} Q\left(\sqrt{\frac{E_b}{2}\left(\frac{2}{N_0}\right)}\right)\right] \\ &+ \binom{2}{2}\rho^2 \frac{1}{2} Q\left(\sqrt{\frac{E_b}{N_T} 2}\right) \end{aligned} \tag{4.52}$$

and

$$\begin{aligned} P_{2.586,2_1} &= \binom{2}{0}(1-\rho)^2 \frac{1}{2} Q\left(\sqrt{\frac{E_b}{N_0} 2.586}\right) \\ &+ \binom{2}{1}\rho(1-\rho)\frac{1}{2}\left[\frac{1}{2} Q\left(\sqrt{\frac{E_b}{2}\left(\frac{0.586}{N_T} + \frac{2}{N_0}\right)}\right) + \frac{1}{2} Q\left(\sqrt{\frac{E_b}{2}\left(\frac{2}{N_T} + \frac{0.586}{N_0}\right)}\right)\right] \\ &+ \binom{2}{2}\rho^2 \frac{1}{2} Q\left(\sqrt{\frac{E_b}{N_T} 2.586}\right) \end{aligned} \tag{4.53}$$

and

$$
\begin{aligned}
P_{2.586,3_1} &= \binom{3}{0}(1-\rho)^3\frac{1}{2}Q\left(\sqrt{\frac{E_b}{N_0}2.586}\right) \\
&+\binom{3}{1}\rho(1-\rho)^2\frac{1}{2}\left[\frac{1}{3}Q\left(\sqrt{E_b\left(\frac{2}{N_0}+\frac{0.586}{N_T}\right)}\right)+\frac{1}{3}Q\left(\sqrt{E_b\left(\frac{0.586}{N_0}+\frac{2}{N_T}\right)}\right)+\frac{1}{3}Q\left(\sqrt{\frac{E_b}{N_0}2.586}\right)\right] \\
&+\binom{3}{2}\rho^2(1-\rho)\frac{1}{2}\left[\frac{1}{3}Q\left(\sqrt{E_b\left(\frac{2}{N_0}+\frac{0.586}{N_T}\right)}\right)+\frac{1}{3}Q\left(\sqrt{E_b\left(\frac{0.586}{N_0}+\frac{2}{N_T}\right)}\right)+\frac{1}{3}Q\left(\sqrt{\frac{E_b}{N_T}2.586}\right)\right] \\
&+\binom{3}{3}\rho^3\frac{1}{2}Q\left(\sqrt{\frac{E_b}{N_T}2.586}\right)
\end{aligned}
\tag{4.54}
$$

The performance with K=1 is shown in Figures 79 and 80. The results in Figures 79 and 80 are obtained for E_b/N_o=11.76 dB, which results in $P_b=10^{-8}$ when $E_b/N_I>>1$. As can be seen, PNI degrades system performance much more than BNI except for $E_b/N_I>>1$, when performance is dominated by E_b/N_o.

For $P_b=10^{-5}$, we require E_b/N_I=13 dB for BNI, while E_b/N_I=27.53 dB is required for PNI with ρ=0.01. The relative degradation in E_b/N_I between BNI and PNI for the worst case ρ is 14.53 dB for K=1 and E_b/N_o=11.76 dB.

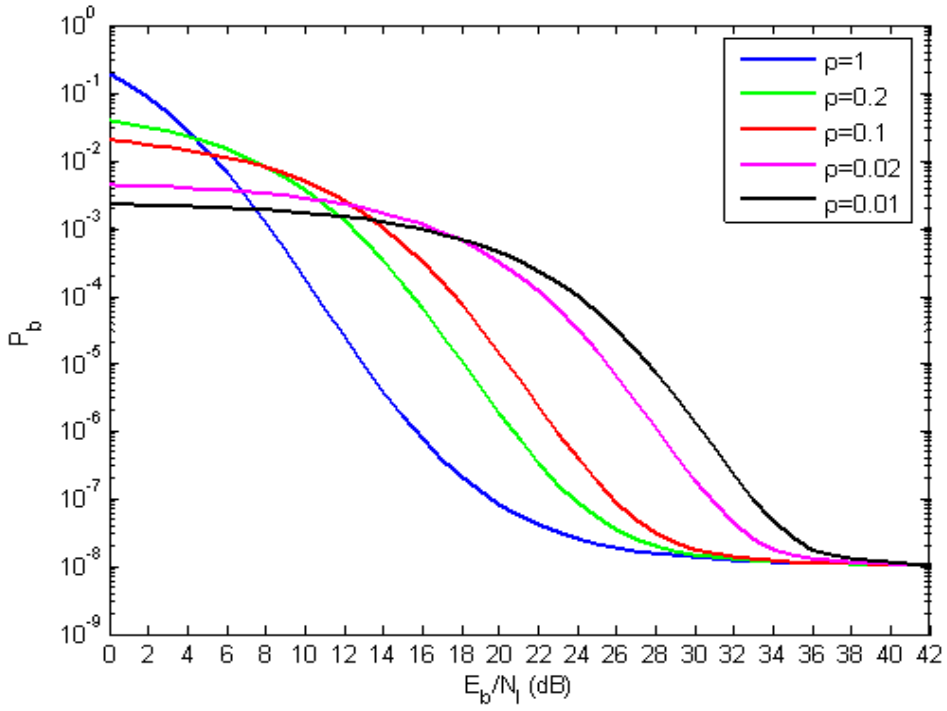

Figure 79. Probability bit error of TCM signals with 8-PSK and r=2/3 convolutional encoding for K=1 in both AWGN and PNI.

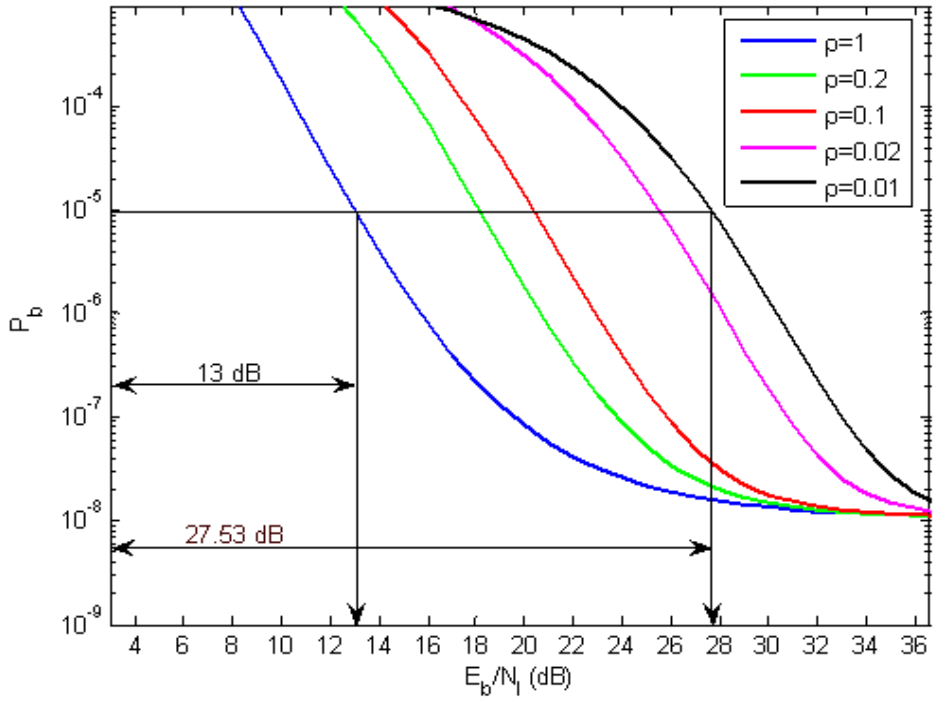

Figure 80. Magnified probability bit error of TCM signals with 8-PSK and r=2/3 convolutional encoding for K=1 in both AWGN and PNI.

2. Probability Bit Error Analysis for K=2

In this subsection we obtain P_b for the TCM system with the r=2/3 convolutional encoder with two memory elements (K=2) shown in Figure 67, and the corresponding state diagram for natural mapped 8-PSK/TCM is shown in Figure 68.

Equation (4.23) from part D of Chapter IV is

$$\left.\frac{\partial T_{ave}(X,Y)}{\partial Y}\right|_{Y=1} = \frac{1}{2}X^{1.758} + \frac{11}{8}X^{2.344} + X^{2.586} + \frac{11}{4}X^{3.172} + \ldots \qquad (4.55)$$

Comparing equation (4.55) with equation (4.29), we obtain the squared-Euclidean distance and the total information weight for all paths having the same squared-Euclidean distance. From Figure 68 the minimum squared-Euclidean distance corresponds to the single path $S_0 - S_2 - S_1 - S_o$, d^2_{free}=1.758, and $\lambda_{1.758}$=1. The average information weight of this path is $B_{1.758}$=1/2. Continuing, we find that two paths, $S_0 - S_2 - S_2 - S_1 - S_o$ and $S_0 - S_2 - S_1 - S_3 - S_o$, have a squared-Euclidean distance d^2=2.344, and the corresponding average information weight is $B_{2.344}$=11/8. Both paths have four branches, and $\lambda_{2.344}$=2. Both paths have the same average probability $P_{d_i^2, l_k}$ because they have equal weight branches so, $P_{2.344,4_1} = P_{2.344,4_2}$. Similarly we find that only one path, $S_0 - S_3 - S_o$, has a squared-Euclidean distance d^2=2.586, and $\lambda_{2.586}$=1. The corresponding average information weight is $B_{2.586}$=1. Finally, we find that two paths, $S_0 - S_2 - S_3 - S_o$ and $S_0 - S_3 - S_2 - S_1 - S_o$, have a squared-Euclidean distance d^2=3.172, and $\lambda_{3.172}$=2. The corresponding average information weight is $B_{3.172}$=11/4. Applying a similar procedure, we can obtain the squared-Euclidean distance and total information weight of each path on the state diagram.

Using the first four terms in the outer summation of equation (4.33), we obtain

$$P_b \approx B_{1.758}P_{1.758,3_1} + \frac{1}{2}B_{2.344}P_{2.344,4_1} + \frac{1}{2}B_{2.344}P_{2.344,4_2} + B_{2.586}P_{2.586,2_1} + \frac{1}{2}B_{3.172}P_{3.172,3_1} + \frac{1}{2}B_{3.172}P_{3.172,4_1}\ldots \qquad (4.56)$$

From equation (4.31), we get

$$P_{1.758,3_1}=\binom{3}{0}(1-\rho)^3\frac{1}{2}Q\left(\sqrt{\frac{E_b}{N_0}1.758}\right)+\binom{3}{1}\rho(1-\rho)^2\frac{1}{2}\left[Q\left(\sqrt{E_b\left(\frac{1.172}{N_0}+\frac{0.586}{N_T}\right)}\right)\right]$$
$$+\binom{3}{2}\rho^2(1-\rho)\frac{1}{2}\left[Q\left(\sqrt{E_b\left(\frac{0.586}{N_0}+\frac{1.172}{N_T}\right)}\right)\right]+\binom{3}{3}\rho^3\frac{1}{2}Q\left(\sqrt{\frac{E_b}{N_T}1.758}\right) \quad (4.57)$$

and

$$P_{2.344,4_1}=\binom{4}{0}(1-\rho)^4Q\left(\sqrt{\frac{E_b}{N_0}2.344}\right)+\binom{4}{1}\rho(1-\rho)^3\left[Q\left(\sqrt{E_b\left(\frac{1.758}{N_0}+\frac{0.586}{N_T}\right)}\right)\right]$$
$$+\binom{4}{2}\rho^2(1-\rho)^2\left[Q\left(\sqrt{E_b\left(\frac{1.172}{N_0}+\frac{1.172}{N_T}\right)}\right)\right]+\binom{4}{3}\rho^3(1-\rho)\left[Q\left(\sqrt{E_b\left(\frac{0.586}{N_0}+\frac{1.758}{N_T}\right)}\right)\right] \quad (4.58)$$
$$+\binom{4}{4}\rho^4Q\left(\sqrt{\frac{E_b}{N_T}2.344}\right)$$

and

$$P_{2.586,2_1}=\binom{2}{0}(1-\rho)^2Q\left(\sqrt{\frac{E_b}{N_0}2.586}\right)+\binom{2}{1}\rho(1-\rho)\frac{1}{2}\left[Q\left(\sqrt{E_b\left(\frac{0.586}{N_0}+\frac{2}{N_T}\right)}\right)+Q\left(\sqrt{E_b\left(\frac{2}{N_0}+\frac{0.586}{N_T}\right)}\right)\right]$$
$$+\binom{2}{2}\rho^2Q\left(\sqrt{\frac{E_b}{N_T}2.586}\right) \quad (4.59)$$

For the two paths $S_0-S_2-S_3-S_o$ and $S_0-S_3-S_2-S_1-S_o$ with a squared-Euclidean distance d^2=3.172, and corresponding average information weight $B_{3.172}$=11/4, the average probability $P_{d_i^2,l_k}$ must be calculated independently for each path on the state diagram, and from equation (4.31) we get

$$
\begin{aligned}
P_{3.172,3_1} &= \binom{3}{0}(1-\rho)^3 Q\left(\sqrt{\frac{E_b}{N_0}3.172}\right) \\
&+\binom{3}{1}\rho(1-\rho)^2\left[\frac{2}{3}Q\left(\sqrt{E_b\left(\frac{2.586}{N_0}+\frac{0.586}{N_T}\right)}\right)+\frac{1}{3}Q\left(\sqrt{E_b\left(\frac{1.172}{N_0}+\frac{2}{N_T}\right)}\right)\right] \\
&+\binom{3}{2}\rho^2(1-\rho)\left[\frac{2}{3}Q\left(\sqrt{E_b\left(\frac{0.586}{N_0}+\frac{2.586}{N_T}\right)}\right)+\frac{1}{3}Q\left(\sqrt{E_b\left(\frac{2}{N_0}+\frac{1.172}{N_T}\right)}\right)\right] \\
&+\binom{3}{3}\rho^3 Q\left(\sqrt{\frac{E_b}{N_T}3.172}\right)
\end{aligned}
\tag{4.60}
$$

and

$$
\begin{aligned}
P_{3.172,4_1} &= \binom{4}{0}(1-\rho)^4 Q\left(\sqrt{\frac{E_b}{N_0}3.172}\right) \\
&+\binom{4}{1}\rho(1-\rho)^3\left[\begin{array}{l}\frac{1}{2}Q\left(\sqrt{E_b\left(\frac{2.586}{N_0}+\frac{0.586}{N_T}\right)}\right)+\frac{1}{4}Q\left(\sqrt{E_b\left(\frac{1.172}{N_0}+\frac{2}{N_T}\right)}\right) \\ +\frac{1}{4}Q\left(\sqrt{\frac{E_b}{N_0}3.172}\right)\end{array}\right] \\
&+\binom{4}{2}\rho^2(1-\rho)^2\left[\begin{array}{l}\frac{1}{6}Q\left(\sqrt{E_b\left(\frac{1.172}{N_0}+\frac{2}{N_T}\right)}\right)+\frac{1}{3}Q\left(\sqrt{E_b\left(\frac{0.586}{N_0}+\frac{2.586}{N_T}\right)}\right) \\ +\frac{1}{3}Q\left(\sqrt{E_b\left(\frac{2.586}{N_0}+\frac{0.586}{N_T}\right)}\right)+\frac{1}{6}Q\left(\sqrt{E_b\left(\frac{2}{N_0}+\frac{1.172}{N_T}\right)}\right)\end{array}\right] \\
&+\binom{4}{3}\rho^3(1-\rho)\left[\begin{array}{l}\frac{1}{2}Q\left(\sqrt{E_b\left(\frac{0.586}{N_0}+\frac{2.586}{N_T}\right)}\right)+\frac{1}{4}Q\left(\sqrt{E_b\left(\frac{2}{N_0}+\frac{1.172}{N_T}\right)}\right) \\ +\frac{1}{4}Q\left(\sqrt{\frac{E_b}{N_T}3.172}\right)\end{array}\right] \\
&+\binom{4}{4}\rho^4 Q\left(\sqrt{\frac{E_b}{N_T}3.172}\right)
\end{aligned}
\tag{4.61}
$$

The performance with K=2 is shown in Figures 81 and 82. The results in Figures 81 and 82 are obtained for E_b/N_o=12.14 dB, which results in $P_b=10^{-8}$ when $E_b/N_I>>1$. As can be seen, PNI degrades system performance much more than BNI except for $E_b/N_I>>1$, when performance is dominated by E_b/N_o.

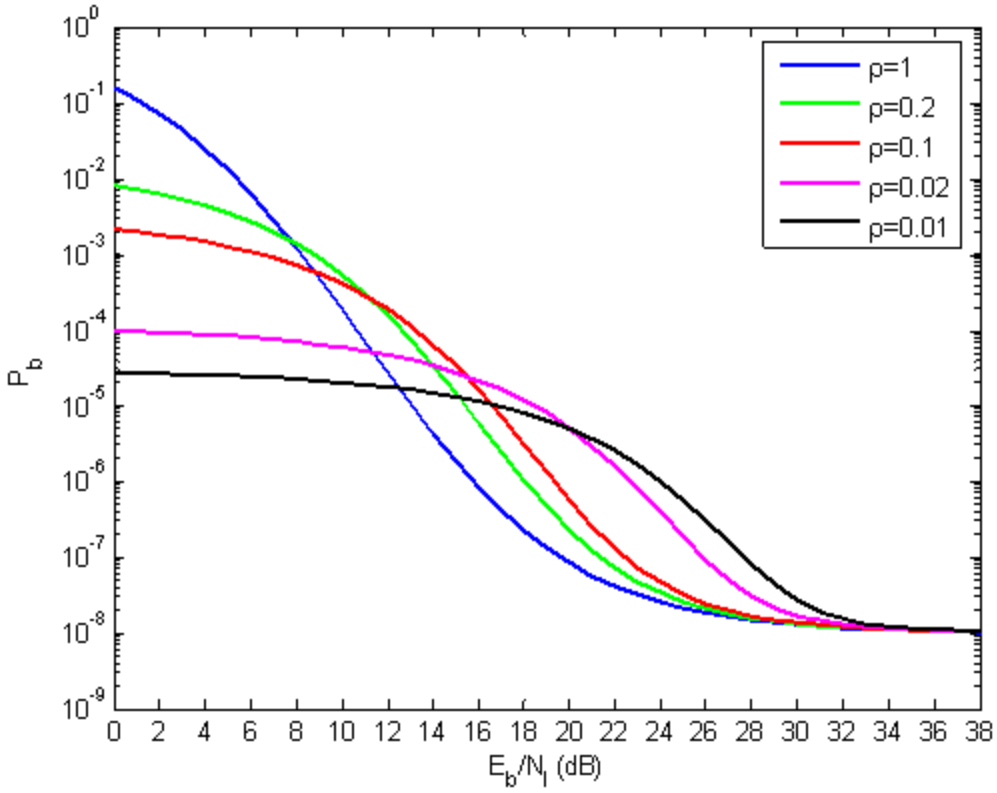

Figure 81. Probability bit error of TCM with 8-PSK and r=2/3 convolutional encoding for K=2 in both AWGN plus PNI.

For $P_b=10^{-5}$, we require E_b/N_I=13.13 dB for BNI, while E_b/N_I=18.4 dB is required for PNI with ρ=0.02. The relative degradation in E_b/N_I between BNI and PNI for the worst case ρ is 5.27 dB for K=2 and E_b/N_o=12.14 dB.

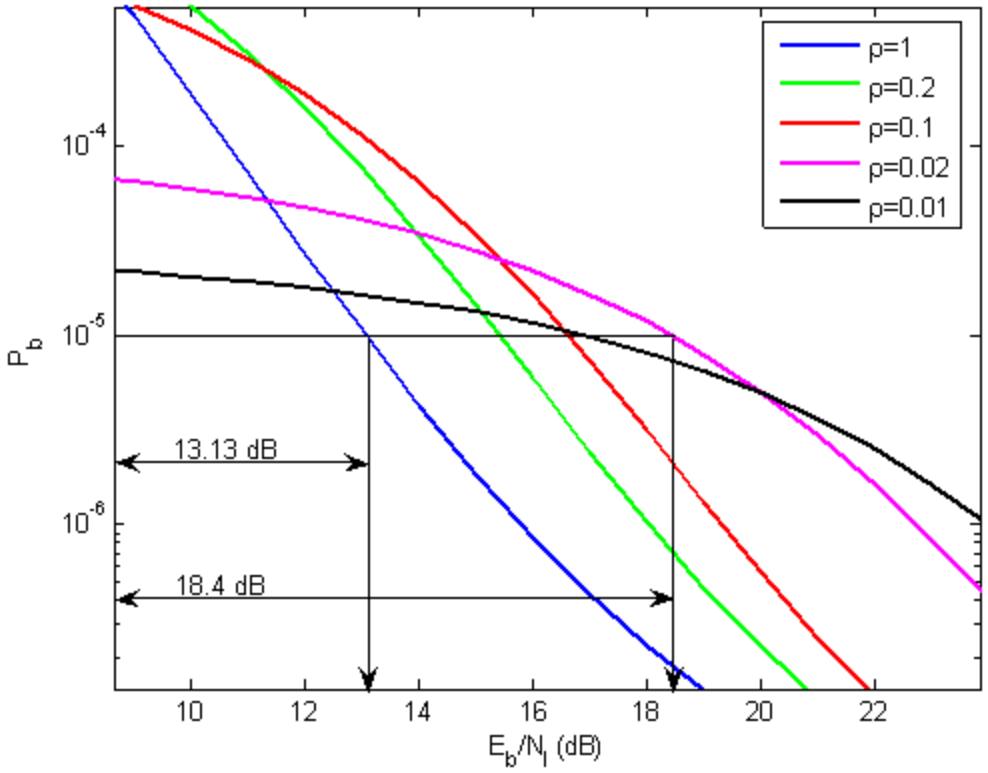

Figure 82. Magnified probability bit error of TCM with 8-PSK and r=2/3 convolutional encoding for K=2 in both AWGN plus PNI.

3. Probability Bit Error Analysis for K=3

In this subsection we obtain P_b for the TCM system with the r=2/3 convolutional encoder with three memory elements (K=3) shown in Figure 69, and the corresponding error trellis for natural mapped 8-PSK/TCM is shown in Figure 70.

Equation (4.26) from part D of Chapter IV is

$$\left.\frac{\partial T_{ave}(X,Y)}{\partial Y}\right|_{Y=1} = 2X^{4.586} + \frac{3}{2}X^{4.586} + \frac{3}{2}X^{4.586}\ldots \qquad (4.62)$$

If we compare equation (4.62) with equation (4.29), we obtain the squared-Euclidean distance and the total information weight for all paths having the same squared-Euclidean distance. From Figure 70 the minimum squared-Euclidean distance corresponds to three

paths, $S_0 - S_1 - S_2 - S_6 - S_o$, $S_0 - S_1 - S_2 - S_4 - S_o$ and $S_0 - S_3 - S_6 - S_o$, d^2_{free}=4.586, and $\lambda_{4.586}$=3. The average information weight of these path is $B_{1.758}$=5. Applying a similar procedure, we can obtain the squared-Euclidean distance and total information weight of each path on the signal flow graph.

Using only the first term in the outer summation of equation (4.33), we obtain

$$P_b \approx \frac{1}{3} B_{4.586} P_{4.586,4_1} + \frac{1}{3} B_{4.586} P_{4.586,4_2} + \frac{1}{3} B_{4.586} P_{4.586,3_1} + \ldots \qquad (4.63)$$

For this example the average probability $P_{d_i^2,l_k}$ is the same for two of the three paths with a squared-Euclidean distance d^2=4.586 because both paths have four branches and the information weight of each branch on each path is the same. From equation (4.31), we get

$$\begin{aligned}
P_{4.586,4_1} = P_{4.586,4_2} &= \binom{4}{0}(1-\rho)^4 \frac{1}{2} Q\left(\sqrt{\frac{E_b}{N_0} 4.586}\right) \\
&+ \binom{4}{1}\rho(1-\rho)^3 \frac{1}{2}\left[\frac{1}{2} Q\left(\sqrt{E_b\left(\frac{2.586}{N_0}+\frac{2}{N_T}\right)}\right) + \frac{1}{4} Q\left(\sqrt{E_b\left(\frac{4}{N_0}+\frac{0.586}{N_T}\right)}\right) + \frac{1}{4} Q\left(\sqrt{\frac{E_b}{N_0} 4.586}\right)\right] \\
&+ \binom{4}{2}\rho^2(1-\rho)^2 \frac{1}{2}\left[\frac{2}{6} Q\left(\sqrt{E_b\left(\frac{2.586}{N_0}+\frac{2}{N_T}\right)}\right) + \frac{2}{6} Q\left(\sqrt{E_b\left(\frac{2}{N_0}+\frac{2.586}{N_T}\right)}\right) + \frac{1}{6} Q\left(\sqrt{E_b\left(\frac{4}{N_0}+\frac{0.586}{N_T}\right)}\right) + \frac{1}{6} Q\left(\sqrt{E_b\left(\frac{0.586}{N_0}+\frac{4}{N_T}\right)}\right)\right] \\
&+ \binom{4}{3}\rho^3(1-\rho) \frac{1}{2}\left[\frac{1}{2} Q\left(\sqrt{E_b\left(\frac{2}{N_0}+\frac{2.586}{N_T}\right)}\right) + \frac{1}{4} Q\left(\sqrt{E_b\left(\frac{0.586}{N_0}+\frac{4}{N_T}\right)}\right) + \frac{1}{4} Q\left(\sqrt{E_b\left(\frac{4.586}{N_T}\right)}\right)\right] \\
&+ \binom{4}{4}\rho^4 \frac{1}{2} Q\left(\sqrt{\frac{E_b}{N_T} 4.586}\right)
\end{aligned} \qquad (4.64)$$

and

$$\begin{aligned}
P_{4.586,3_1} &= \binom{3}{0}(1-\rho)^3 \frac{1}{2} Q\left(\sqrt{\frac{E_b}{N_0} 4.586}\right) \\
&+ \binom{3}{1}\rho(1-\rho)^2 \frac{1}{2}\left[\frac{2}{3} Q\left(\sqrt{E_b\left(\frac{2.586}{N_0}+\frac{2}{N_T}\right)}\right) + \frac{1}{3} Q\left(\sqrt{E_b\left(\frac{4}{N_0}+\frac{0.586}{N_T}\right)}\right)\right] \\
&+ \binom{3}{2}\rho^2(1-\rho) \frac{1}{2}\left[\frac{2}{3} Q\left(\sqrt{E_b\left(\frac{2}{N_0}+\frac{2.586}{N_T}\right)}\right) + \frac{1}{3} Q\left(\sqrt{E_b\left(\frac{0.586}{N_0}+\frac{4}{N_T}\right)}\right)\right] \\
&+ \binom{3}{3}\rho^3 \frac{1}{2} Q\left(\sqrt{\frac{E_b}{N_T} 4.586}\right)
\end{aligned} \qquad (4.65)$$

The performance with K=3 is shown in Figures 83 and 84. The results in Figures 83 and 84 are obtained for E_b/N_o=8.58 dB, which results in $P_b=10^{-8}$ when $E_b/N_I>>1$. As can be seen, PNI degrades system performance much more than BNI except for $E_b/N_I>>1$, when performance is dominated by E_b/N_o.

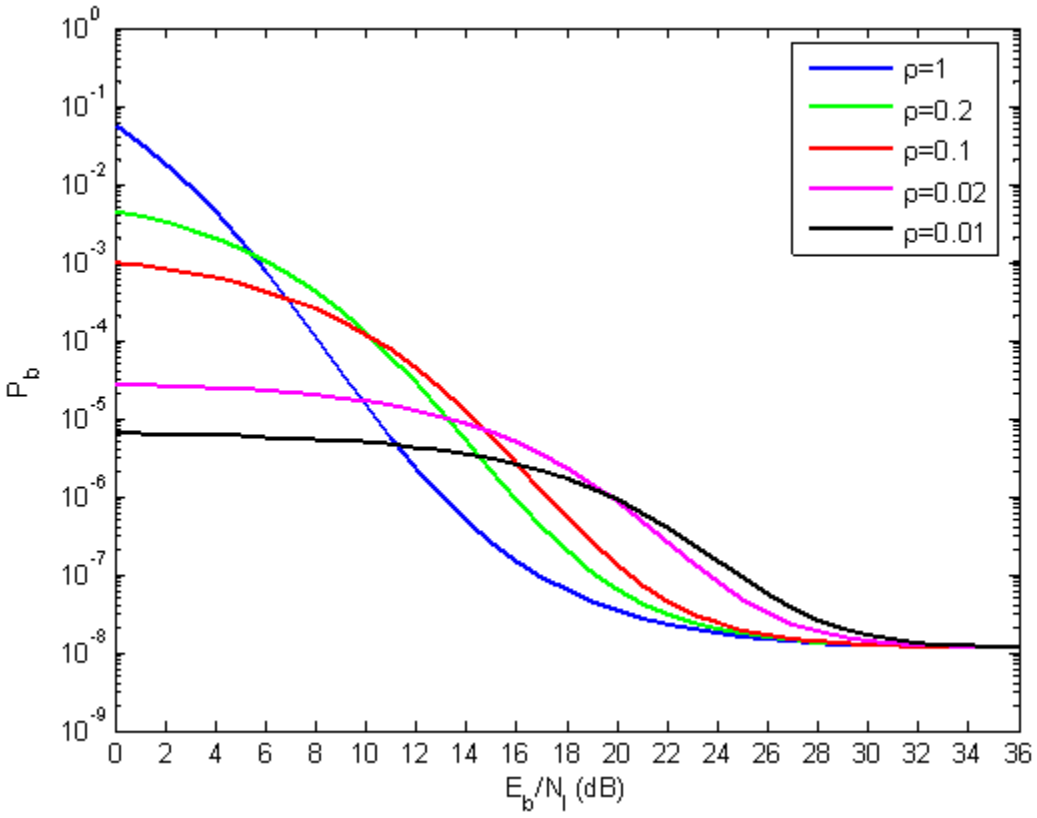

Figure 83. Probability bit error of TCM with 8-PSK and r=2/3 convolutional encoding for K=3 in both AWGN plus PNI.

For $P_b=10^{-5}$, we require E_b/N_I=10.39 dB for PNI, while E_b/N_I=14.21 dB is required for PNI with ρ=0.1. The relative degradation in E_b/N_I between BNI and PNI for the worst case ρ is 3.82 dB for K=1 and E_b/N_o=8.58 dB.

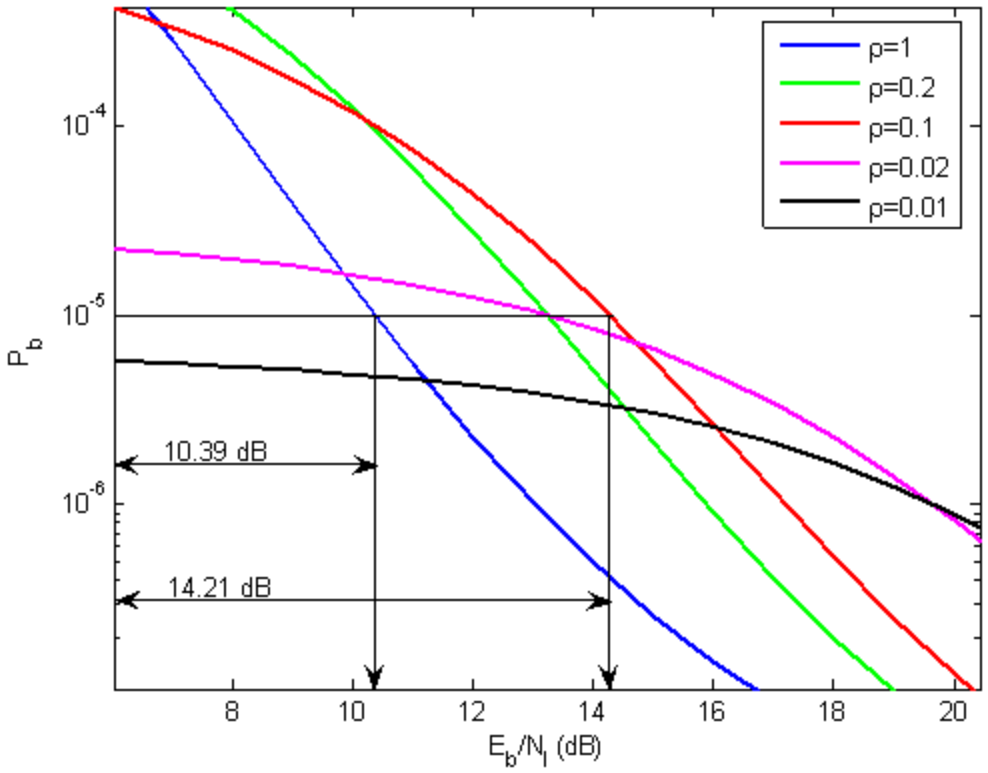

Figure 84. Magnified probability bit error of TCM with 8-PSK and r=2/3 convolutional encoding for K=3 in both AWGN plus PNI.

Table 15. Performance of 8-PSK/TCM with r=2/3 convolutional encoding in AWGN and PNI.

K	Absolute E_b/N_I for $P_b=10^{-5}$ and ρ=1	Absolute E_b/N_I for $P_b=10^{-5}$ and worst case ρ	Relative E_b/N_I degradation for $P_b=10^{-5}$
1	13 dB	27.53 dB	14.53 dB
2	13.13 dB	18.4 dB	5.27 dB
3	10.39 dB	14.21 dB	3.82 dB

Table 15 is a summary of the performance of the 8-PSK, r=2/3 TCM system. For $P_b=10^{-5}$, the relative degradation in E_b/N_I between BNI and PNI for the worst case ρ is 14.53 dB for K=1 and E_b/N_o=11.76 dB, 5.27 dB for K=2 and E_b/N_o=12.14 dB, and 3.82 dB for K=3 and E_b/N_o=8.58 dB. From these results we see that as the number of encoder

memory elements increases, the performance of the TCM system improves both in an absolute sense, the E_b/N_I and E_b/N_o required to achieve $P_b=10^{-5}$ both decrease as K increases, and in a relative sense, since the TCM system has greater resistance to PNI, the difference in E_b/N_I between BNI and PNI with worst case ρ for $P_b=10^{-5}$ is reduced as K increases.

Table 16. Performance of TCM and non-TCM signals applied to same rate convolutional encoders with 8-PSK modulation in an AWGN and PNI environment.

Non-TCM signals with 8-PSK modulation and r=2/3 convolutional encoding with HDD in AWGN and PNI			
K	E_b/N_I for $P_b=10^{-5}$ and ρ=1	E_b/N_I for $P_b=10^{-5}$ and worst case ρ	E_b/N_I degradation for $P_b=10^{-5}$
2	15.89 dB	24.51 dB	8.62 dB
3	15.77 dB	23.56 dB	7.79 dB
4	15.36 dB	19.79 dB	4.43 dB
TCM signals with 8-PSK modulation and r=2/3 convolutional encoding in AWGN and PNI			
K	E_b/N_I for $P_b=10^{-5}$ and ρ=1	E_b/N_I for $P_b=10^{-5}$ and worst case ρ	E_b/N_I degradation for $P_b=10^{-5}$
2	13.13 dB	18.4 dB	5.27 dB
3	10.39 dB	14.21 dB	3.82 dB
4	8.97 dB	11.76 dB	2.79 dB

The results listed in Table 16 for K=4 TCM signals with 8-PSK modulation and r=2/3 convolutional encoding in AWGN and PNI were derived in [19] and are used for comparison purposes. From Table 16 we see that TCM with 8-PSK and r=2/3 convolutional encoding has a significant advantage compared to non-TCM system.

For K=2, 3, and 4, the difference in E_b/N_I for the TCM and the non-TCM systems are 6.11 dB, 9.35 dB, and 8.03 dB, respectively. The relative degradation in E_b/N_I for $P_b=10^{-5}$ for the two systems is 3.35 dB, 3.97 dB, and 1.64 dB, respectively.

We can compare the results listed in Tables 14 and 15, which are combined in Table 17, and we see that TCM with 4-PAM and r=1/2 convolutional encoding individually modulating the I and Q channels is preferred to 8-PSK with r=2/3 convolutional encoding. The point is that it is easier to increase K for the former system than for the latter without making overall decoding complexity impractical. With the latter system, a maximum of K=8 is practical, but with the former, K=8 in each encoder, for a total of K=16, is practical. Based on the trends seen in Table 17, this should yield excellent immunity to PNI as well as significant coding gain.

Table 17. Performance of TCM signals implemented with different modulation types and different code rates.

TCM with 4-PAM modulation and r=1/2 convolutional encoding in AWGN and PNI			
K	E_b/N_I for $P_b=10^{-5}$ and ρ=1	E_b/N_I for $P_b=10^{-5}$ and worst case ρ	E_b/N_I degradation for $P_b=10^{-5}$
1	13.5 dB	24.24 dB	10.74 dB
2	11.12 dB	14.44 dB	3.32 dB
3	10.8 dB	12.45 dB	1.65 dB
TCM with 8-PSK modulation and r=2/3 convolutional encoding in AWGN and PNI			
K	E_b/N_I for $P_b=10^{-5}$ and ρ=1	E_b/N_I for $P_b=10^{-5}$ and worst case ρ	E_b/N_I degradation for $P_b=10^{-5}$
1	13 dB	27.53 dB	14.53 dB
2	13.13 dB	18.4 dB	5.27 dB
3	10.39 dB	14.21 dB	3.82 dB
4	8.97 dB	11.76 dB	2.79 dB

The results displayed in Table 17 allow a comparison between 8-PSK, r=2/3 TCM when the encoder has K memory elements and 4-PAM, r=1/2 TCM when each encoder has K memory elements for a total of 2K memory elements. Clearly, TCM signals independently transmitting data on the I and Q channels with 4-PAM and r=1/2 encoding has a significant advantage in decoding complexity. TCM with 8-PSK and r=2/3 convolutional encoding does not perform as well in both AWGN and PNI when K is the same for all encoders. As a consequence, when both AWGN and PNI are present, both decreased decoding complexity and improved resistance to the effects of PNI are obtained by using 4-PAM, r=1/2 TCM instead of 8-PSK, r=2/3 TCM.

To sum up, TCM with 4-PAM and r=1/2 convolutional encoding has a clear advantage over 8-PSK, r=2/3 TCM both in a relative and an absolute sense. The 4-PAM, r=1/2 system is more immune in PNI and has the advantage of reduced decoding complexity.

Another comparison of interest is to compare the two systems for the same total number of encoder memory elements. To be specific, if the 8-PSK, r=2/3 TCM system has K memory elements, then the 4-PAM, r=1/2 TCM system encoders will have K/2 memory elements for a total of K memory elements. For this comparison, the 8-PSK, r=2/3 TCM system has better immunity to PNI than the 4-PAM, r=1/2 TCM system. Clearly, increasing the decoding complexity of the 4-PAM, r=1/2 TCM system by increasing the total number of encoder memory elements improves the overall performance of the system both in terms of E_b/N_o and E_b/N_I while still resulting in a less complex decoding requirement than when 8-PSK, r=2/3 TCM is used.

The results derived from the comparison of the two TCM schemes having the same bandwidth and data rate give us the message that the type of comparison we use plays a vital role in the selection which system will be used. We can choose to either sacrifice coding gain in favor of reducing decoding complexity, or we can maximize coding gain at the expense of decoding complexity. In some situations, both reduced decoding complexity with improved coding gain can be obtained at the same time.

In this chapter, the performance of TCM systems in AWGN and PNI was analyzed. In the final chapter, the main conclusions of the analyses are summarized and proposals for future work are presented.

THIS PAGE INTENTIONALLY LEFT BLANK

V. CONCLUSIONS AND FUTURE WORK

A. CONCLUSIONS

Trellis-coded modulation (TCM) is a technique that introduces FEC coding without increasing the bandwidth of the channel signal. TCM combines binary convolutional codes with *M*-ary modulation in one operation. The waveform is assumed to be transmitted over a channel with both AWGN and PNI. In addition to a TCM waveform consisting of a rate r=2/3 convolutional code with 8-PSK modulation (analogous to the *IEEE* 802.11*g* TCM mode) and a TCM system consisting of two rate r=1/2 convolutional codes encoding data that is modulated on the I and Q channels, respectively, with 4-PAM is examined. As compared to an r=2/3, 8-PSK TCM system, the decoding complexity of the r=1/2, 4-PAM TCM system is significantly less when the number of encoder memory elements is large.

Initially, in this thesis the performance of a non-TCM system with rate r=2/3 convolutional coding and 8-PSK modulation in both AWGN and PNI for flat, slowly fading Nakagami channels with the number of encoder memory elements K as a parameter was evaluated. In AWGN, performance of the non-TCM system improves as the number of encoder memory elements K increases. In both AWGN and PNI, as K increases, the performance of the system improves in terms of both E_b/N_o and E_b/N_I . PNI is less effective as the number of memory elements increases. For flat, slowly fading Nakagami channels with AWGN, the effect of the Nakagami fading channel decreases as the fading figure m increases, and the Nakagami fading channel has the least effect when K=8 as compared to K=2. For flat, slowly fading Nakagami channels with both AWGN and PNI, as m increases performance improves. PNI only degrades the performance when $m>1$, and for $1/2 \leq m \leq 1$, PNI does not degrade performance but actually improves it. Another interesting point is that for $m>2$, the effect of the Nakagami fading channel does not significantly change the performance of the system with respect to PNI as m increases. For K=8, the system performance is significantly better, both in an absolute and a relative sense, compared to K=2.

Next, the performance of the two different TCM waveforms previously mentioned was investigated for the AWGN channel. The performance of the two TCM systems was compared with conventional systems, all designed such that the data rate and signal bandwidth are the same. The two TCM systems were compared in two different ways. First, the two TCM systems were compared for the same number of encoder memory elements devoted to overall encoding. In other words, if the 8-PSK/TCM r=2/3 encoder has K memory elements, then each of the r=1/2 encoders in the 4-PAM/TCM alternative system has K/2 memory elements for a total of K memory elements. Second, the two TCM systems were compared when, if the 8-PSK/TCM r=2/3 encoder has K memory elements, then each of the 4-PAM/TCM r=1/2 encoders has K memory elements for a total of 2K memory elements.

As compared to an r=2/3, 8-PSK TCM system, the decoding complexity of the r=1/2, 4-PAM TCM system is significantly less when the number of encoder memory elements is large; hence, the latter system has an advantage compared to the former system. If we consider both coding gain improvement and decoding complexity, the r=1/2, 4-PAM TCM system is preferred since the coding gain disadvantage, when it exists, is insignificant (a maximum of 0.67 dB) compared to the advantage of decreased decoding complexity. When the two TCM systems are compared for the same total number of encoder memory elements, the r=2/3, 8-PSK TCM system is superior to the r=1/2, 4-PAM TCM system.

In addition to AWGN, the performance of the two TCM systems in PNI was investigated. For both TCM systems, the effect of varying the number of encoder memory elements when PNI is present was examined. It was found that as the number of encoder memory elements increases the negative effect of PNI decreases. When the total number of memory elements in the r=1/2, 4-PAM TCM system is twice that of the r=2/3, 8-PSK TCM system (each r=1/2 encoder has the same number of memory elements as the r=2/3 encoder), the r=1/2, 4-PAM TCM system has better immunity to PNI than the r=2/3, 8-PSK TCM system. When the two TCM systems were compared for the same total number of encoder memory elements, the r=2/3, 8-PSK TCM system has better immunity to PNI than the r=1/2, 4-PAM TCM system.

The results derived from the comparison of the two TCM schemes having the same bandwidth and data rate imply that the type of comparison used plays a vital role in the selection of which system will be used. We can choose to either sacrifice coding gain in favor of reducing decoding complexity, or we can maximize coding gain at the expense of decoding complexity. In some situations, both reduced decoding complexity and improved coding gain can be obtained simultaneously.

B. FUTURE WORK

Due to the increased complexity of the analysis of TCM as K increases when PNI is present, the evaluation of the performance for larger K should be done by simulation. A simulation would also allow the performance of TCM waveforms to be examined for more realistic interference noise signals than the PNI assumed in this thesis.

It would be interesting to investigate performance of the two TCM systems under the effect of pseudo noise jamming signals. This kind of noise jamming signal is implemented by frequency modulating (FM) a voltage tunable power oscillator using bandlimited AWGN or bandlimited AWGN plus a periodic waveform. Noise quality (GNQ) is a figure of merit that represents the effectiveness of pseudo noise jamming signals, and GNQ is related to various parameters such as baseband noise bandwidth, periodic waveform shape, periodic waveform frequency, and receiver bandwidth. An effective way to evaluate GNQ is by simulation where we can examine the effect of the different signal parameters of the FM jammer [20].

By examining the TCM systems considered in this thesis for more realistic noise signals like pseudo noise jamming signals, we get more realistic results since pseudo noise jamming signals are typical of real military electronic warfare systems [20].

THIS PAGE INTENTIONALLY LEFT BLANK

LIST OF REFERENCES

[1] WHITE PAPER, "IEEE 802.11g New Draft Standard Clarifies Future of Wireless LAN", William Carney, TEXAS INSTRUMENTS.

[2] R. C. Robertson and C. Kalogrias, "Performance analysis of the IEEE 802.11a WLAN standard optimum and sub-optimum receiver in frequency-selective, slowly fading Nakagami channels with AWGN and pulsed-noise interference", *Proc. IEEE Military Comm. Conf.*, vol. 2, pp. 736 – 743, Nov. 2004.

[3] C. E. Shannon, "A Mathematical Theory of Communication ", Bell Syst. Tech. J., pp.379-423 Part(1), July 1948; pp. 623-56 Part(2), Oct. 1948.

[4] D. J. Costello, S. Lin, *Error Control Coding: Fundamental and Applications*, 2nd edition, Prentice-Hall, Upper Saddle River, NJ, 2004.

[5] R. C. Robertson, class notes for EC4580 (Trellis-Coded Modulation), Naval Postgraduate School, Monterey, CA, 2005 (unpublished).

[6] G. Ungerboeck and I. Csajka, "On improving data-link performance by increasing the channel alphabet and introducing sequence coding," *Proc. Int. Symp. Inform. Th.*, Session B4, p. 53, June 1976.

[7] G. Ungerboeck, "Channel coding with multilevel phase signals" *IEEE Trans. Inform. Theory*, vol. IT-28, pp. 55-67, Jan. 1982.

[8] G. Ungerboeck, "Trellis-Coded Modulation with Reduntant Signal Sets. Part I: Introduction," *IEEE Commun. Mag*., vol. 25, pp. 5-11, Feb. 1987.

[9] J.G. Proakis, *Digital Communications*, 4th edition, McGraw Hill, New York, NY, 2001.

[10] B. Sklar, *Digital Communications: Fundamental and Applications*, 2nd edition, Prentice-Hall, Upper Saddle River, NJ, 2001.

[11] Ezio Bigliery, Dariush Divsalar, Peter J. McLane, Marvin K. Simon, *Introduction to Trellis-coded Modulation with applications*, Prentice-Hall, Inc., May 1991.

[12] R. C. Robertson, class notes for EC4580 (Error Correction Coding), Naval Postgraduate School, Monterey, CA, 2001 (unpublished).

[13] R. C. Robertson, class notes for EC4550 (*M*-ary Digital Communication Systems), Naval Postgraduate School, Monterey, CA, 2001 (unpublished).

[14] R. C. Robertson, class notes for EC3510 (Communications Engineering), Naval Postgraduate School, Monterey, CA, 2001 (unpublished).

[15] S. T. Rappaport, *Wireless Communications Principles and Practice*, 2nd edititon, Prentice Hall, Upper Saddle River, NJ, 2002.

[16] Yi Gong, K.B Letaief, "Performance of space-time trellis coding over Nakagami fading channel", vol. 2, pp. 1405 – 1409, 2001.

[17] R. C. Robertson and G. Zouros, "Performance analysis of BPSK with errors and erasures decoding to mitigate the effects of pulse-noise interference", *Proc. IEEE Military Comm. Conf*., pp.1-6, 2006.

[18] K. Pyloudis, "Low Spectral Efficiency Trellis Coded Modulation Systems" M.S. thesis, Naval Postgraduate School, Monterey, CA, 2006.

[19] I. Katzourakis, "Performance analysis of a variable data rate TCM waveform transmitted over a channel with AWGN and pulse-noise interference", M.S. thesis, Naval Postgraduate School, Monterey, CA, 2007.

[20] J. B. Knorr and D. T. Karantanas, "Simulation Optimizes Noise Jammer Design", *Microwave Journal*, pp. 273-277, May 1985.

INITIAL DISTRIBUTION LIST

1. Defense Technical Information Center
   Ft. Belvoir, Virginia

2. Dudley Knox Library
   Naval Postgraduate School
   Monterey, California

3. Chairman, Code EC
   Department of Electrical and Computer Engineering
   Naval Postgraduate School
   Monterey, California

4. Professor R. Clark Robertson, Code EC/Rc
   Department of Electrical and Computer Engineering
   Naval Postgraduate School
   Monterey, California

5. Professor Tri Ha, Code EC/Ha
   Department of Electrical and Computer Engineering
   Naval Postgraduate School
   Monterey, California

6. Embassy of Greece,
   Office of Naval Attaché
   Washington, DC

7. LTJG Drivas Athanasios
   Hellenic Navy General Staff
   Athens, Greece